3-12-2008

Uncorrelated Track Avoidance

Darrell L. Grob

UNCORRELATED TRACK AVOIDANCE

THESIS

Darrell L. Grob, Captain, USAF

AFIT/GA/ENY/08-M10

DEPARTMENT OF THE AIR FORCE
AIR UNIVERSITY

AIR FORCE INSTITUTE OF TECHNOLOGY

Wright-Patterson Air Force Base, Ohio

The views expressed in this thesis are those of the author and do not reflect the official policy or position of the United States Air Force, Department of Defense, or the United States Government.

AFIT/GA/ENY/08-M10

UNCORRELATED TRACK AVOIDANCE

THESIS

Presented to the Faculty

Department of Aeronautical and Astronautical Engineering

Graduate School of Engineering and Management

Air Force Institute of Technology

Air University

Air Education and Training Command

In Partial Fulfillment of the Requirements for the

Degree of Master of Science in Astronautical Engineering

Darrell L. Grob, BSAE

Captain, USAF

March 2008

AFIT/GA/ENY/08-M10

UNCORRELATED TRACK AVOIDANCE

Darrell L. Grob, BSAE
Captain, USAF

Approved:

William E. Wiesel — 12 Mar '08

Dr. William E. Wiesel (Chairman) — Date

12 Mar 08

Lt. Col. Kerry Hicks (Member) — Date

12 Mar 08

Lt. Col. Nathan Titus (Member) — Date

Abstract

The purpose of this thesis is to examine what data requirements are necessary to avoid continual series of uncorrelated tracks when gathering observations. The constants of the motion for simple two-body motion for a satellite orbiting the Earth, known as the classical orbital elements or COEs, do not remain constant due to zonal and sectoral harmonic variations in the Earth's gravitational field. There are other elements of the motion that should be considered and this paper discusses the constancy of three elements: the Hamiltonian ($\mathcal{H}$) of the Earth-Centered Rotating System, $\hat{Z}$-component of inertial angular momentum (H_k), and the time rate of change of the right ascension of the ascending node ($\dot{\Omega}$).

With an understanding of the constancy of these elements, simulated data was used to determine the effects sensor performance and observation quantity have on the ability to effectively estimate these constants. This information was used to determine an appropriate level of fidelity for a model to be utilized as a supplement in fitting observation data with current data available in the Satellite Catalog.

To my loving wife

Acknowledgements

I would like to extend my sincere gratitude to my faculty advisor, Dr. William Wiesel, for his continuous support and guidance on my thesis work. Dr. Wiesel's knowledge and insight are a great source of inspiration. I would also like to thank Dr. Chris Sabol of Air Force Research Laboratories for proposing the idea and sponsoring my thesis work.

Darrell L. Grob

Table of Contents

Page

List of Figures

List of Tables

List of Symbols

Symbol		Page
$\mathcal{H}$	Hamiltonian Function	iv
H_k	$\hat{Z}$-Component of Inertial Angular Momentum	iv
$\dot{\Omega}$	Time Rate of Change of the Right Ascension of the Ascending Node	iv
θ_{GMST}	Greenwich Meridian Sidereal Time	4
q	Generalized Coordinate	5
$\omega_{\oplus}$	Rotation of the Earth	6
$\dot{q}$	Generalized Velocity	6
T	Kinetic Energy	6
V	Potential Energy	6
L	Lagrangian	7
p	Generalized Momentum	7
ϕ	Geocentric Longitude	8
θ	Colatitude	8
$\vec{R}_{IJK}$	Inertial Position Vector	10
$\vec{V}_{IJK}$	Inertial Velocity Vector	10
$\vec{H}_{IJK}$	Inertial Angular Momentum	17
Ω	Right Ascension of the Ascending Node	26
a	Semi-Major Axis	26
e	Eccentricity	26
i	Inclination	26
$\vec{n}$	Line of Nodes	28
$\vec{R}$	Position Vector	35
$\vec{V}$	Velocity Vector	35
$\vec{g}$	Gravitational Acceleration	35
m	Meters	35
s	Seconds	35

Symbol		Page
Δt	Time Step	35
z_d	Observed Data	35
Φ	State Transition Matrix	36
G	Observation Relation	37
T	Observation Matrix	37
Q	Instrumental Covariance Matrix	38
P_X	Covariance Matrix	38
X_p	Particular Solution	38
$\vec{r}$	Residual Vector	39

List of Abbreviations

UNCORRELATED TRACK AVOIDANCE

I. Introduction

1.1 Background

Since the first man-made satellite Sputnik was launched by the former Soviet Union in 1957, the number of Earth orbiting satellites continues to grow at a rapid pace. Currently, the Earth is surrounded by thousands of satellites and other objects, such as expended rocket bodies and debris left from broken-up satellites orbiting at numerous altitudes above the Earth. These objects create a region of increased risk around the Earth for objects returning into the Earth's atmosphere or objects being launched into space.

These problems are not new to anyone in the space business but they do require full time operations to monitor and track all of these objects. Currently, the United States uses the "Satellite Catalog (SATCAT)" [6] to track over 8,500 objects approximately as small as a softball [1]. In order to track these different objects, current operations entail obtaining observational data and comparing the new data with databases filled with archived information on current objects. Then, based on best-fit algorithms like least squares, the tracked satellite is fit to an existing track in the database and the information for that object is updated; if the new orbit cannot be fit with an existing object in the database, it is labeled as an uncorrelated track and inserted into the database as a new object. In the business where accuracy is of utmost importance and information is essential, it is beneficial to keep uncorrelated tracks at a minimum. Tracking all of these objects is quite a task especially with all of the disturbing forces that are acting on these objects, varying with each orbit. Despite the difficulty of the task and the standing army required to manage the problem, there are ideas to reduce the size of the objects being tracked from softball size

to approximately golf ball size which will substantially increase the number of objects being tracked.

1.2 Problem Statement

As the number of objects being tracked increases, one can naturally expect that the number of uncorrelated tracks will increase at the same rate. However, the problem is not based on numbers alone and because the objects being tracked are smaller in size, the objects may only be in-view when they pass overhead or nearly-overhead. Based on the orbit of the object and the location of the tracking station, these objects might only be tracked once every two weeks. That means the information in the catalog may not be current when the object is viewed again, giving rise for more error in the attempt to fit the new track with one in the database. The higher error increases the likelihood of adding identical objects multiple times into the catalog. Therefore, in order to limit the redundancy in the Satellite Catalog by minimizing the number of uncorrelated tracks, there is a need to enhance the process by including information about the orbit that remains more accurate for a longer period of time.

1.3 Research Focus

The focus of this research is to investigate the constancy of the Hamiltonian Function (Chapter III), the constancy of the $\hat{Z}$-component of the inertial angular momentum (Chapter IV) and the constancy of the time rate of change of the right ascension of the ascending node (Chapter V). The constancy of these elements is established through analysis of different levels of fidelity for the gravitational geopotential expansion. The level of accuracy attainable for each of these elements is then utilized in establishing a basis for a supplemental model (Chapter VI) that can be used in data mining to aide in the minimization of uncorrelated tracks by fitting two or more uncorrelated tracks.

II. Coordinate Systems

2.1 Earth-Centered Coordinate Frames

There are two coordinate systems that are referenced in this paper and a short description of each coordinate system is addressed in this chapter. The first coordinate frame is the Earth-Centered Inertial (ECI) Frame, also known as the Geocentric Equatorial Coordinate System or IJK Frame. The origin, as suggested in the name, lies at the center of the Earth. The fundamental plane for this system is the Earth's equatorial plane and the first axis ($\hat{I}$) points toward the vernal equinox or the first point of Aries. The second axis ($\hat{J}$) is picked ninety degrees off of the first and chosen so that applying the right-hand rule, the third component of the coordinate system ($\hat{K}$) is aligned with the Earth angular velocity vector, through the North Pole [8, 157]. Figure 2.1 shows the ECI Coordinate Frame and comes from Vallado [8, 157].

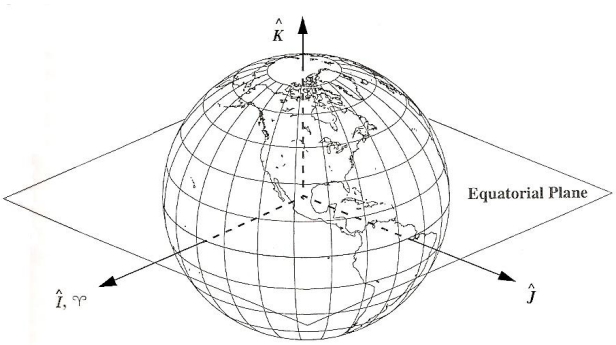

Figure 2.1: Earth-Centered Inertial Frame

The second coordinate system that is referenced in this paper is the Earth-Centered Rotating (ECR) Frame, also known as the Body-Fixed Coordinate System or International Terrestrial Reference Frame (ITRF). This coordinate system shares the origin and fundamental plane of the ECI, but the main difference is that the coordinate system rotates with the Earth. The first axis ($\hat{X}$) points from the origin toward the Prime Meridian, or Greenwich Meridian, which is zero degrees longitude. Similar to the ECI, the second axis ($\hat{Y}$) is selected ninety degrees East of first axis such that the third axis ($\hat{Z}$) is aligned with the Earth spin axis using the right-hand rule.

As stated above, one difference between these two coordinate systems is that ECR rotates with the Earth and a link between these two coordinate frames is the angle known as Greenwich Meridian Sidereal Time (θ_{GMST}). Greenwich Meridian Sidereal Time is the angle measured from the first axis of the ECI ($\hat{I}$) to the Earth's meridian [5, 137]. Figure 2.2 is taken from Vallado [8, 189] but some of the information was removed in order to focus on the angles of interest. Additionally, due to slight

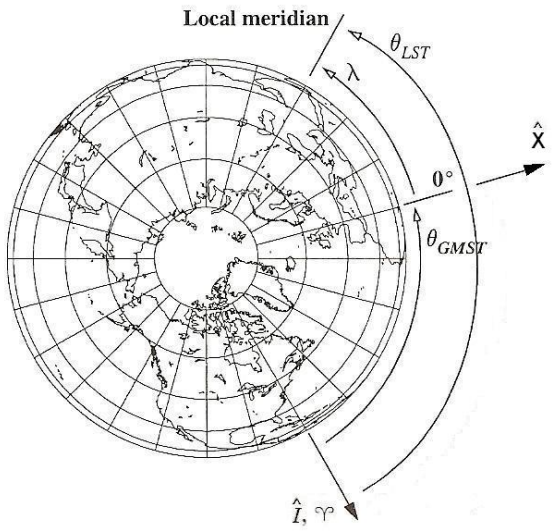

Figure 2.2: Greenwich Meridian Sidereal Time

movements over time by the equatorial plane and the equinox, nutation and precession models are also required to link the two coordinate systems [8, 158].

III. Integrals of Satellite Motion

3.1 Introduction

The first element the author analyzed for constancy is the Hamiltonian Function. Solving for the Hamiltonian Function is accomplished by utilizing analytical mechanics. The advantages to using analytical mechanics is that instead of focusing on vector quantities like force and momentum, the focus shifts to scalars like kinetic energy and the Hamiltonian. Not only does changing from vectors to scalars make things easier, but the acceleration vector is not required in analytical mechanics. Additionally, analytical mechanics allows the use of generalized coordinates allowing selection of an ideal coordinate system to calculate the above mentioned scalars. [7, 45]

3.2 Deriving the Hamiltonian Function

In formulating the Hamiltonian Function, x, y, and z in the Earth-Centered Rotating Frame are chosen to be the "generalized coordinates" (q) [7, 45]:

$$\bar{q} = \begin{pmatrix} q_1 \\ q_2 \\ q_3 \end{pmatrix} = \begin{pmatrix} x \\ y \\ z \end{pmatrix} \tag{3.1}$$

The next step is to take the derivative of the generalized coordinates to find the "generalized velocities" [7, 94] and because the $q_k's$ are in a rotating frame, we must apply the following equation, taken from Wiesel [9, 12] to find the inertial derivative:

$$\frac{^i d}{dt}(\ ) = \frac{^s d}{dt}(\ ) + \omega^{si} \times (\ ) \tag{3.2}$$

Note that in the above equation ω^{si} is ω of the Earth and it is labeled as $\omega_{\oplus}$. Taking the derivative of the coordinates produces the following generalized velocities ($\dot{q}$):

$$\frac{^{i}d}{dt}\begin{pmatrix} q_1 \\ q_2 \\ q_3 \end{pmatrix} = \begin{pmatrix} \dot{x} \\ \dot{y} \\ \dot{z} \end{pmatrix} + \omega_{\oplus} \times \begin{pmatrix} q_1 \\ q_2 \\ q_3 \end{pmatrix} \tag{3.3}$$

Executing the cross product in the above equation yields the following:

$$\begin{pmatrix} \dot{q}_1 \\ \dot{q}_2 \\ \dot{q}_3 \end{pmatrix} = \begin{pmatrix} \dot{x} - \omega_{\oplus} q_2 \\ \dot{y} + \omega_{\oplus} q_1 \\ \dot{z} \end{pmatrix} \tag{3.4}$$

Now obtaining the generalized velocities makes it possible to calculate the kinetic energy (T) by using the following equation [7, 14]:

$$T = \frac{1}{2} m \begin{pmatrix} \dot{q}_1 \\ \dot{q}_2 \\ \dot{q}_3 \end{pmatrix} \cdot \begin{pmatrix} \dot{q}_1 \\ \dot{q}_2 \\ \dot{q}_3 \end{pmatrix} \tag{3.5}$$

However, because the interest is in the specific kinetic energy, there is no need for mass in the above equation. Taking out the mass term and inputting the results from Equation 3.4 the specific kinetic energy is calculated to be:

$$T = \frac{1}{2}\left[(\dot{x} - \omega_{\oplus} q_2)^2 + (\dot{y} + \omega_{\oplus} q_1)^2 + (\dot{z})^2\right] \tag{3.6}$$

Along with the specific kinetic energy of the system, the potential energy (V) of the system is also of interest. The potential energy can be written in the geopotential form with $r = \sqrt{q_1^2 + q_2^2 + q_3^2}$ as follows [10, 108]:

$$V = -\frac{\mu}{r}\sum_{n=0}^{\infty}\sum_{m=0}^{n}\left(\frac{r}{R_{\oplus}}\right)^{-n} P_n^m\left(\frac{q_3}{r}\right) \times \left[C_{nm}\, cos\, m\, tan^{-1}\left(\frac{q_2}{q_1}\right) + S_{nm}\, sin\, m\, tan^{-1}\left(\frac{q_2}{q_1}\right)\right] \tag{3.7}$$

The C_{nm} and S_{nm} terms were defined in a study conducted by a team comprised of individuals from the National Geospatial-Intelligence Agency and National Aeronautics and Space Administration. The study assigned values for the geopotential expansion out through $n = m = 50$ [2]. The final n and m values desired for the geopotential expansion will be referred to as J_n^m for the remainder of this paper. This provides the n and m values required for the summations to determine the values for C_{nm}, S_{nm} and P_n^m in Equation 3.7.

After obtaining values for the specific kinetic energy and potential energy of the system, the next step is to find the Lagrangian (L) [7, 68]. The Lagrangian is defined as:

$$L = T - V \tag{3.8}$$

Inserting Equation 3.6 and 3.7 into Equation 3.8 the Lagrangian is found to be:

$$L = \frac{1}{2}\left[(\dot{x} - \omega_{\oplus} q_2)^2 + (\dot{y} + \omega_{\oplus} q_1)^2 + (\dot{z})^2\right] - V(q_1, q_2, q_3) \tag{3.9}$$

The next step is to calculate the "generalized momenta" (p) [7, 80]. The momenta are defined as:

$$p_k = \frac{\partial L}{\partial \dot{q}_k} = \frac{\partial T}{\partial \dot{q}_k} \tag{3.10}$$

Applying equation 3.10 it is possible to find the generalized momenta:

$$\begin{pmatrix} p_1 \\ p_2 \\ p_3 \end{pmatrix} = \begin{pmatrix} \dot{x} - \omega_{\oplus} q_2 \\ \dot{y} + \omega_{\oplus} q_1 \\ \dot{z} \end{pmatrix} \tag{3.11}$$

Which shows that the generalized momenta are the same as the inertial derivative of the coordinates or the generalized velocities. Therefore, the momenta for this non-inertial system are the components of the inertial velocity. Rearranging the above

equation to solve for the $\dot{q_k}'s$ the following is found:

$$\begin{pmatrix} \dot{q_1} \\ \dot{q_2} \\ \dot{q_3} \end{pmatrix} = \begin{pmatrix} \dot{x} \\ \dot{y} \\ \dot{z} \end{pmatrix} = \begin{pmatrix} p_1 + \omega_{\oplus} q_2 \\ p_2 - \omega_{\oplus} q_1 \\ p_3 \end{pmatrix} \tag{3.12}$$

The last step is to formulate the Hamiltonian [7, 94]. The Hamiltonian Function is defined as:

$$\mathcal{H} = \sum_{k=1}^{n} p_k \dot{q_k} - L \tag{3.13}$$

but the generalized velocities must not be in the Hamiltonian Function [7, 94]; therefore, substituting in for the generalized velocities, as defined in Equation 3.12, results in a Hamiltonian Function as defined below:

$$\mathcal{H} = \frac{1}{2}\left(p_1^2 + p_2^2 + p_3^2\right) + \omega_{\oplus}\left(p_1 q_2 - p_2 q_1\right) + V(q_1, q_2, q_3) \tag{3.14}$$

Equation 3.14 shows that the Hamiltonian Function is not directly dependent on time making it a constant of the motion.

It is worth noting that the above expression can be simplified by incorporating polar coordinates. In polar coordinates, r is the radius as defined above, ϕ is defined as the geocentric longitude and θ is defined as the colatitude [10, 105]. These coordinates are related to the generalized coordinates in the following manner:

$$\phi = tan^{-1}\left(\frac{q_2}{q_1}\right) \tag{3.15}$$

$$\theta = cos^{-1}\left(\frac{q_3}{\sqrt{q_1^2 + q_2^2 + q_3^2}}\right) \tag{3.16}$$

Substituting Equations 3.15 and 3.16 into Equation 3.7 results in the Hamiltonian Function expressed in polar coordinates as defined in Wiesel [10, 108]. Now working with the Hamiltonian Function in polar coordinates it is possible to calculate the

change in the generalized momenta using the following equation [7, 94]:

$$\dot{p}_k = -\frac{\partial \mathcal{H}}{\partial q_k} \tag{3.17}$$

Taking the partial as described in 3.17 results in a change in the generalized momenta for the geocentric longitude (ϕ) as shown below [10, 110]:

$$\dot{p}_\phi = \frac{\mu}{r} \sum_{n=0}^{\infty} \sum_{m=0}^{n} \left(\frac{r}{R_\oplus} \right)^{-n} P_n^m \left(cos\,\theta \right) \times m \left[-C_{nm}\, sin\, m \left(\phi - \omega_\oplus t \right) + S_{nm}\, cos\, m \left(\phi - \omega_\oplus t \right) \right] \tag{3.18}$$

This result shows that for cases where $m = 0$ the change in $\dot{p}_\phi$ is equal to zero making the inertial angular momentum a constant of the motion. This is the topic of discussion for Chapter IV.

3.3 Constancy of the Hamiltonian

In order to show the constancy of the Hamiltonian Function, the author used Matlab® to create a computer program (see Appendix B) which takes position and velocity vectors in the Earth-Centered Rotating (ECR) Frame and computes the Hamiltonian as described in Equation 3.14 using simulated data. The following is a complete list of the tests run to determine the constancy of the Hamiltonian Function:

- Case 1: Includes geopotential expansion through J_0^0 term
- Case 2: Includes geopotential expansion through J_2^0 term
- Case 3: Includes geopotential expansion through J_2^2 term
- Case 4: Includes geopotential expansion through J_4^0 term
- Case 5: Includes geopotential expansion through J_4^4 term
- Case 6: Includes geopotential expansion through J_8^0 term
- Case 7: Includes geopotential expansion through J_8^8 term
- Case 8: Includes geopotential expansion through J_{21}^0 term

- Case 9: Includes geopotential expansion through J_{21}^{21} term

The above cases were run using four different scenarios. The first scenario is a near-circular orbit, inclined at 30 degrees, evaluated for 2000 TU or approximately 18 days. The second scenario is a circular orbit, inclined at 45 degrees, evaluated for 2000 TU. The third scenario is the same orbit as Scenario 1 with an evaluation period of 20000 TU or approximately six months. The final scenario is the same orbit as Scenario 2 with an evaluation period of 20000 TU. The initial conditions for position ($\vec{R}_{IJK}$) and velocity ($\vec{V}_{IJK}$) for Scenarios 1 and 3 are:

$$\vec{R}_{IJK} = \begin{pmatrix} 1.05 \\ 0.0 \\ 0.0 \end{pmatrix} [DU] \tag{3.19}$$

$$\vec{V}_{IJK} = \begin{pmatrix} 0.0 \\ 0.845154254 \\ 0.453464763 \end{pmatrix} \left[\frac{DU}{TU}\right] \tag{3.20}$$

The initial conditions for Scenarios 2 and 4 are:

$$\vec{R}_{IJK} = \begin{pmatrix} 0.0 \\ -1.15678606465 \\ 0.0 \end{pmatrix} [DU] \tag{3.21}$$

$$\vec{V}_{IJK} = \begin{pmatrix} 0.65744356375 \\ 0.0 \\ 0.65744356375 \end{pmatrix} \left[\frac{DU}{TU}\right] \tag{3.22}$$

For each of the nine cases and four scenarios the process of gathering the data is the same. The desired initial conditions and geopotential value are input into Dr. Wiesel's orbit propagator by altering the input file to specify the initial conditions as well as the n and m values for the geopotential expansion. The orbit propagator

outputs position and velocity data in both the ECI and ECR Frames which are then read into the Matlab® program. Then data showing all the values for the Hamiltonian for each J_n^m term at each time step is output.

Applying the initial conditions for Scenario 1, the first test case was evaluated in which $n = m = 0$ to find the two-body constancy of the Hamiltonian Function. Taking the output data from the computer program and importing it into Excel® a graph of the values at each time step was created. Because this case is the two-body case, there are no geopotential terms to alter the constancy of the system and, therefore, a constant value for $\mathcal{H}$ for the entire data collection period is expected.

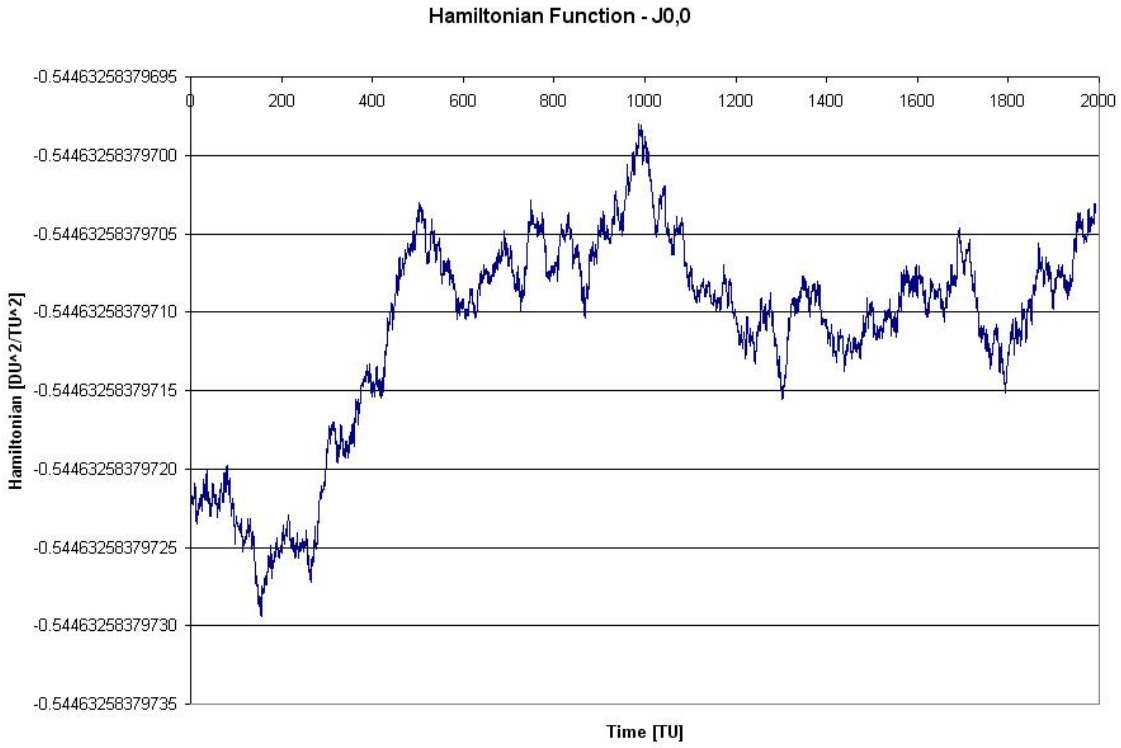

Figure 3.1: Scenario 1, Case 1: $\mathcal{H}$ versus time

Figure 3.1 verifies that indeed the Hamiltonian Function is constant up to approximately order 10^{-13}. Because the value of the Hamiltonian Function is calculated using canonical units, the original values are of order one, making the $\mathcal{H}$ constant to

twelve significant figures. This result was expected for the two-body case and will be used as a comparison for the remainder of the cases.

The next case evaluated was Case 2 with geopotential terms out to J_2^0. Using the same process stated above data was gathered and the results are plotted in Figure 3.2. This figure shows that the constancy of $\mathcal{H}$ remains at approximately 10^{-13} even with the oblateness of the Earth factored into the equation. The importance of these results is that although the geopotential J_2^0 term is added the constancy of $\mathcal{H}$ remains on the same order as the two-body case. When analyzing the COEs, there is a noticeable change in the accuracy of these constants with the oblateness term added and equations for the secular change can be found in Wiesel [10, 141-146]. Unlike the classical orbital elements though, $\mathcal{H}$ retains the same order of constancy with the inclusion of the gravity geopotential expansion through the J_2^0 term.

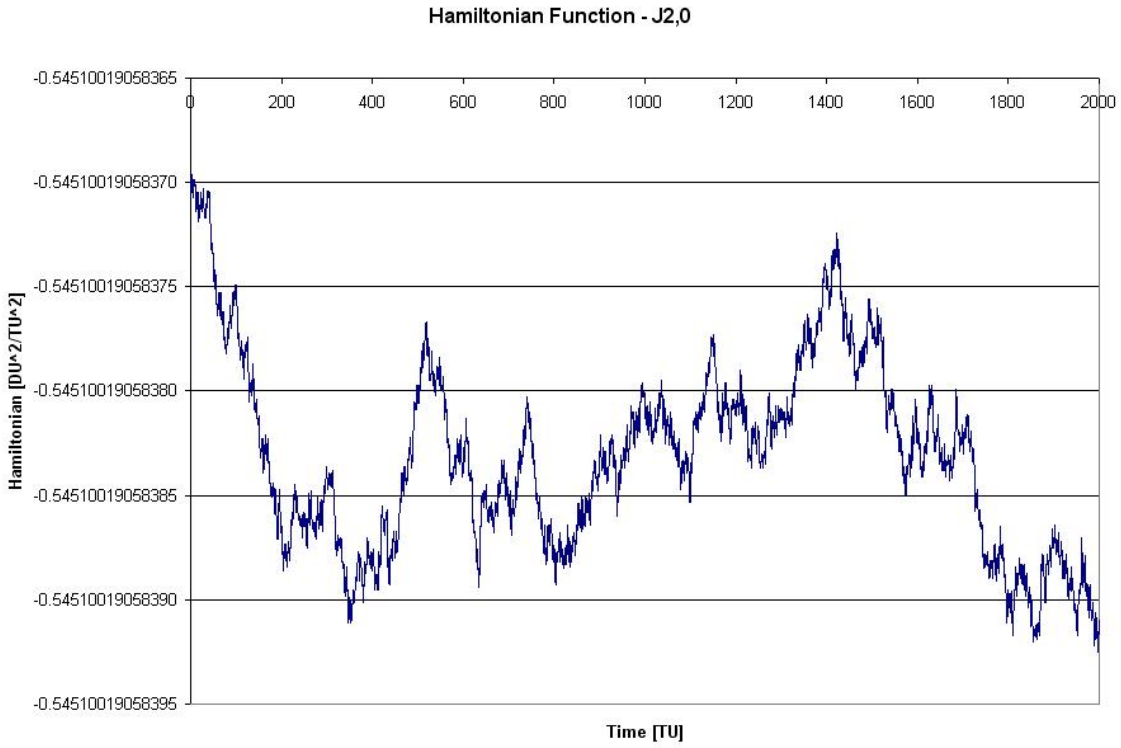

Figure 3.2: Scenario 1, Case 2: $\mathcal{H}$ versus time

Continuing to add terms from the geopotential does not affect the accuracy of the Hamiltonian Function. Executing all cases in the first scenario results in no change to the level of constancy of $\mathcal{H}$. The constancy of $\mathcal{H}$ remains at approximately order 10^{-13}. Scenario 1, Case 9 validates that adding geopotential terms through the J_{21}^{21} term the Hamiltonian Function remains at a constancy of approximately the same order of magnitude as the two-body case. Figure 3.3 is a graph of Scenario 1, Case 9 graphically showing that for 2000 TU, $\mathcal{H}$ remains constant to approximately order 10^{-13}. As was stated above all of the cases in this scenario have approximately the same constancy as Case 1 and the graphs for Scenario 1 not explicitly discussed in this section are attached in Appendix A along with graphs for Scenario 2.

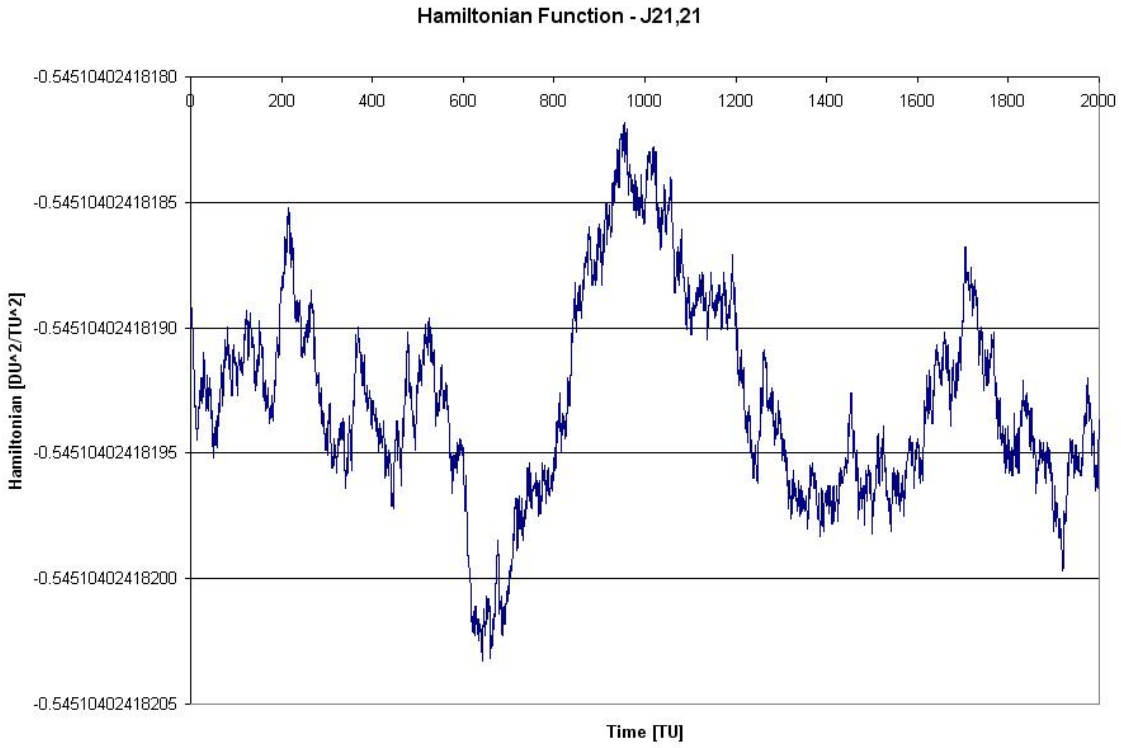

Figure 3.3: Scenario 1, Case 9: $\mathcal{H}$ versus time

In addition to graphing the data, analysis was done in order to find the maximum change from the initial Hamiltonian Function value. In order to do this, the data was inserted into an Excel® file and the absolute value of the difference of $\mathcal{H}(t) - \mathcal{H}(t_0)$

was calculated in one column. Then using a built-in Excel® function the maximum value in that column was identified. For each of the four scenarios and nine cases in each scenario, the data was evaluated in the same manner and the results from all of these cases are summarized in Table 3.1. Note the asterisk next to Scenario 3, Case 1; it is there to signify that data was not collected for the entire 20000 TU. For unknown reasons, the orbit propagator did not produce data for the entire time interval and therefore the data is based on a shorter time period. This is insignificant since it is only the two-body case and we expect it to remain constant for the entire time.

	Scenario 1	**Scenario 2**	**Scenario 3**	**Scenario 4**
Case 1	2.46E-13	8.80E-14	3.29E-13*	6.29E-13
Case 2	2.18E-13	4.68E-13	1.51E-12	9.73E-13
Case 3	4.56E-13	1.13E-13	8.19E-13	5.79E-13
Case 4	4.17E-13	2.44E-13	3.96E-13	9.52E-13
Case 5	2.92E-13	1.15E-13	7.99E-13	1.10E-12
Case 6	4.16E-13	8.20E-14	1.44E-12	7.37E-13
Case 7	1.79E-13	2.15E-13	6.67E-12	5.45E-13
Case 8	2.86E-13	1.23E-13	1.35E-12	3.11E-13
Case 9	1.35E-13	1.68E-13	4.18E-13	4.39E-13

Table 3.1: Hamiltonian Function Constancy Results

The final analysis done with the Hamiltonian Function was to come up with a comparison for how well a lower geopotential expansion estimate does with a specific data set. The motivation behind this analysis is to determine a level of constancy for the Hamiltonian Function based on position and velocity accuracy attainable for a specific sensor. For example, it may not be feasible to use the geopotential expansion through the J_{21}^{21} term if the position accuracy for a sensor is on the order of a kilometer. This analysis will provide a basis for the discussion in Chapter VI to determine an appropriate geopotential expansion level for models based on position and velocity accuracy attainable by a sensor. In order to accomplish this, position and velocity data was created by running Dr. Wiesel's orbit propagator for each of the four scenarios detailed above. The geopotential input into the propagator calls for the $n = 21$ and $m = 21$ values indicating the geopotential expansion through the J_{21}^{21}

term. As discussed previously, the output from the orbit propagator is used as input into the Hamiltonian Function Matlab® code. Then Hamiltonian data is gathered to show the accuracy of each of the different cases as defined above. So for Case 1, the Hamiltonian data created for the geopotential expansion through the J_{21}^{21} term was evaluated using only the two-body terms in the Matlab® program. Then taking the output from the computer program and importing it into Excel® the data was analyzed as described above. A column of data was created containing the absolute value of the difference between $\mathcal{H}(t) - \mathcal{H}(t_0)$ and then using the built-in Excel® function the maximum difference from the initial Hamiltonian value was calculated and inserted into Table 3.2. The accuracy of the Hamiltonian Function with Case 1 assumptions was very low, on the order of 10^{-4}. The J_2^0 case increases the constancy of $\mathcal{H}$ by about an order of magnitude, but is still not very constant. It turns out that Case 2 is about as accurate as the "zonal harmonic" cases will get [10, 113]. Note in the table that using J_{21}^0 yields approximately the same constancy. However, it should be noted that as more terms are added to the geopotential in the Matlab® program, the constancy of the Hamiltonian Function increases. These results are summarized in Table 3.2 and the table ends with the constancy obtained by using the geopotential through J_{21}^{21} exactly what was used to create the position and velocity vector in the orbit propagator. The final results in Table 3.2 match the constancy in the final row of Table 3.1 because the data input into the propagator and Matlab® program is identical.

	Scenario 1	**Scenario 2**	**Scenario 3**	**Scenario 4**
Case 1	3.23E-04	5.23E-04	3.23E-04*	5.25E-04
Case 2	2.12E-05	1.23E-05	2.13E-05	1.24E-05
Case 3	1.15E-05	7.28E-06	1.24E-05	7.30E-06
Case 4	2.11E-05	1.23E-05	2.11E-05	1.23E-05
Case 5	8.17E-06	2.56E-06	8.20E-06	2.58E-06
Case 6	2.12E-05	1.23E-05	2.12E-05	1.23E-05
Case 7	3.46E-06	6.03E-07	3.93E-06	6.03E-07
Case 8	2.13E-05	1.23E-05	2.13E-05	1.23E-05
Case 9	1.35E-13	1.68E-13	4.18E-13	4.39E-13

Table 3.2: Hamiltonian Function Comparison

IV. Angular Momentum

4.1 Introduction

Another component evaluated for constancy is the $\hat{Z}$-component of inertial angular momentum of the system. Starting in the Earth-Centered Inertial Frame and neglecting all disturbing forces other than the zonal harmonics in the geopotential, the inertial angular momentum stays constant with a symmetric Earth, this result was proved in Chapter III. Inertial angular momentum ($\vec{H}_{IJK}$) is defined as:

$$\vec{H}_{IJK} = \vec{R}_{IJK} \times \vec{V}_{IJK} \tag{4.1}$$

As noted above, as long as the Earth is symmetric about the polar axis, the inertial angular momentum of the system will stay constant. The constancy of the $\hat{Z}$-component of inertial angular momentum was evaluated using a Matlab® program (see Appendix B). This program reads in the ECI position and velocity vectors and computes the angular momentum at each time step. As noted in the previous chapter, the position and velocity vectors are calculated using Dr. Wiesel's custom-made orbit propagator.

4.2 Changing the Zonal Harmonics

In order to quantify the constancy of the $\hat{Z}$-component of inertial angular momentum analysis of the same four scenarios as stated in Chapter III was accomplished. The four cases include the near-circular orbit with a thirty degree inclination and the circular orbit with a forty-five degree inclination evaluated for 2000 TU and 20000 TU for each of these two orbits. Additionally, each of these four scenarios was analyzed using the same nine cases as discussed in the previous chapter, but the analysis was done in a different order. The modification to the order is used to point out the difference between a symmetric and non-symmetric Earth. Initially, analysis for the scenarios in which only the "zonal harmonics" are considered was accomplished, keeping the Earth's gravitational geopotential symmetric [10, 113]. The five initial

cases run on each scenario to determine the constancy of the $\hat{Z}$-component of the inertial angular momentum are listed below:

- Case 1: Includes geopotential expansion through the J_0^0 term
- Case 2: Includes geopotential expansion through the J_2^0 term
- Case 4: Includes geopotential expansion through the J_4^0 term
- Case 6: Includes geopotential expansion through the J_8^0 term
- Case 8: Includes geopotential expansion through the J_{21}^0 term

Similarly, the initial conditions for the two scenarios remain the same as stated in Chapter III. Initial conditions for Scenarios 1 and 3 are:

$$\vec{R}_{IJK} = \begin{pmatrix} 1.05 \\ 0.0 \\ 0.0 \end{pmatrix} [DU] \tag{4.2}$$

$$\vec{V}_{IJK} = \begin{pmatrix} 0.0 \\ 0.845154254 \\ 0.453464763 \end{pmatrix} \left[\frac{DU}{TU}\right] \tag{4.3}$$

Initial conditions for Scenarios 2 and 4 are:

$$\vec{R}_{IJK} = \begin{pmatrix} 0.0 \\ -1.15678606465 \\ 0.0 \end{pmatrix} [DU] \tag{4.4}$$

$$\vec{V}_{IJK} = \begin{pmatrix} 0.65744356375 \\ 0.0 \\ 0.65744356375 \end{pmatrix} \left[\frac{DU}{TU}\right] \tag{4.5}$$

The first case analyzed is Scenario 1, Case 1, where $n = m = 0$ in the geopotential (Equation 3.7). In order to verify the constancy, the $\hat{Z}$-component of the

inertial angular momentum, ($\hat{H}_k$), is plotted against time represented in canonical time units [TU]. This was accomplished by calculating inertial angular momentum using a Matlab® program and the $\hat{Z}$-component values were output along with each associated time. The data was then imported into Excel® and plotted, showing the constancy of H_k versus time.

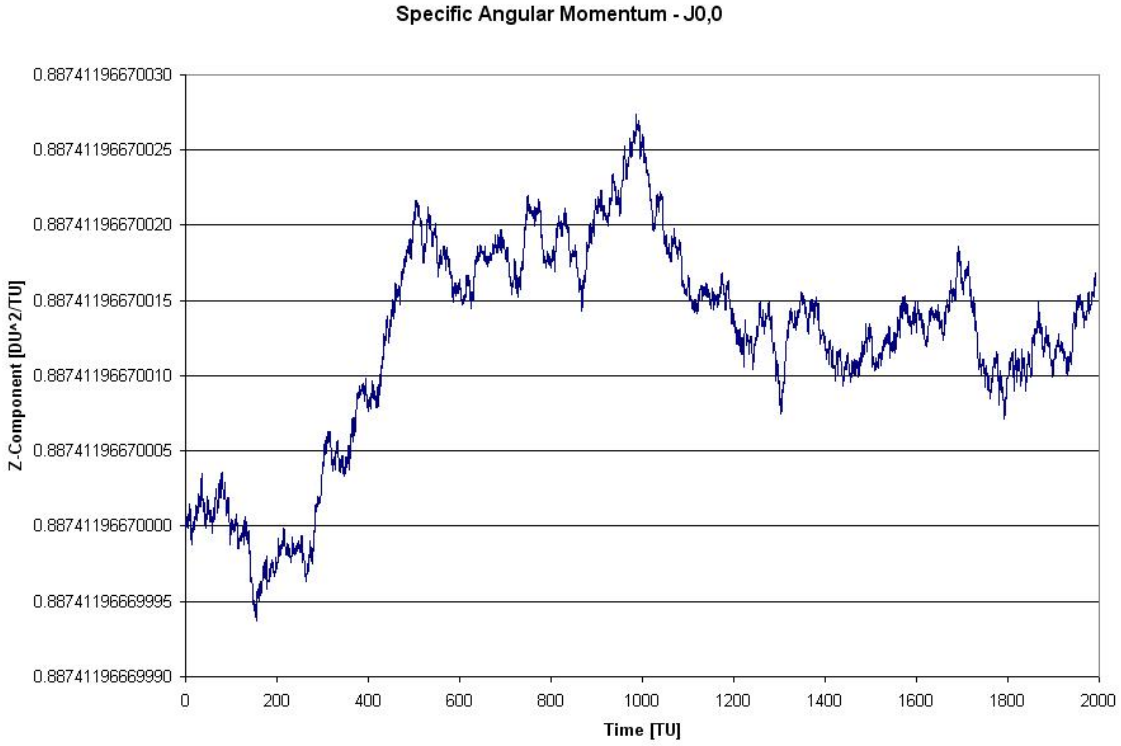

Figure 4.1: Scenario 1, Case 1: H_k versus time

Figure 4.1 shows that for the initial conditions stated in Equations 4.2 and 4.3, the $\hat{Z}$-component of the inertial angular momentum is constant to approximately order 10^{-14} over a period of 2000 TU, or just over two weeks. This was expected since the first case is merely the two-body case without the effects of the geopotential, the $\hat{Z}$-component of the inertial angular momentum is constant along with all the other classical orbital elements. This first case will be used for comparison with the remaining cases within this scenario.

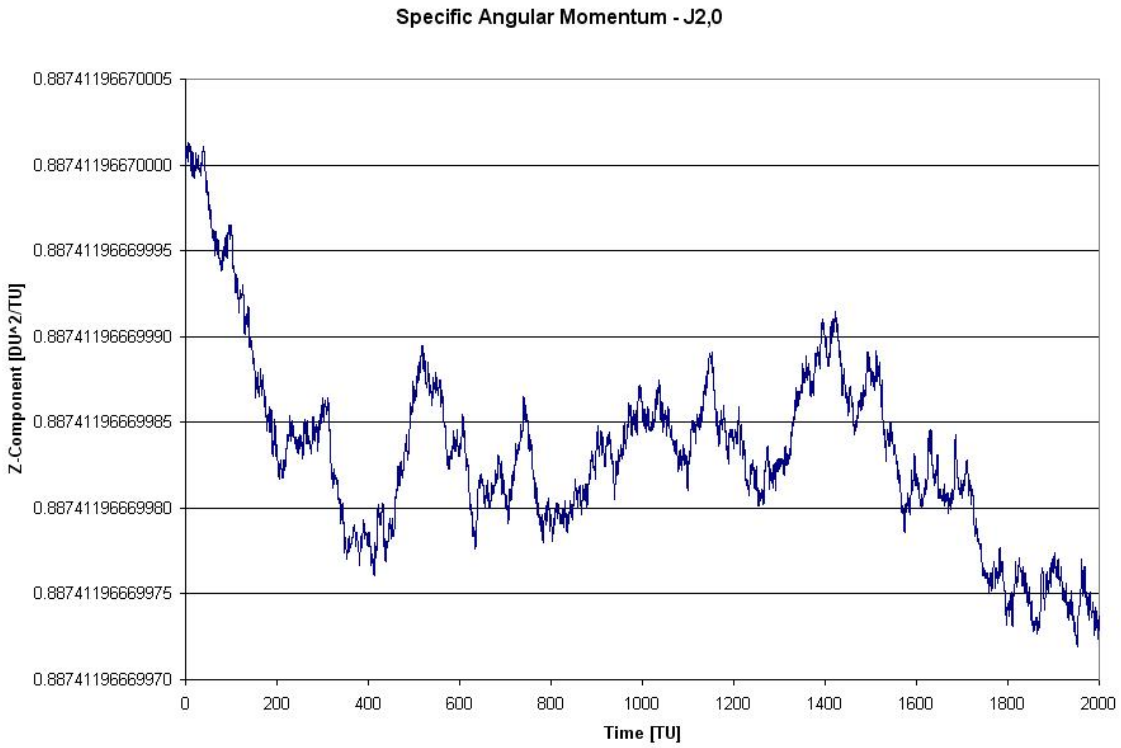

Figure 4.2: Scenario 1, Case 2: H_k versus time

The next case evaluated is Case 2, which accounts for the oblateness of the Earth, or the Earth's "equatorial bulge" [10, 114]. Running the same Matlab® program as before and importing the data into Excel®, a similar graph is created. Figure 4.2 plots the $\hat{Z}$-component of the inertial angular momentum against time and shows the constancy remaining at approximately order 10^{-13} with the stated initial conditions. This continues to validate the assertion that the $\hat{Z}$-component of the inertial angular momentum remains constant over a symmetric Earth. This first zonal change in the geopotential creates a symmetric change in the Earth's gravitational field therefore, leaving the $\hat{Z}$-component of the inertial angular momentum constant.

This trend continues for all cases where the geopotential contains no "sectoral harmonics" or "tesseral harmonics", or where $m = 0$ [10, 114-115]. Figure 4.3 is a graph of the results calculated for the J_{21}^0 case and it shows that the constancy of the $\hat{Z}$-component of the inertial angular momentum continues to remain at a constant

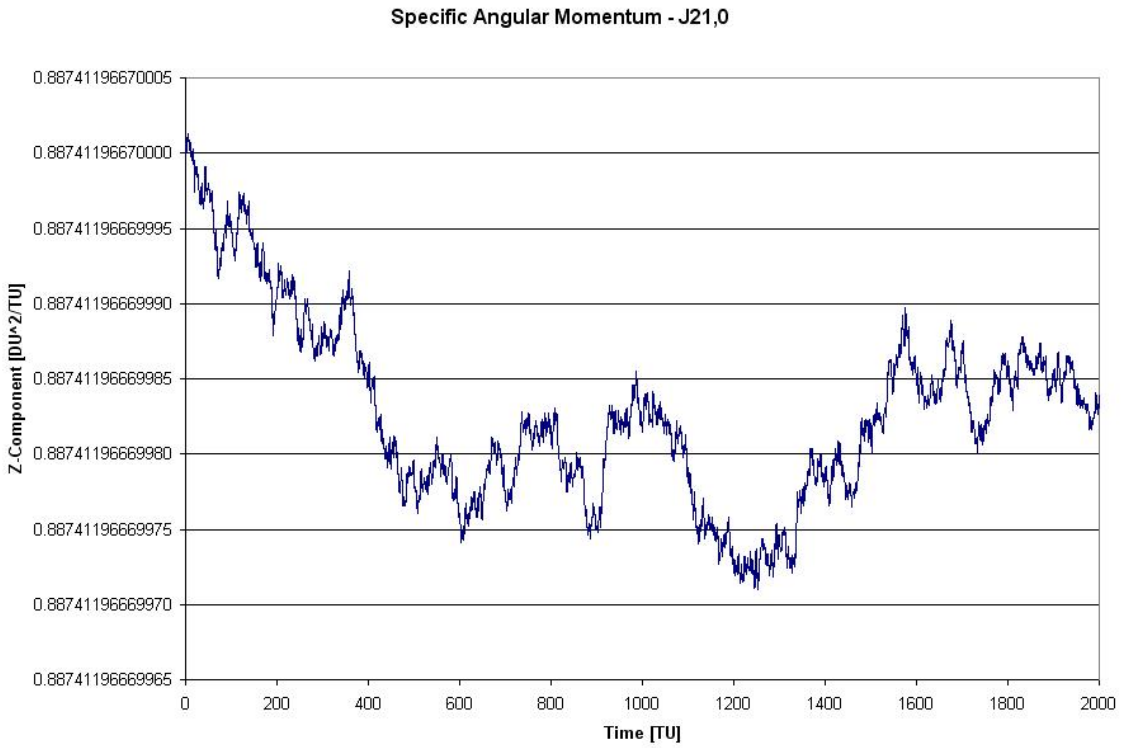

Figure 4.3: Scenario 1, Case 8: H_k versus time

value to within approximately order 10^{-13}. Case 8 is the final case that was analyzed to verify the constancy of the $\hat{Z}$-component of the inertial angular momentum for Scenario 1. The constancy of this case is unchanging from the previous cases including the two-body case showing that for a symmetric Earth, the $\hat{Z}$-component of the inertial angular momentum will remain constant to approximately order 10^{-13}. Graphs from Scenario 2 and cases not cited in this section can be found in Appendix A.

4.3 Including the Tesseral and Sectoral Harmonics

Although making use of the assumption that the Earth's gravitational field is symmetric allows for great constancy in the $\hat{Z}$-component of the inertial angular momentum, it does not represent the Earth's actual gravitational field. Including the tesseral and sectoral harmonics in the calculations enhances our ability to more

accurately model the actual effects that the Earth's geopotential has on orbiting objects. Now utilizing the same four scenarios as above, the constancy of the $\hat{Z}$-component of the inertial angular momentum was evaluated using the following four cases:

- Case 3: Includes geopotential expansion through the J_2^2 term
- Case 5: Includes geopotential expansion through the J_4^4 term
- Case 7: Includes geopotential expansion through the J_8^8 term
- Case 9: Includes geopotential expansion through the J_{21}^{21} term

Each of these cases includes the geopotential expansion through a term where $n = m$. These terms are referred to as "sectoral harmonics" [10, 114].

The first case to be analyzed is Case 3. In Scenario 1, the near-circular, 30 degree inclined orbit, was evaluated by adding tesseral and sectoral harmonics up to J_2^2. A graph was created to show the value of the $\hat{Z}$-component of the inertial angular momentum versus time. The data collected from Matlab® was imported into Excel® and plotted for 2000 TU. Figure 4.4 shows that the constancy of the $\hat{Z}$-component of the inertial angular momentum decreases from order 10^{-14} as seen in Case 1 and order 10^{-13} as seen in Case 8 to a constancy on the order of approximately 10^{-5}. This is a huge reduction in constancy and is due solely to the non-symmetric nature of the tesseral and sectoral harmonics. It can be noted in Figure 4.4 that each time the object orbits the Earth there are periodic effects causing the $\hat{Z}$-component of the inertial angular momentum to vary equally over the same location of the Earth. It appears that the period of these cyclic variances is related to the period of the orbit.

The next case evaluated in this scenario is Case 5. This data was collected and analyzed in an identical fashion as the previous case, but instead of having the simple sinusoidal pattern as seen in Case 3, the variance in the geopotential is seen through different fluctuations in the value of the $\hat{Z}$-component of the inertial angular momentum but the constancy of this component remains at approximately 10^{-5}.

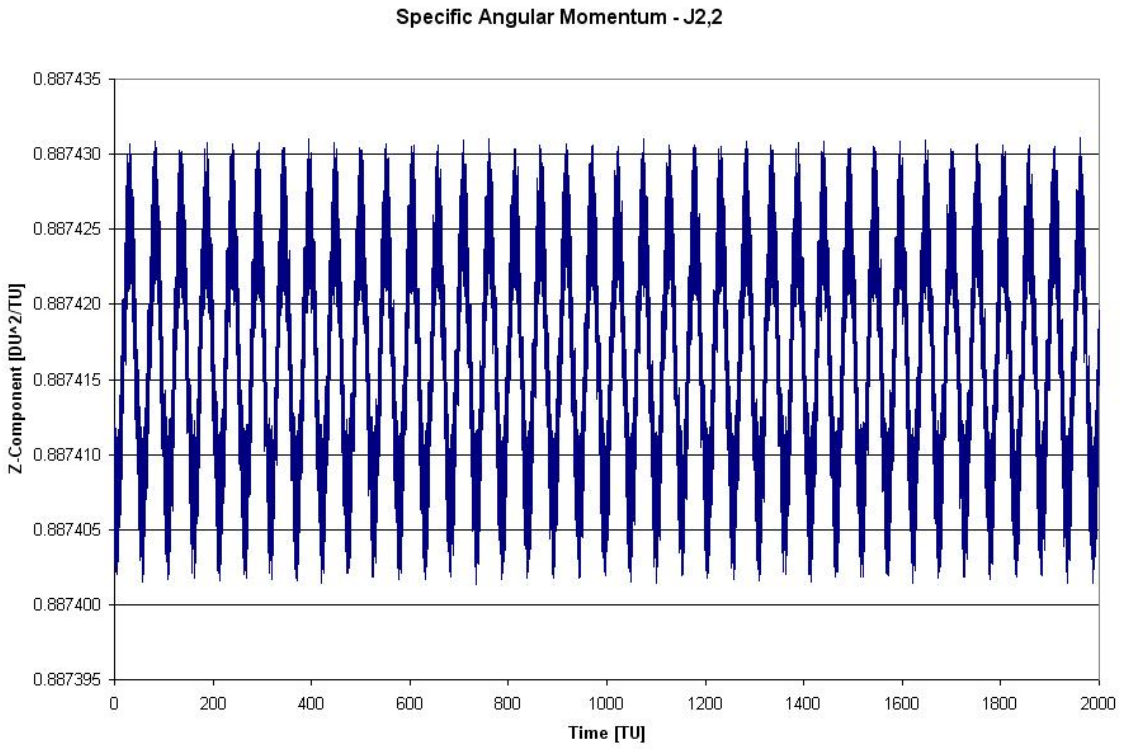

Figure 4.4: Scenario 1, Case 3: H_k versus time

Although there are more random-looking variations in this graph, the graph continues to be cyclic. However, the period of these variations appears to be two-times the period of the J_2^2 case. This implies that the repetition seen in the previous graph shows the variations run coincidentally with the half-period of the object's orbit and the repetition in Figure 4.5 is coincident with the period of the orbit.

The last case analyzed in Scenario 1 is the J_{21}^{21} case. The constancy of the $\hat{Z}$-component of the inertial angular momentum does not get any worse with the increased order of complexity in the geopotential. The higher order terms utilized in Cases 3, 5, 7 and 9 limit the constancy to approximately order 10^{-5} as is shown in Figures 4.4, 4.5 and 4.6. Additionally, the variations seen in Figure 4.6 run coincidentally with the variations in Figure 4.5 validating the assumption that the variations are coincident with the period of the orbit. Because including the tesseral and sectoral harmonics represent a more realistic geopotential for the Earth's gravitational field

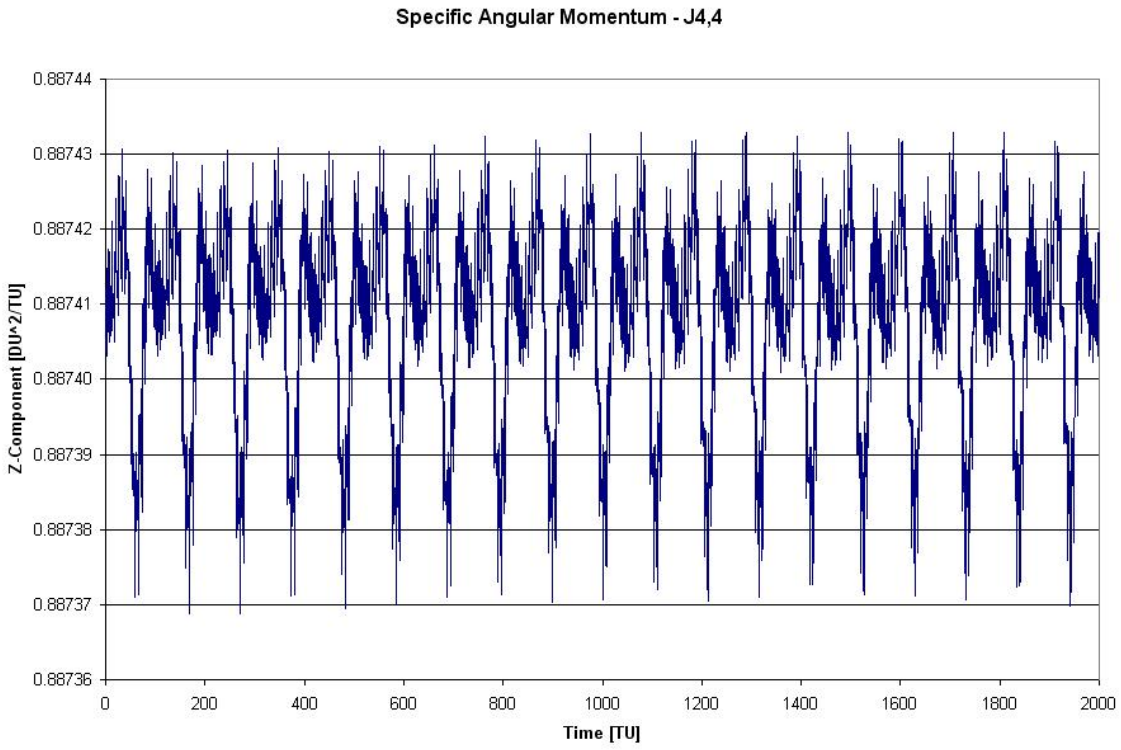

Figure 4.5: Scenario 1, Case 5: H_k versus time

than the spherical model or the symmetric model developed with the zonal harmonics only, 10^{-5} is the the level of constancy that can be expected from the $\hat{Z}$-component of inertial angular momentum. Graphs from Scenario 2 and the cases not cited in this section can be found in Appendix A.

In addition to graphing the results from the Matlab® program, the data was imported into Excel® and analyzed to find the maximum change in the $\hat{Z}$-component of the inertial angular momentum. In order to do this, within Excel®, a column was created to calculate the absolute value of the difference between $H_k(t) - H_k(t_0)$. Then utilizing the built-in function in Excel® maximum value in that column was determined. The results for all four scenarios and the nine cases in each scenario are summarized in Table 4.1.

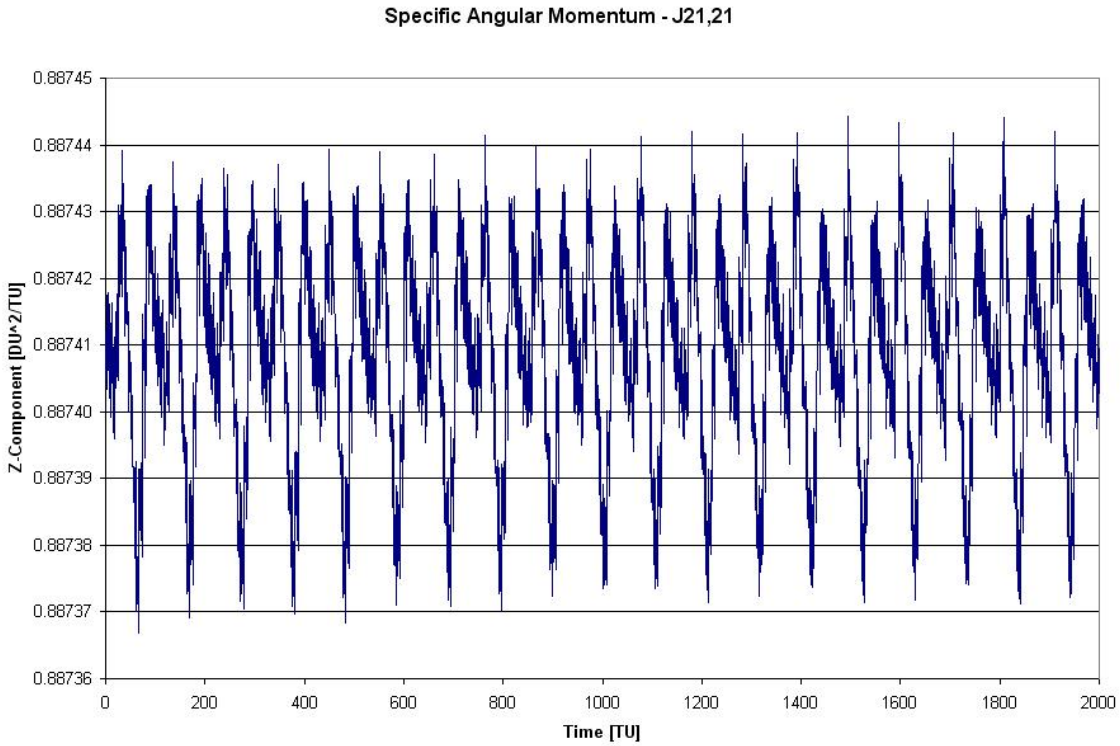

Figure 4.6: Scenario 1, Case 9: H_k versus time

	Scenario 1	**Scenario 2**	**Scenario 3**	**Scenario 4**
Case 1	2.74E-14	1.23E-13	3.88E-13*	3.01E-13
Case 2	2.81E-13	4.16E-13	1.65E-12	9.21E-13
Case 3	1.91E-05	2.81E-05	1.91E-05	2.81E-05
Case 4	4.64E-13	3.11E-13	3.91E-12	7.33E-13
Case 5	4.31E-05	2.84E-05	4.37E-05	2.85E-05
Case 6	3.74E-13	1.34E-13	1.12E-12	6.60 E-13
Case 7	4.50E-05	2.85E-05	4.63E-05	2.87E-05
Case 8	2.90E-13	1.13E-13	1.31E-12	2.63E-13
Case 9	4.48E-05	2.97E-05	4.54E-05	3.00E-05

Table 4.1: Inertial Angular Momentum Constancy Results

V. Right Ascension of the Ascending Node

5.1 Introduction

The third element analyzed for constancy is the time rate of change of the right ascension of the ascending node (RAAN) ($\dot{\Omega}$). Much research has been done on the effect of the Earth's oblateness term in the geopotential, J_2^0, and information can be found in several different books and papers. The author chose to use Dr. Wiesel's *Modern Astrodynamics* book as a reference on this topic. In the two-body problem, five of six COEs remain constant regardless of time, but as stated before, the introduction of the gravity geopotential limits the constancy of these elements. The effect on the right ascension of the ascending node (Ω) is the focus of this chapter. In his book, Dr. Wiesel addresses the rate at which the Node changes and gives an equation in the "Lagrange Planetary Equations Disturbing Function Form" [10, 98]:

$$\frac{d\Omega}{dt} = \frac{1}{na^2\sqrt{1-e^2}\,sin\,i}\frac{\partial R}{\partial i} \tag{5.1}$$

where n is the mean motion of the satellite, a is the semi-major axis, e is the eccentricity of the orbit and i is the inclination.

The equation for $\dot{\Omega}$ is not useful yet, so it is essential to determine the contributions that the J_2^0 term of the geopotential adds to this equation. Therefore, taking Equation 3.7 and letting $n = 2$ and $m = 0$ results in the following for the disturbing function:

$$R_2 = -\frac{\mu R_\oplus^2 J_2}{2r^3}\left(3\,cos^2\,\theta - 1\right) \tag{5.2}$$

In order to take the partial of the disturbing function $\frac{\partial R}{\partial i}$, the disturbing function through J_2^0 needs to be written in terms of the COEs [10, 137]. Dr. Wiesel's book contains the detailed derivation from the Lagrange Planetary Equation form to the COE form [10, 137-140]. Rewriting Equation 5.2 in terms of the classical orbital elements through order e^2, it can be shown that [10, 140]:

$$R_{2,sec} = -\frac{\mu R_\oplus^2 J_2}{2a^3}\left(\frac{3}{2}sin^2\,i - 1\right)\left(1 + \frac{3}{2}e^2\right) \tag{5.3}$$

Now taking the partial of the disturbing function in Equation 5.3 with respect to inclination as detailed in Equation 5.1 the following is an expression for the time rate of change of the node [10, 141]:

$$\dot{\Omega} = \frac{d\Omega}{dt} = -\frac{3nJ_2R_{\oplus}^2}{2a^2\left(1-e^2\right)^2}\,cos\,i \tag{5.4}$$

The results of deriving Equation 5.4 is that there exists a real value that can be calculated describing how Ω changes with respect to time. The result is based on the J_2^0 term in the geopotential and related to the other classical orbital elements. Although other equations exist applying the Brouwer-Lyddane method and incorporating J_2, J_3, J_4, J_5 and $(J_2)^2$ terms, Equation 5.4 is sufficient for this analysis [3]. Additionally, it is worth stating that the node will regress for prograde orbits, precess for retrograde orbits and is unchanging for the Molniya orbit. For this paper, the example scenarios are prograde orbits and the discussion pertains to prograde orbits.

5.2 Analyzing the Constancy of the Change in the RAAN

In order to determine the constancy in the time rate of change of the right ascension of the ascending node, the results created by Dr. Wiesel's obit propagator serve as inputs for another Matlab® program (See Appendix B). The same four scenarios were tested but Case 1 was not analyzed because in the two-body case Ω does not change, so the results from that case are meaningless. The remaining eight cases (Case 2 - Case 9) as stated in previous chapters were analyzed using the following initial conditions:

The initial conditions for Scenarios 1 and 3 are:

$$\vec{R}_{IJK} = \begin{pmatrix} 1.05 \\ 0.0 \\ 0.0 \end{pmatrix} [DU] \tag{5.5}$$

$$\vec{V}_{IJK} = \begin{pmatrix} 0.0 \\ 0.845154254 \\ 0.453464763 \end{pmatrix} \left[\frac{DU}{TU}\right] \tag{5.6}$$

The initial conditions for Scenarios 2 and 4 are:

$$\vec{R}_{IJK} = \begin{pmatrix} 0.0 \\ -1.15678606465 \\ 0.0 \end{pmatrix} [DU] \tag{5.7}$$

$$\vec{V}_{IJK} = \begin{pmatrix} 0.65744356375 \\ 0.0 \\ 0.65744356375 \end{pmatrix} \left[\frac{DU}{TU}\right] \tag{5.8}$$

The constancy of the time rate of change of the right ascension of the ascending node is evaluated by inputting the inertial position and velocity vectors calculated by Dr. Wiesel's orbit propagator into the Matlab® program which calculates the value of the right ascension of the ascending node at each time step. This is done by first calculating the Inertial Angular Momentum using Equation 4.1 and then calculating the line of nodes ($\vec{n}$) using the following equation [8, 118]:

$$\vec{n} = \hat{K} \times \vec{H}_{IJK} \tag{5.9}$$

Using the fact that the line of nodes lies in the Earth's equatorial plane we know the following to be true [9, 62]:

$$\hat{n} = \frac{\vec{n}}{\|\vec{n}\|} = cos\,\Omega\hat{I} + sin\,\Omega\hat{J} \tag{5.10}$$

Applying Equation 5.10 it is possible to solve for Ω using the following equation:

$$\Omega = cos^{-1}\frac{n_I}{|\vec{n}|} \tag{5.11}$$

The final step in the calculation of Ω is to do a quadrant check and then verify that the data falls in a good range, where $0 \leq \Omega \leq 2\pi$.

The Matlab® program calculates Ω for each time step and outputs the data in a format easily imported into Excel®. Once the data is imported into Excel®, a graph summarizing the data was created. The first case analyzed is Scenario 1 Case 2, which includes the geopotential expansion through the J_2^0 term.

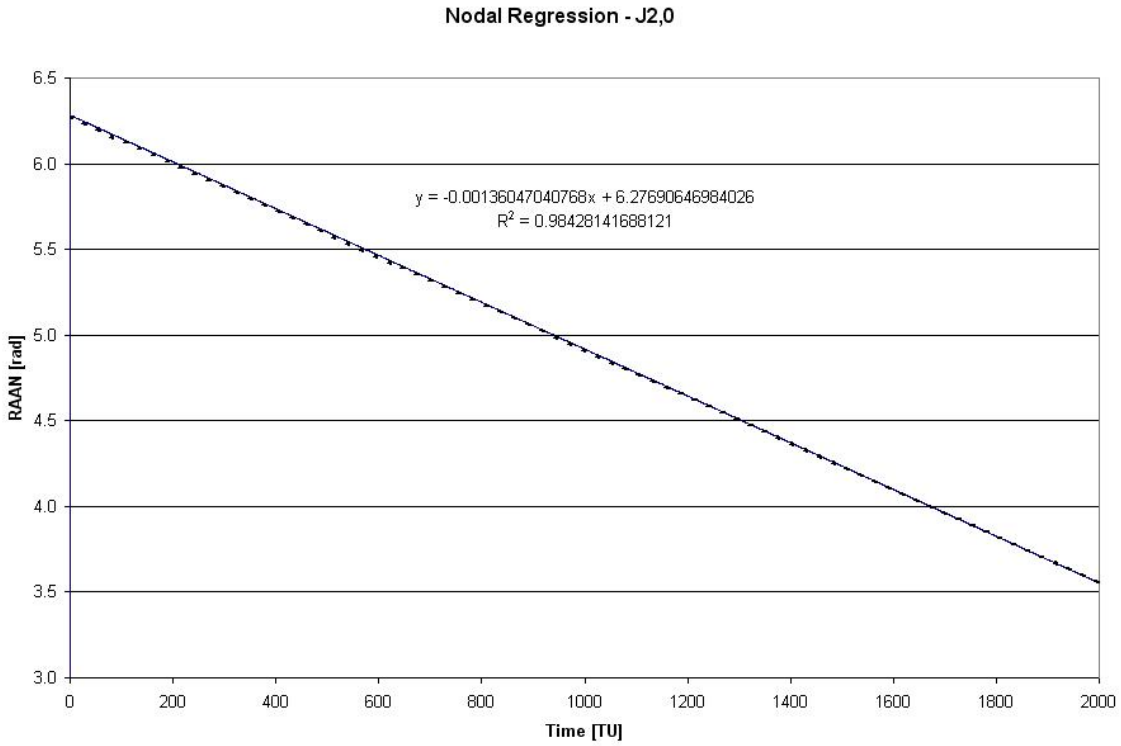

Figure 5.1: Scenario 1, Case 2: $\dot{\Omega}$ versus time

Figure 5.1 shows that the time rate of change of the RAAN is very close to being linear with time. To emphasize this point, a best-fit trendline is plot over the data. The trendline is the black dotted line spanning the plotted data. The equation and the value for R^2, defined as "the fraction of the total squared error that is explained by the model", are also noted on the plot [4]. The R^2 value is close to 1, showing how close to linear $\dot{\Omega}$ is with respect to time and giving a sense of the level of predictability for this data. Additionally, the slope of the line is the value determined by Equation

5.4. In order to determine if using the change in the right ascension of the ascending node produced by the geopotential expansion through the J_2^0 term is appropriate, the slope from Case 2 will be compared with the slopes from the remaining cases in this scenario.

The next case analyzed is Case 3, which includes zonal, tesseral and sectoral harmonics in the geopotential expansion through J_2^2. This case allows us to see the differences brought about by including the tesseral and sectoral harmonics in the geopotential expansion. Figure 5.2 shows a nearly identical regression of the node

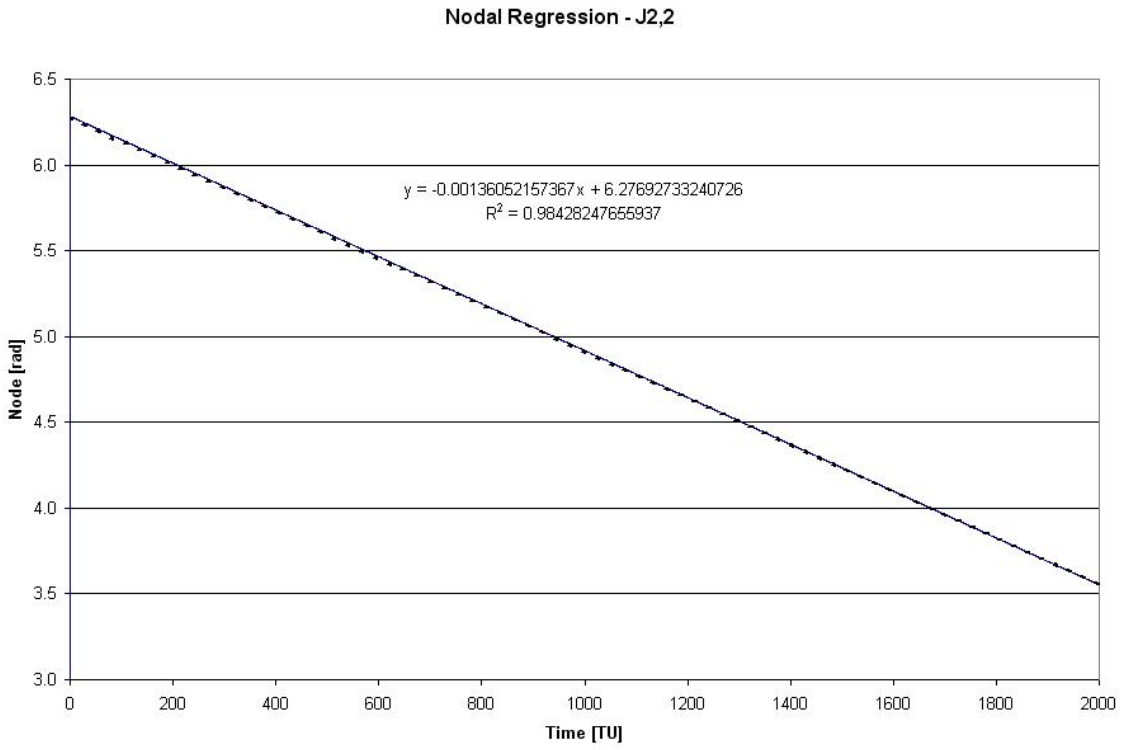

Figure 5.2: Scenario 1, Case 3: $\dot{\Omega}$ versus time

with respect to time. The slope of the equation defining the time rate of change of RAAN is constant to approximately order 10^{-8}, but because the value is of order 10^{-3} the result is constancy to five significant figures. Adding a few tesseral and sectoral harmonics to the geopotential did not seem to affect the linearity of $\dot{\Omega}$ as shown in the R^2 term. From the change in the slope, the effect these first tesseral and sectoral

harmonic terms have on the time rate of change of RAAN is approximately order 10^{-6}. This implies that through the J_2^2 term in the expansion, the J_2^0 derived time rate of change of RAAN is an adequate estimation. It is also interesting to note that the R^2 term actually increased slightly showing that this case is more linear than Case 2.

Noting the minimal difference in the slope from Case 2 to Case 3, analysis continued with the next case evaluated being Case 4. Case 4 includes terms through J_4^0 in the geopotential expansion. This case gives an idea of how well the J_2^0 case does with the inclusion of more zonal, tesseral and sectoral harmonics in the geopotential expansion. Figure 5.3 shows a familiar graph to the first two but this time the

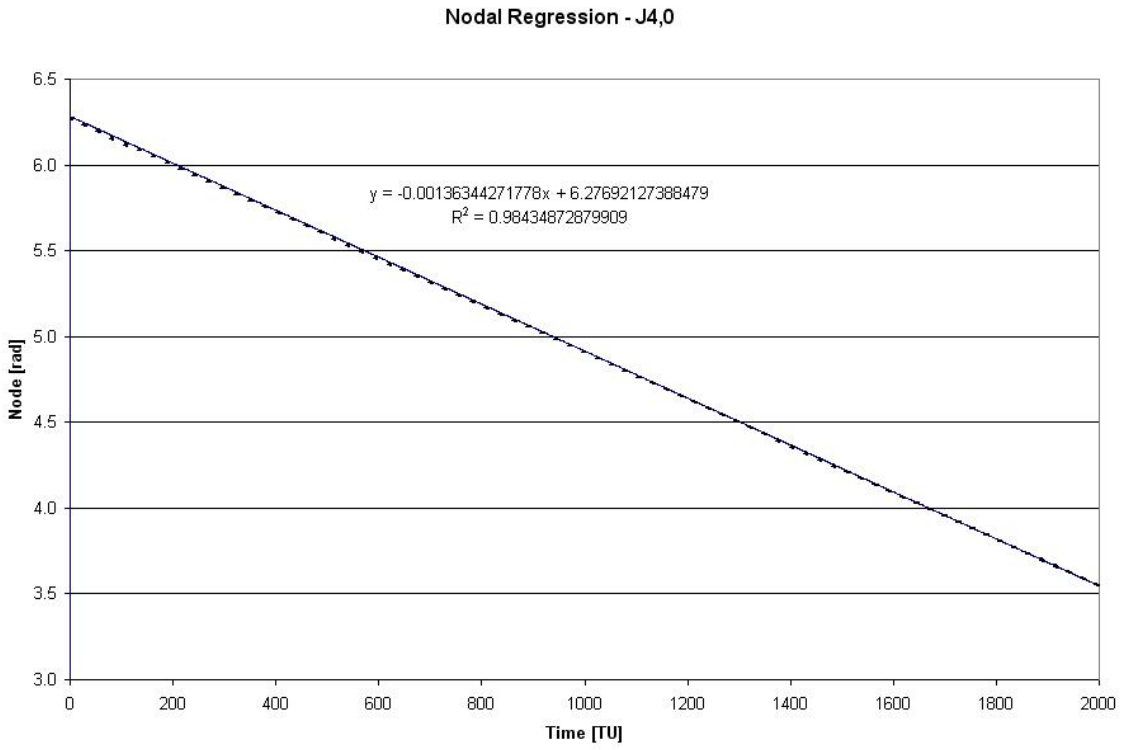

Figure 5.3: Scenario 1, Case 4: $\dot{\Omega}$ versus time

precision of the slope in the best-fit equation reduces to approximately order 10^{-6}. As discussed above, because the original value is of order 10^{-3} the result is accuracy to three significant figures. Once again, it is interesting to note that the R^2 value slightly

increased getting even closer to 1. So although the accuracy of the J_2^0 assumption is decreased to three significant figures, the results are showing a more linear regression in the node.

The final case analyzed is Case 9. This includes the full expansion of the geopotential through the J_{21}^{21} term. Despite the significant increase in terms added, the slope of the best-fit line stayed at approximately order 10^{-6}. This result shows that there is no impact on the plausibility of using the J_2^0 assumption. The significant variance came from adding terms through J_4^0. Any further expansion of the geopotential has little to no effect on the accuracy of this assumption. Additionally, the R^2 value increased slightly showing that for this orbit and cases evaluated, Case 9 is the most linear case.

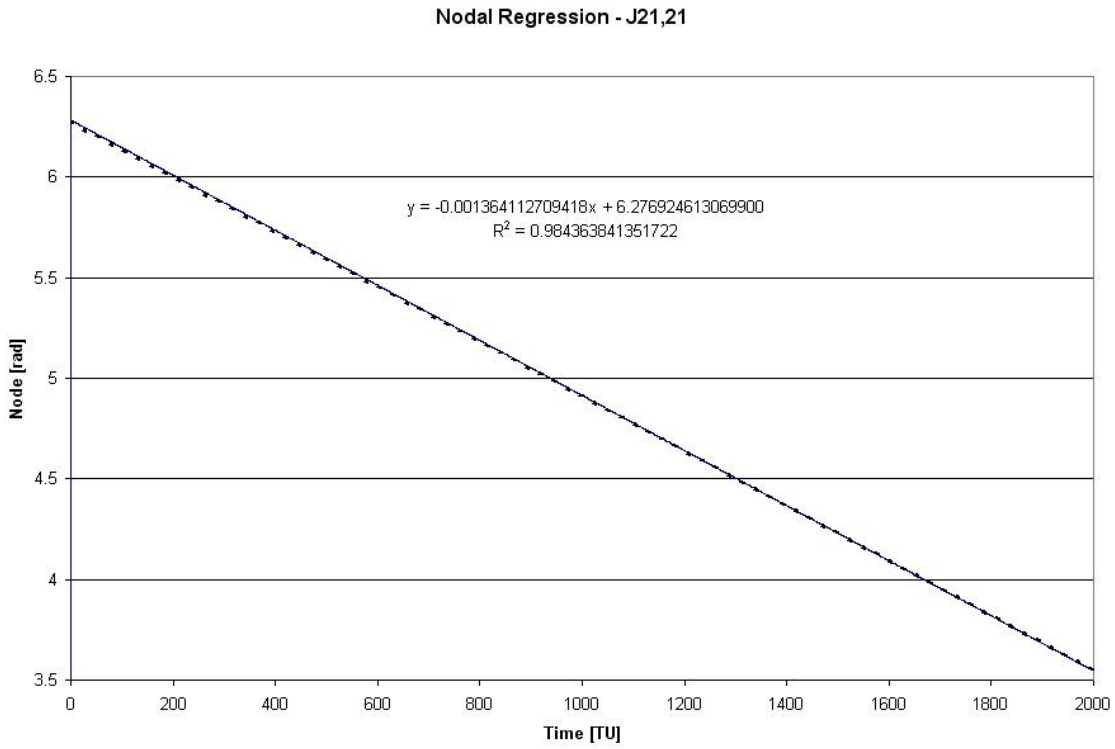

Figure 5.4: Scenario 1, Case 9: $\dot{\Omega}$ versus time

Although there is not a full description of all the scenarios and cases in this chapter, a summary of the information gathered for each case was created. In order

to analyze the data, all the data was imported into Excel® and a plot was created. On each one of the graphs there is a best-fit trendline and the R^2 value annotated. Tables 5.1 and 5.2 show a summary of the results for all relevant cases in Scenarios 1 and 2 respectively. Additionally, figures are available in Appendix A for Scenario 2 and the cases not specifically addressed in this chapter.

Scenario 1		
	Best-Fit Trendline	**R^2**
Case 2	-0.00136047040768t + 6.27690646984026	0.984281416881
Case 3	-0.00136052157367t + 6.27692733240726	0.984282476559
Case 4	-0.00136344271778t + 6.27692127388479	0.984348728799
Case 5	-0.00136349596607t + 6.27695859934003	0.984349746613
Case 6	-0.00136394677915t + 6.27691182676157	0.984360161509
Case 7	-0.00136398333024t + 6.27692569650047	0.984360916666
Case 8	-0.00136408012100t + 6.27690812910590	0.984363189205
Case 9	-0.00136411270942t + 6.27692461306990	0.984363841352

Table 5.1: Scenario 1, $\dot{\Omega}$ Results

Scenario 2		
	Best-Fit Trendline	**R^2**
Case 2	-0.00069216082930t + 4.71238962787044	0.999999421426
Case 3	-0.00069213563793t + 4.71237847388094	0.999999420218
Case 4	-0.00069240615521t + 4.71239121808520	0.999999422356
Case 5	-0.00069237544806t + 4.71235911459945	0.999999419109
Case 6	-0.00069220307448t + 4.71239091720158	0.999999422679
Case 7	-0.00069216655269t + 4.71236023876455	0.999999419493
Case 8	-0.00069215279270t + 4.71239087276285	0.999999422789
Case 9	-0.00069211664459t + 4.71235730338259	0.999999419370

Table 5.2: Scenario 2, $\dot{\Omega}$ Results

VI. Data Accuracy

6.1 Introduction

Now that a constancy level for $\mathcal{H}$, H_k, and $\dot{\Omega}$ has been evaluated, it is necessary to investigate the levels of accuracy for these constants attainable using different sensors. There are a few different types of sensors being used currently to track satellites and other objects orbiting the Earth. The most popular in this application are optical, radar and laser instruments. Different types of sensors have varying limitations based on the technology and quality of equipment installed in the sensor. Vallado provides a table with limitations and biases of United States owned sensors, but for simplicity the author will evaluate generalized cases with no ties to current sensors to get an idea of how different parameters affect the quality of the acquired data [8, 245].

In order to investigate the levels of accuracy obtainable by different sensors, position and velocity data will be simulated. The data will be simulated using a simple dynamics model and the amount of error introduced into the data based on observation quality and quantity will be determined. Then the simulated data and observed data will be propagated using the full geopotential through the J_{21}^{21} term to determine the correlation with observation accuracy and the accuracy attainable for the Hamiltonian Function, $\hat{Z}$-component of inertial angular momentum and the time rate of change of the right ascension of the ascending node. Finally, the constancy in $\mathcal{H}$, H_k and $\dot{\Omega}$ attainable utilizing the simulated data will be compared with previously determined constancies for $\mathcal{H}$, H_k and $\dot{\Omega}$ to establish the basis for a supplemental model that can be used as a tool for data mining.

6.2 Simulating R and V Data

In order to determine the quality of data produced by a specific sensor, a simplified least squares estimator was written in Matlab®. The first thing required in the program is to produce data to observe. Since this is a simplified estimator, a *flat-Earth* model was selected to represent the data. The data was created using basic

physics kinematic equations, assuming a constant acceleration:

$$\vec{R}(t) = \vec{R}_0 + \vec{V}_0 t + \frac{1}{2}\vec{g}t^2 \tag{6.1}$$

$$\vec{V}(t) = \vec{V}_0 + \vec{g}t \tag{6.2}$$

where $\vec{R}$ is the position vector and $\vec{V}$ is the velocity vector at a given time. The subscript "$_0$" indicates the initial value where $t = 0$, and $\vec{g}$ is the acceleration due to gravity. For this model, the assumed value of $\vec{g}$ is the local gravity at the surface of the Earth or 9.81 $\frac{m}{s^2}$ toward the center of the Earth. Using Equation 6.1, and inputting the following initial conditions:

$$\vec{R}_0 = \begin{pmatrix} 6697043.85 \\ 0 \\ 0 \end{pmatrix} [m] \tag{6.3}$$

$$\vec{V}_0 = \begin{pmatrix} 0 \\ 6538.656905 \\ 3600.9857675 \end{pmatrix} \left[\frac{m}{s}\right] \tag{6.4}$$

Simulated data was produced for a ten minute interval. A time interval of ten minutes was selected because that is an approximate in-view time for a satellite being tracked by a scanning sensor on Earth. The time step, Δt, is varied from 0.01 s to 60 s and is used to identify the impact that the time step has on obtaining a good estimate, which will be addressed later. Now in order to make this data look more like actual data, noise was incorporated into the data. Matlab® has a built in function that creates random numbers. The random number was then multiplied by the value *sigma*, which represents the order of magnitude of the noise in the data, and subsequently added to the simulated data. This creates more realistic data which is then incorporated into least squares as z_d, the observed data.

Although the dynamics model is not linear, using the observed data, it is possible to run linear least squares to get an approximate initial state as input into the non-linear least squares problem. This step is not mandatory, an approximate initial state, or an educated guess, would be sufficient input into the non-linear least squares problem, but the author chose to get an estimate through the linear least squares method. Linear least squares attempts to estimate "the state of a linear dynamical system at *epoch* time" [11, 67]. The initial state is given by:

$$X_0 = \begin{pmatrix} \vec{R}_0 \\ \vec{V}_0 \end{pmatrix} \tag{6.5}$$

There is a detailed process by which the following equations are derived in Dr. Wiesel's *Modern Orbit Determination* book but these derivations will not be discussed in this paper [11, 67-70]. The first step in solving for the initial state using linear least squares is to find the "state transition matrix" (Φ) [11, 32]. The state transition matrix is the term that transitions the state from one time to a different time and can be calculated using the following equation:

$$\Phi\left(t, t_0\right) = \frac{\partial X(t)}{\partial X(t_0)} \tag{6.6}$$

Applying Equations 6.1 and 6.2 the state as a function of time is given by:

$$X(t) = \begin{pmatrix} x_0 + \dot{x}_0\, t \\ y_0 + \dot{y}_0\, t \\ z_0 + \dot{z}_0\, t + \frac{1}{2}\, g\, t^2 \\ \dot{x}_0 \\ \dot{y}_0 \\ \dot{z}_0 + g\, t \end{pmatrix} \tag{6.7}$$

Taking the partial derivatives in Equation 6.6 gives a state transition matrix as follows:

$$\Phi\left(t, t_0\right) = \begin{pmatrix} 1 & 0 & 0 & t & 0 & 0 \\ 0 & 1 & 0 & 0 & t & 0 \\ 0 & 0 & 1 & 0 & 0 & t \\ 0 & 0 & 0 & 1 & 0 & 0 \\ 0 & 0 & 0 & 0 & 1 & 0 \\ 0 & 0 & 0 & 0 & 0 & 1 \end{pmatrix} \tag{6.8}$$

The next step is to define a matrix, the "observation relation", $G(t)$ that predicts the data $z_d(t)$ [11, 75]. The assumption is that observation data is the inertial position vector. Therefore, $G(t)$ is given by the following equation:

$$G(t) = \begin{pmatrix} x(t) \\ y(t) \\ z(t) \end{pmatrix} \tag{6.9}$$

Additionally, the H matrix is the linearization of the observation relation and can be found in the following manner [11, 76]:

$$H = \frac{\partial G(t)}{\partial X(t)} \tag{6.10}$$

taking the partial derivative results in the following for the H matrix:

$$H = \begin{pmatrix} 1 & 0 & 0 & 0 & 0 & 0 \\ 0 & 1 & 0 & 0 & 0 & 0 \\ 0 & 0 & 1 & 0 & 0 & 0 \end{pmatrix} \tag{6.11}$$

Now, for short-hand, we will define the T matrix, also referred to as the "observation matrix" [11, 67]:

$$T(t) = H \;\; \Phi(t, t_0) \tag{6.12}$$

Then, it is possible to define the "instrumental covariance matrix" Q as equal to $sigma^2$, where *sigma* is the order of magnitude of the noise in the data due to the quality of the instrument [11, 68]. At this point, applying the previous equations makes it possible to solve for the "state covariance" (P_X) defined by the following equation [11, 70]:

$$P_X = \left(\sum_{i=1}^{N} T_i^T Q_i^{-1} T_i \right)^{-1} \tag{6.13}$$

The covariance is calculated by first running a *for* loop for the summation and then taking the inverse. The final step in linear least squares is to calculate the initial state and it is determined by the following equation [11, 70]:

$$X_0 = P_X \sum_{i=1}^{N} T_i^T Q_i^{-1} z_i \tag{6.14}$$

Once again making sure that the summation is accomplished in the afore mentioned *for* loop.

Now an initial guess for the state at epoch time has been obtained and will be applied as an input to the non-linear least squares estimator. Although making an educated guess would make it possible to skip the above process, the afore mentioned process provides a methodical technique for obtaining an estimate and introduces many of the terms used in non-linear least squares. Now with this estimate for the initial state, an update of the state is required and can be found using the following equation:

$$X(t) = \Phi(t, t_0)\, X_{ref}(t_0) + X_p \tag{6.15}$$

where $X_{ref}(t_0)$ is the estimate calculated in the previous step with the notation updated to avoid future confusion and the state transition matrix is the same as defined in Equation 6.8. The X_p is a particular solution that is added to the state to account

for the non-linear terms and it is defined below:

$$X_p = \begin{pmatrix} 0 \\ 0 \\ \frac{1}{2} g\, t^2 \\ 0 \\ 0 \\ g\, t \end{pmatrix} \tag{6.16}$$

Since the non-linear terms are taken care of by adding a particular solution every time the state is updated, the remainder of the problem can be treated as a linear problem [11, 82-83]. The next step is to calculate observation relation, the G matrix, as defined in Equation 6.9. The easiest way to do this is to multiply the H matrix by the updated state which leaves the estimated position vector. Then calculating the "residual vector" ($\vec{r}$) is accomplished using the relationship between the observed data and the observation relation matrix [11, 77]:

$$\vec{r}(t) = z_d(t) - G(t) \tag{6.17}$$

Now using Equation 6.12 the T matrix is calculated and it is used to calculate the change in the covariance matrix $P_{\delta X}$ as defined in Equation 6.18 [11, 77]:

$$P_{\delta X} = \left(T^T\, Q^{-1}\, T\right)^{-1} \tag{6.18}$$

Then the change required to be made to the initial state estimate is calculated to account for the non-linear terms over-looked in the original estimate:

$$\delta X_0 = P_{\delta X}\, T^T\, Q^{-1}\, \vec{r} \tag{6.19}$$

A new initial state is then calculated using the following equation:

$$X_0 = X_{ref}(t_0) + \delta X_0 \tag{6.20}$$

Now because the covariance and the change to the initial state needs to be calculated for every Δt, a summation is calculated, similar to what was done in the linear case, to determine the total values of $P_{\delta X}$ and $T^T Q^{-1} \vec{r}$ as defined in Equations 6.18 and 6.19. Finally, because it is possible to gain access to the actual initial state, the error can be calculated by subtracting the initial state determined through least squares from the initial state used in creating the simulated data (Equations 6.3 and 6.4). The absolute value of the difference between these terms is output by Matlab® for each of the position and velocity components as well as the magnitude of these vectors (see code in Appendix B). In order to validate the computer program, the noise was not included with the data and executing the Matlab® program the following results for the error were obtained:

Position error is: 0.000000000000e+000
x-direction 0.000000000000e+000
y-direction 4.758828049570e-012
z-direction 6.984919309616e-010
Velocity error is: 0.000000000000e+000
x-direction 7.185018701990e-015
y-direction 0.000000000000e+000
z-direction 4.547473508865e-013

Just for note, the program was run with Δt equal to 1 s and *sigma* equal to 1 m. The results from this run of the program show that the error between the calculated initial state and the initial state input into the program to simulate the data is zero. This validates that the program is working as expected. Now that a computer program has been written to simulate the data, analysis will be done to identify the correlation

between observation quality and quantity and the error in the position and velocity vectors.

6.3 Quantifying the Data

Utilizing the computer code for the least squares estimator written in Matlab®, there are two different input values that were altered to assess the impact on the quality of the estimate for the initial state obtainable. The first parameter altered is the noise level in the data and it is based on the quality of the sensor being used, defined by the instrumental covariance matrix. In order to test the impact that this parameter has on the quality of the data, values from 0.1 m to 1000 m as the *sigma* in increments of 0.1 m were input into the program. The second parameter altered is the time step, Δt. For each increment in *sigma* and for a given Δt, the program outputs the absolute value of the error between the scalar value of the estimated position and velocity vector and the initial position and velocity vector inserted to create the data. In this analysis, time steps varying from 0.05 s up to 60 s were implemented. Below, Figure 6.1 shows the error in position versus *sigma* for the shortest time step.

In this analysis, each time step was plotted on a separate graph to show how position error changes with respect to the accuracies of the sensor for a specific time step. The first case where the time step is very small, the position error grows linear with respect to *sigma*. A trendline is plotted over the data and the best-fit equation is shown on the graph along with the R^2 term. The equation shows that with an R^2 value of 0.9995, the position error is approximately one-half of the *sigma* value. This trend continues for each time step evaluated, but the R^2 value continually decreases for each increase in the time step. The decrease in the R^2 value implies that the data is more scattered providing data with higher variances from the trendline. For comparison, the position error versus *sigma* for the final time step, where Δt is equal to 60 seconds, was plotted. Once again, Figure 6.2 shows that the trend for the data is found to be at approximately one-half of the input *sigma* value. However, because the R^2 term is much lower than it was in Figure 6.1 there are more data

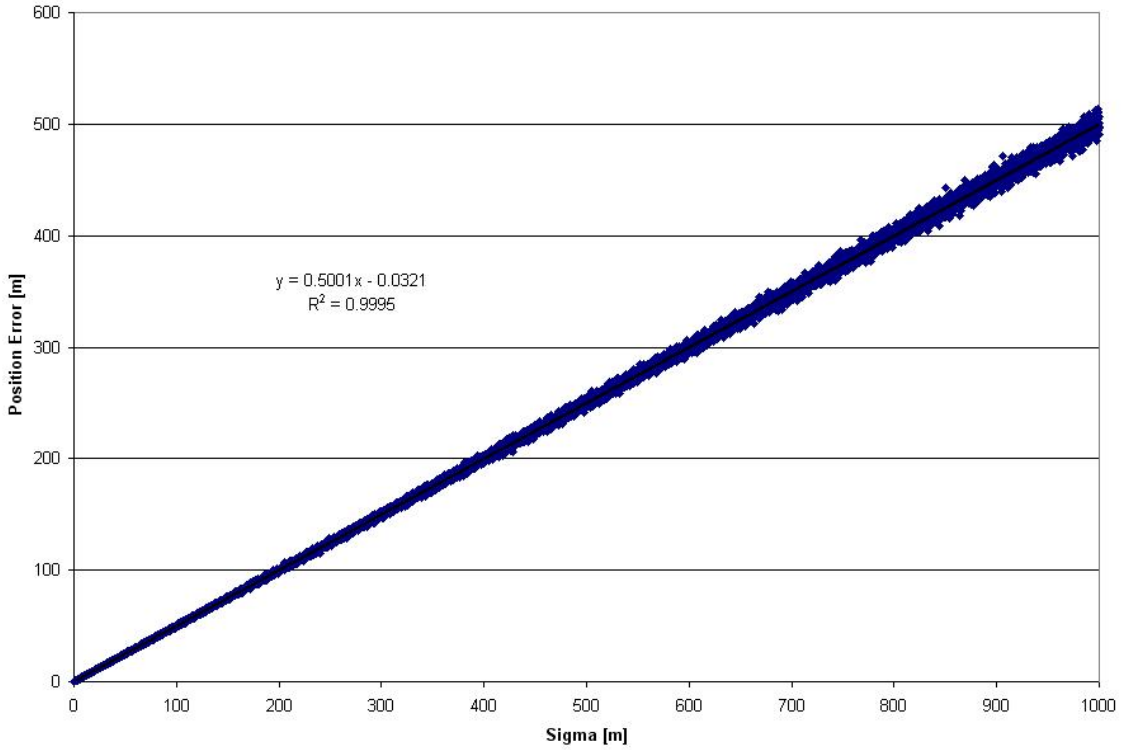

Figure 6.1: Initial Position Error vs Sigma for $\Delta t = 0.05s$

points nearing the *sigma* value. Additionally, an analysis was done to calculate the best-fit trendline and the R^2 value for each time step and the results for all the cases are summarized in Table 6.1. The graphs for time steps not explicitly discussed in this section are available in Appendix A. The significance of this analysis is that for

Time (s)	Best-Fit Trendline	R^2
0.05	0.5001x - 0.0321	0.9995
0.1	0.4999x + 0.0269	0.9991
0.5	0.5003x - 0.0911	0.9957
1	0.4996x + 0.1348	0.9911
5	0.5003x + 0.0737	0.9571
30	0.4962x + 0.6413	0.8071
60	0.4984x + 0.5105	0.7078

Table 6.1: Initial Position Error Results

this simplified model of the dynamics, the mean value of the data is on the order of one-half *sigma*. This means that for a *sigma* value of one meter, the error in position

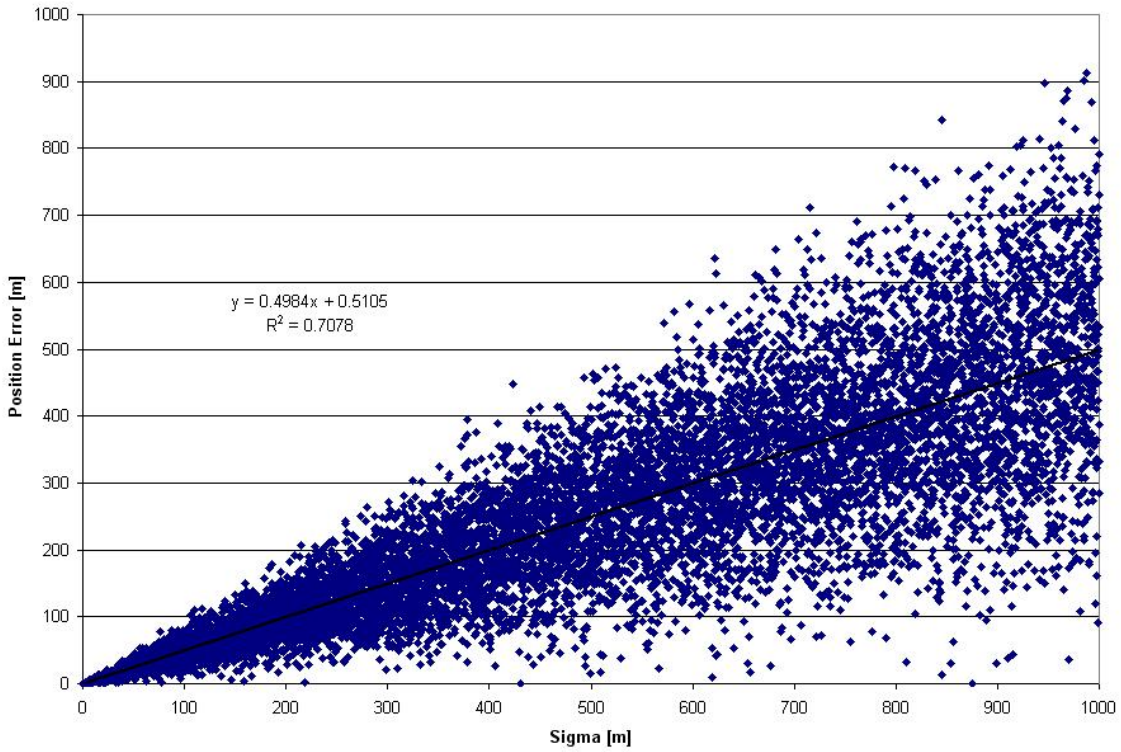

Figure 6.2: Initial Position Error vs Sigma for $\Delta t = 60s$

is approximately 0.5 m. Now, because position is on the order of 10^6 m, an error of 0.5 m provides an accuracy in position to seven significant figures or order 10^{-8}. As the time step increases, the R^2 value decreases resulting in larger variances from the best-fit trendline. However, for further analysis, the values as they appear on the best-fit trendline will be used as a basis for the accuracy level. Therefore, the range of accuracies in the position vector for all time steps goes from eight significant figures for *sigma* equal to 0.1 m down to four significant figures for *sigma* equal to 1000 m. Keep in mind though, that as the time step increases the probability that the error will fall on or near the best-fit line decreases, as evident through the R^2 term. At a time step of 60 seconds this could increase the error to the order of the *sigma* value, which would give a range of accuracy from seven to three significant figures. The accuracies obtainable using the mean value (value obtained from the trendline) will

be used in the following section to determine the impact this error has on $\mathcal{H}$, H_k and $\dot{\Omega}$.

In addition to position error, analysis was completed to determine the error in the velocity vector. Similarly to what was done for position, the absolute value of the error between the least squares calculated velocity and the original velocity vector used to create the simulated data was calculated. However, a slight modification to the process for collecting data to determine the mean value is made and approximately 100 data points for every magnitude increase in *sigma* will be evaluated. Then, as before, the time step is varied from 0.05 s to 60 s and the error is plotted for each time step. In order to best show the changes in error as *sigma* increases, the data is plotted on a logarithmic plot. Figure 6.3 shows the first time step analyzed.

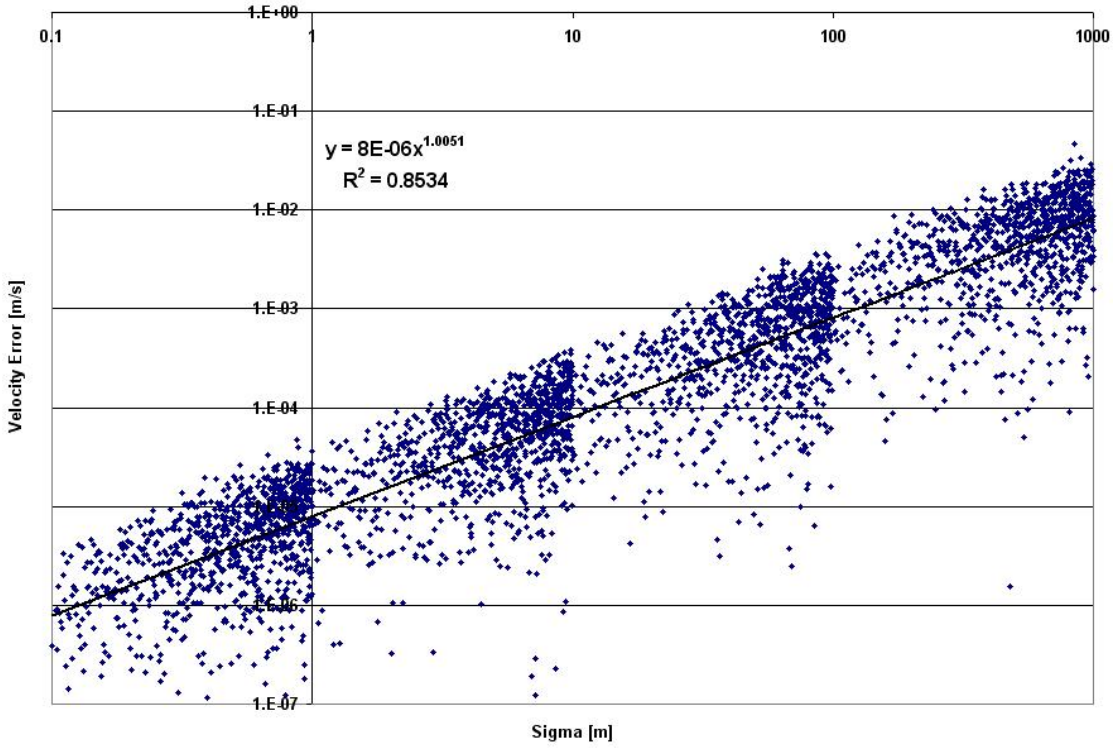

Figure 6.3: Initial Velocity Error vs Sigma for $\Delta t = 0.05s$

Unfortunately, the plot of initial velocity error versus *sigma* does not give us a strictly linear relation; therefore, a power law equation was fit to the data. Although

the R^2 term is not extremely high, the power law fit provides a nice mean value to be used in determining the accuracy attainable in the velocity. Using the power law fit equation plotted in Figure 6.3, it can be shown that the velocity error ranges from order 10^{-7} $\frac{m}{s}$ at *sigma* equal to 0.1 m up to order 10^{-3} $\frac{m}{s}$ where *sigma* is equal to 1000 m. Because the velocity is on the order of 10^{3} $\frac{m}{s}$, accuracies for velocity range from ten to six significant figures. Similar to the position error, the average velocity error increases approximately one order of magnitude for every order of magnitude increase for *sigma*. However, unlike the position error the velocity error changes with respect to the Δt term. Using a time step of two times the first, $t = 0.1$ s, results in an order of magnitude increase in the velocity error for all *sigma* values. Figure 6.4 shows this

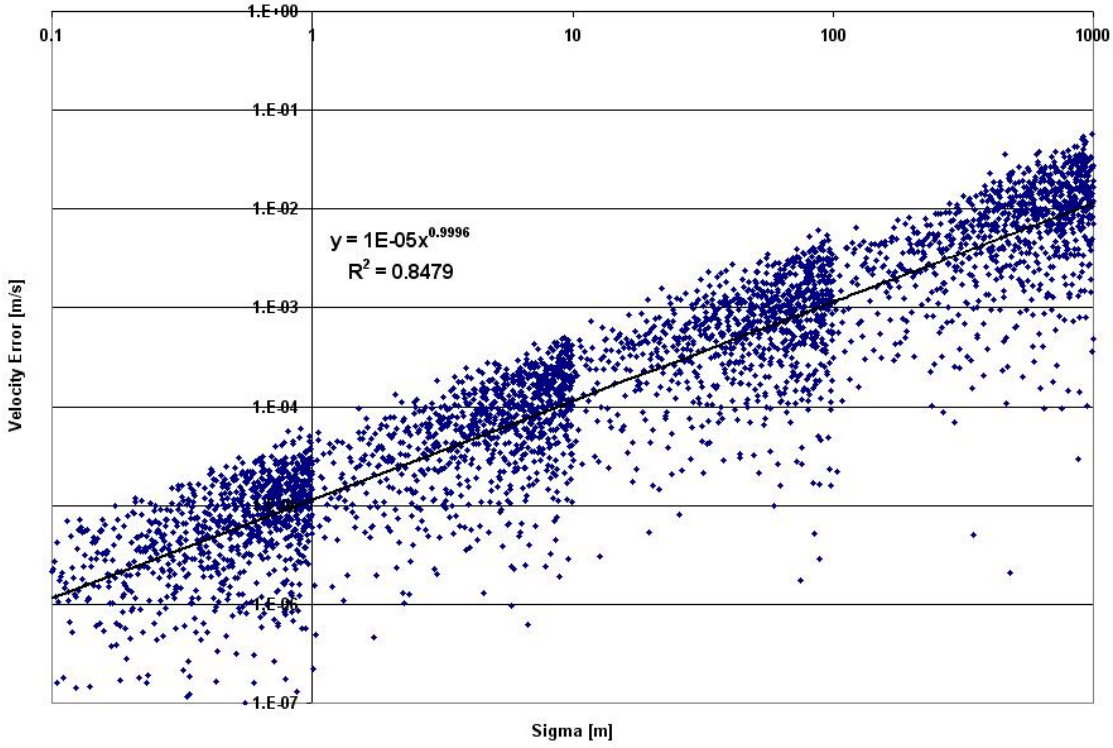

Figure 6.4: Initial Velocity Error vs Sigma for $\Delta t = 0.1s$

increase in the velocity error and the power law fit equation can be used to calculate the average velocity error for this time step. The velocity error starts at order 10^{-6} $\frac{m}{s}$ for a *sigma* value of 0.1 m and increases to order 10^{-2} $\frac{m}{s}$ for *sigma* equal to 1000

m. The basic structure of the plot remains the same showing power dependence on *sigma*. The order of magnitude error in velocity seen at a time step of 0.1 s is the same for Δt values of 0.5, 1, and 5 seconds. The plots for each of these cases will not be shown here but are included in Appendix A. The velocity error increases again by an order of magnitude for the 30 and 60 second time steps.

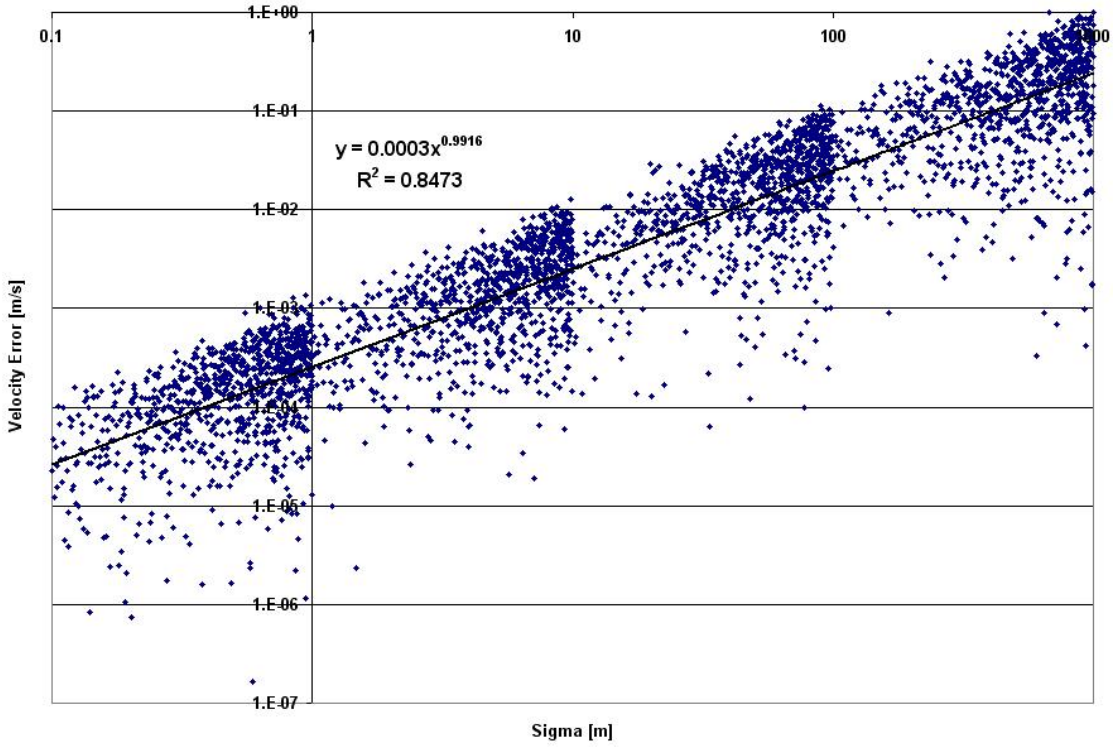

Figure 6.5: Initial Velocity Error vs Sigma for $\Delta t = 60s$

Figure 6.5 shows the initial velocity error determined using least squares with a time step of 60 seconds. As mentioned previously, the error for this time step is one order of magnitude higher for all values of *sigma* as compared with Δt equal to 0.1 s and two orders of magnitude higher than Δt equal to 0.05 s. The power law fit equation for this data was used to calculate the range of velocity error expected for *sigma* values from 0.1 to 1000 meters. The mean value of the initial velocity error is calculated to be of order 10^{-5} $\frac{m}{s}$ at the lowest *sigma* value, and increases to order 10^{-1} $\frac{m}{s}$ at the highest *sigma* value. Although the graph for the 30 second time step

is not included in this section, it is included in Appendix A. Additionally, the power law fit equation and R^2 values for each of the time steps analyzed are summarized in Table 6.2.

Time (s)	Power Law Fit Equation	R^2
0.05	$0.00000793x^{1.00506942}$	0.85337492
0.1	$0.00001147x^{0.99959821}$	0.84789666
0.5	$0.00002480x^{1.00269564}$	0.85068946
1	$0.00003516x^{1.00350272}$	0.84703331
5	$0.00007833x^{1.00023009}$	0.84223989
30	$0.00018685x^{0.99491486}$	0.85111477
60	$0.00025541x^{0.99164799}$	0.84730417

Table 6.2: Initial Velocity Error Results

Now, with the initial position and velocity errors created through the simplified least squares estimator, it is possible to use the average error calculated from the best-fit trendline and power law fit equation to estimate the impact these errors have on $\mathcal{H}$, H_k and $\dot{\Omega}$.

6.4 Impact on the Constants

In order to assess the impact of the initial position and velocity error on $\mathcal{H}$, H_k and $\dot{\Omega}$, the initial position and velocity vectors (Equations 6.3 and 6.4) used as inputs to create the data were converted to canonical units and input into Dr. Wiesel's orbit propagator using the full geopotential expansion through the J_{21}^{21} term. In a similar fashion as discussed in each of the previous chapters, the output position and velocity vectors from the propagator were used to calculate the expected $\mathcal{H}$, H_k and $\dot{\Omega}$ values to use as a baseline. Then importing the data into Excel®, baseline values for $\mathcal{H}$, H_k and $\dot{\Omega}$ were included in separate spreadsheets. Next, the position and velocity vectors calculated using the Matlab® least squares estimator, with errors approximately equal to the value defined by the associated trendlines (see Tables 6.1 and 6.2), were propagated using Dr. Wiesel's orbit propagator incorporating the full geopotential expansion through the J_{21}^{21} term. Then using the output files, $\mathcal{H}$, H_k

and $\dot{\Omega}$ values associated with these initial conditions were calculated using Matlab®. Since the author is interested in the error caused in these three constants as a result of the error in the initial position and velocity vectors, the new values for $\mathcal{H}$, H_k and $\dot{\Omega}$ were input into the respective Excel® spreadsheets and the maximum difference between these values and the baseline values for each constant over the ten minute time interval was calculated. Analysis for all time steps was completed to include the minimum and maximum values for *sigma* mentioned previously. Tables 6.3 through 6.5 show the results for maximum error calculated during the propagation time for the Hamiltonian Function, $\hat{Z}$-component of inertial angular momentum and the time rate of change of the right ascension of the ascending node.

	0.1 m	1000 m
0.05 s	6.76150E-09	6.62014E-05
0.1 s	6.85740E-09	6.81668E-05
0.5 s	6.85740E-09	7.33783E-05
1 s	6.48999E-09	6.87841E-05
5 s	6.93561E-09	5.31149E-05
30 s	9.34998E-09	5.54704E-05
60 s	1.16882E-08	8.75611E-05

Table 6.3: Hamiltonian Function Impacts

	0.1 m	1000 m
0.05 s	9.21223E-09	8.07959E-05
0.1 s	9.04901E-09	8.33492E-05
0.5 s	9.04901E-09	8.59880E-05
1 s	8.22583E-09	8.38054E-05
5 s	8.31630E-09	6.38745E-05
30 s	9.50784E-09	8.00142E-05
60 s	8.29201E-09	1.40391E-04

Table 6.4: $\hat{Z}$-Component of Inertial Angular Momentum Impacts

The error in the Hamiltonian Function and the $\hat{Z}$-component of inertial angular momentum are on the same order of magnitude as the error in the initial position vectors. As mentioned earlier, initial position error was on the order of one-half *sigma* which gives us a range from eight significant figures for the minimum value

	0.1 m	1000 m
0.05 s	2.40150E-07	2.30941E-03
0.1 s	2.44420E-07	2.38862E-03
0.5 s	2.44420E-07	2.58224E-03
1 s	2.31306E-07	2.41162E-03
5 s	2.49130E-07	1.85890E-03
30 s	3.44855E-07	1.84797E-03
60 s	4.43634E-07	3.03183E-03

Table 6.5: Nodal Regression Impacts

of *sigma* analyzed down to four significant figures for the maximum value of *sigma*. The Hamiltonian Function and $\hat{Z}$-component of inertial angular momentum follow the same pattern showing that the accuracy of these constants is directly related to the accuracy of the position attainable, which is related to the accuracy of the sensor. The time step does not appear to be directly related to the errors in $\mathcal{H}$ and H_k but that is a result of selecting data near the trendline. As the time step increases, the probability that these values will be on or near the trendline decreases, possibly impacting the accuracies up to one order of magnitude as stated previously.

The error in the time rate of change of the right ascension of the ascending node appears different from the others because it is not solely dependent on the position accuracy. With an error starting at order 10^{-7} for the minimum value of *sigma* and increasing to order 10^{-3} for the maximum value of *sigma* is two orders of magnitude lower than would be expected if the error was limited by the accuracy of the position alone. The data created for the nodal regression shows that initially the error is on the order of 10^{-9} and 10^{-5} for *sigma* values of 0.1 and 1000 m respectively, but as the propagation time progresses the error increases showing the dependence on time as well. Therefore, analysis was done to find the slope related to the regression of the node for each case. Then the absolute value of the difference between the slope of the baseline case with each of the remaining cases was determined. The difference in the slope for each case analyzed is summarized in Table 6.6. Therefore the combination of the initial error in the position and the time period for which the data was propagated

	0.1 m	1000 m
0.05 s	7.7701E-11	7.57278E-07
0.1 s	7.8852E-11	7.83315E-07
0.5 s	7.8852E-11	8.47747E-07
1 s	7.465E-11	7.92397E-07
5 s	8.1049E-11	6.05814E-07
30 s	1.11668E-10	6.11538E-07
60 s	1.43509E-10	9.87744E-07

Table 6.6: Nodal Regression Slope Impacts

contributed to the error in the regression of the RAAN as seen in Table 6.5. With this information it is now possible to look at what level of fidelity of the geopotential expansion is appropriate for application in a supplemental model.

6.5 A Supplemental Model

According to the level of accuracies attained in the Hamiltonian Function by using simulated data it does not appear necessary to use geopotential terms through J_{21}^{21}. Comparing the order of magnitude in Table 6.3 with Table 3.2, geopotential expansion through J_2^0 is sufficient for sensors with *sigma* on the order of 1000 m. This is because the error seen in the Hamiltonian is on the order of 10^{-5} which matches the level of constancy found when evaluating the Hamiltonian Function through J_2^0. For a slightly better sensor where *sigma* is on the order of 100 m, an increase in the geopotential terms through J_4^4 is appropriate. Table 3.2 shows that the constancy attained in the Hamiltonian Function with geopotential expansion through this term was approximately order 10^{-6}, which matches the error level for a 100 m sensor. In order to get accuracies of 10^{-9} more cases similar to those listed in Table 3.2 were analyzed and it was found that just decreasing the geopotential expansion to J_{20}^{20} results in accuracies on the order of 10^{-7} which would not be sufficient to observe order 10^{-9} errors in the Hamiltonian Function. Therefore, sensors attaining meter accuracy or better require a model incorporating a geopotential expansion through the J_{21}^{21} term.

The $\hat{Z}$-component of inertial angular momentum results displayed in Table 6.4 show that for higher *sigma* values, the error is on the order of 10^{-5} which coincides with the highest level of constancy that can be expected for H_k. Table 4.1 shows that for any geopotential (ignoring the zonal harmonics only cases) the highest level of constancy is of order 10^{-5} when using geopotential terms from J_2^2 all the way through J_{21}^{21}. Therefore, it is not necessary to include any more terms in the geopotential expansion beyond the J_2^2 term.

Finally, looking at the results from the time rate of change of the right ascension of the ascending node, the change in the slope shown in Table 6.6 is so low, the difference would not be noticeable in the model as discussed in Chapter V. Table 5.1 shows that the maximum difference between slopes is on the order of 10^{-6}. Therefore, the minor differences brought about by this particular data set are not the limiting factor in the accuracy attainable in the time rate of change of the right ascension of the ascending node and the model should be developed based on the highest level of accuracy attainable in the slope using the lowest possible geopotential expansion. As previously stated, the largest variance occurs between J_2^0 and J_4^0 and adding geopotential terms beyond this term results in no additional variance. Therefore, a model utilizing the geopotential expansion through the J_4^0 is appropriate. Table 6.7 summarizes the level of geopotential expansion appropriate for different *sigma* values. Current systems have *sigma* values on the order of hundreds of meters, implying that

	Meter or Better	Tens to Hundreds of Meters	Thousands of Meters
$\mathcal{H}$	J_{21}^{21}	J_4^4	J_2^0
H_k	J_2^2	J_2^2	J_2^2
$\dot{\Omega}$	J_4^0	J_4^0	J_4^0

Table 6.7: Summary of Supplemental Model

the geopotential expansion appropriate with this order of *sigma* would be sufficient for implementation in data mining techniques.

VII. Conclusion

7.1 A Growing Problem

As the number of objects orbiting the Earth continue to increase through current launch operations, failing satellites and a decrease in the size of objects being tracked, the probability that an object will be input into the Satellite Catalog multiple times increases. Additionally, because tracking satellites requires high-level precision, extraneous data in the SATCAT is highly undesirable. In order to limit the number of uncorrelated tracks being added to the SATCAT, it is beneficial to supplement the current system for tracking and updating orbits with a model that uses elements of the motion that remain more constant than the classical orbital elements.

7.2 Analysis Summary

In order to develop an appropriate supplemental model, research was conducted to determine the constancy of three elements of the motion, the Hamiltonian Function, $\hat{Z}$-component of angular momentum and the time rate of change of the right ascension of the ascending node. In addition to the investigation of the constancy attainable by these three elements, simulated data was analyzed to identify accuracies attainable through current estimation procedures based on the quality and quantity of the observations.

The Hamiltonian Function was shown to provide accuracies on the order of twelve significant figures. Additionally, the simulated data showed that using a sensor with accuracies of meter level or better would require using a geopotential expansion through the J_{21}^{21} term. Sensors with accuracies on the order of ten meters to hundreds of meters would require a model using a geopotential expansion through the J_4^4 term, while a sensor on the order of 1000 meters would only require expansion through the J_2^0 term. Therefore, depending on the accuracy of the sensor in use, the fidelity of the model will need to be adjusted.

The $\hat{Z}$-component of inertial angular momentum is another element that was evaluated to determine constancy. Using several zonal and sectoral cases, the con-

stancy of this element was shown to be on the order of four significant figures with the inclusion of the tesseral and sectoral harmonics. The theoretical level of accuracy coincides with the level of accuracy attainable using a sensor with accuracy on the order of 1000 meters. Therefore, the model should use the geopotential expansion through the J_2^2 term in order to attain the best available accuracy in the $\hat{Z}$-component of inertial angular momentum.

The final element of the motion evaluated for accuracy is the time rate of change of the right ascension of the ascending node. The right ascension of the ascending node decreases linearly with time at a rate dependent on the classical orbital elements. The most significant variance in $\dot{\Omega}$ occurs with the expansion through the J_4^0 term resulting in accuracies of approximately three significant figures. The simulated data was producing errors of much lower values than the model at this geopotential expansion will show. Therefore, an appropriate model is one utilizing the geopotential expansion through the J_4^0 term.

7.3 A Model for Improvement

Each of the elements of the motion evaluated for constancy require a slightly different level of expansion for the geopotential to be used in the model. Utilization of this model for data mining, along with the current method has potential to enhance the level of accuracy of objects being tracked by introducing elements of the motion that remain constant for longer periods of time. An increase in tracking accuracy will decrease the number of uncorrelated tracks appearing in the Satellite Catalog, thereby improving the available data and enhancing awareness of the objects orbiting the Earth.

Appendix A. Additional Figures

A.1 Scenario 1: Hamiltonian Function Graphs

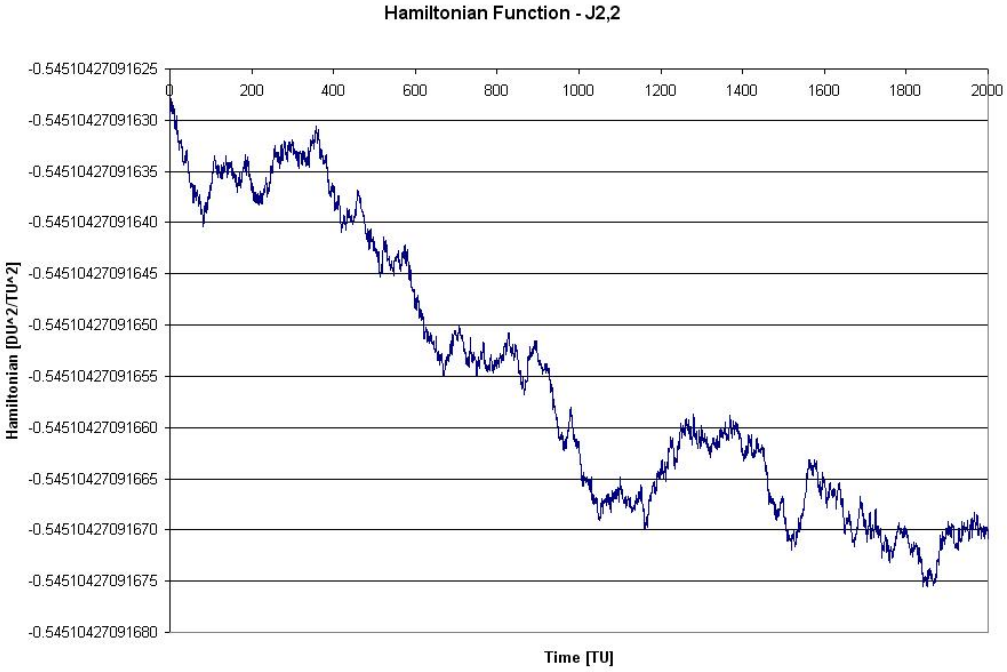

Figure A.1: Scenario 1, Case 3: $\mathcal{H}$ versus time

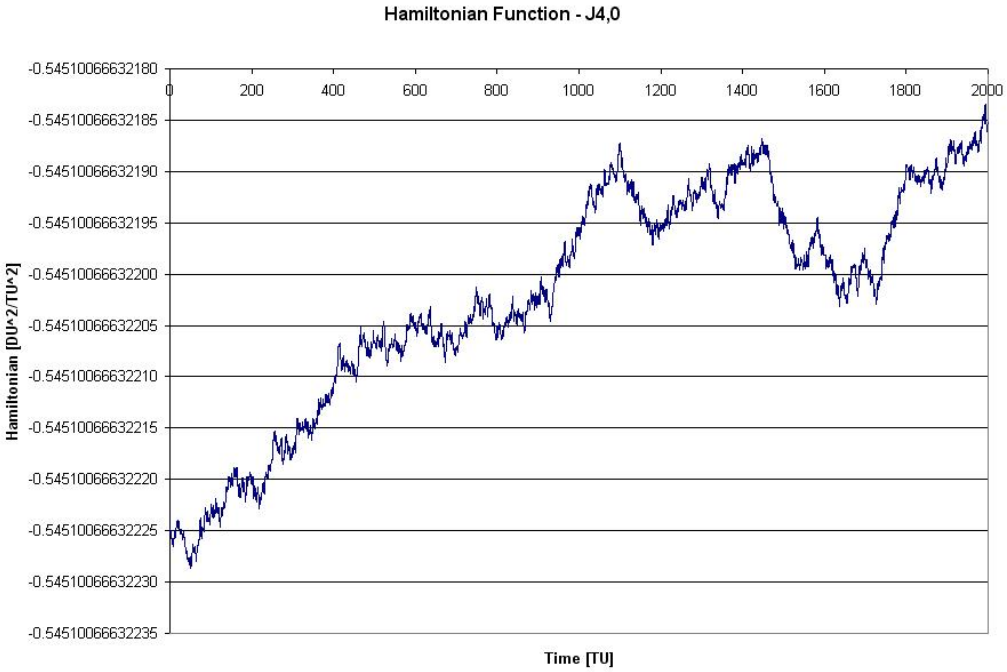

Figure A.2: Scenario 1, Case 4: $\mathcal{H}$ versus time

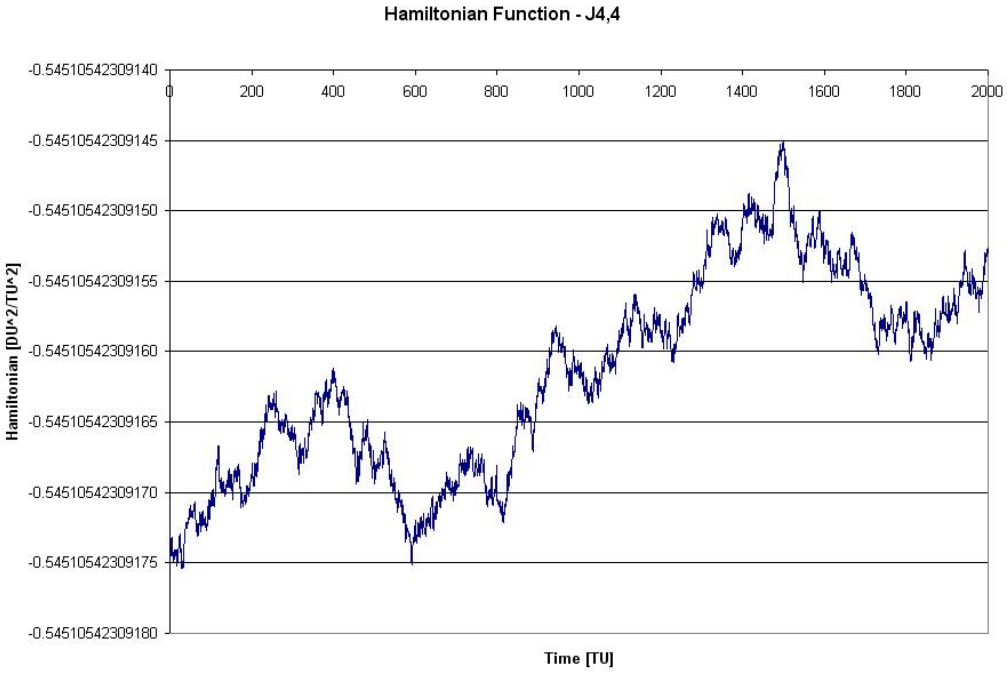

Figure A.3: Scenario 1, Case 5: $\mathcal{H}$ versus time

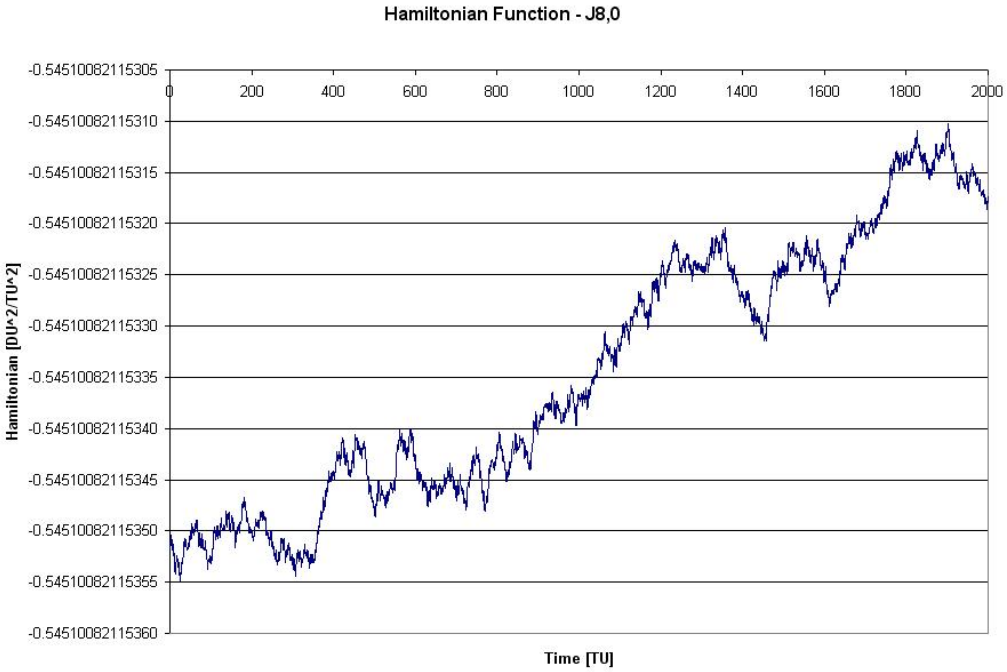

Figure A.4: Scenario 1, Case 6: $\mathcal{H}$ versus time

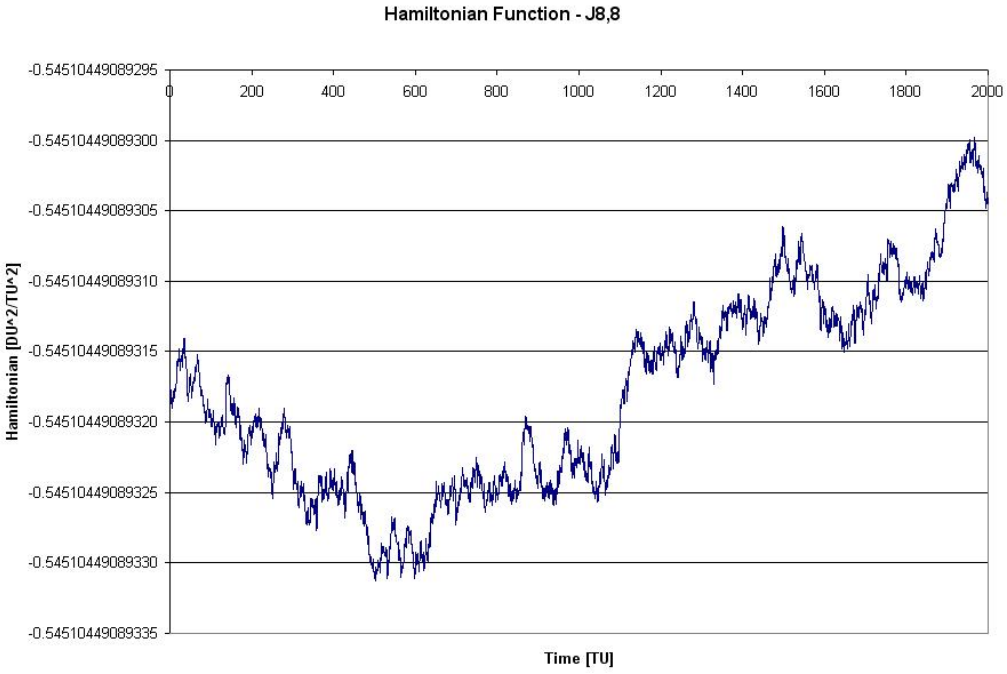

Figure A.5: Scenario 1, Case 7: $\mathcal{H}$ versus time

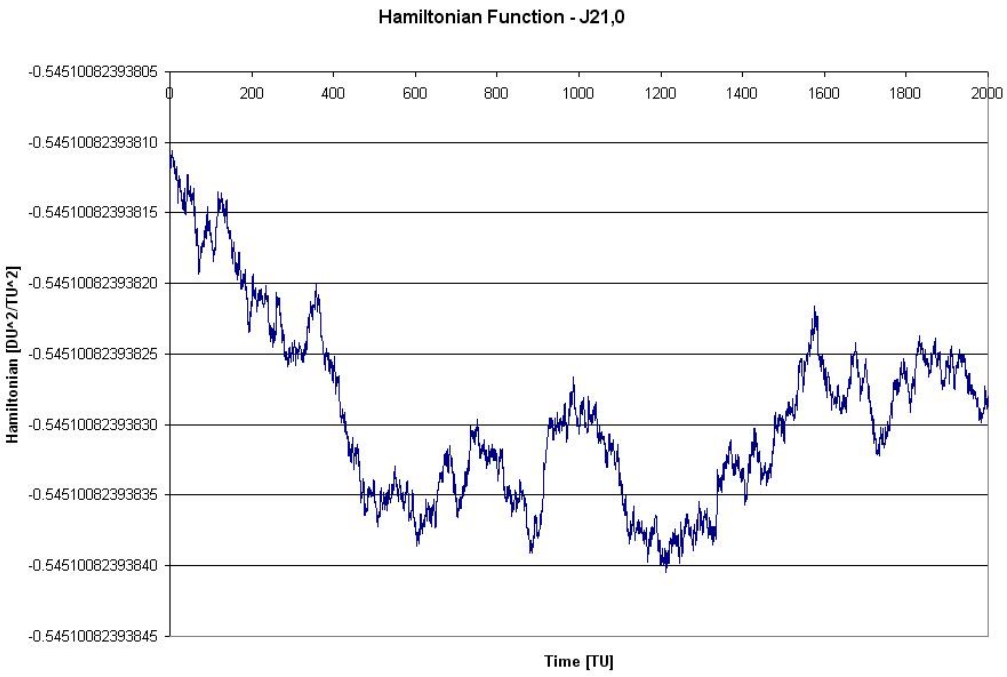

Figure A.6: Scenario 1, Case 8: $\mathcal{H}$ versus time

A.2 Scenario 1: Angular Momentum Graphs

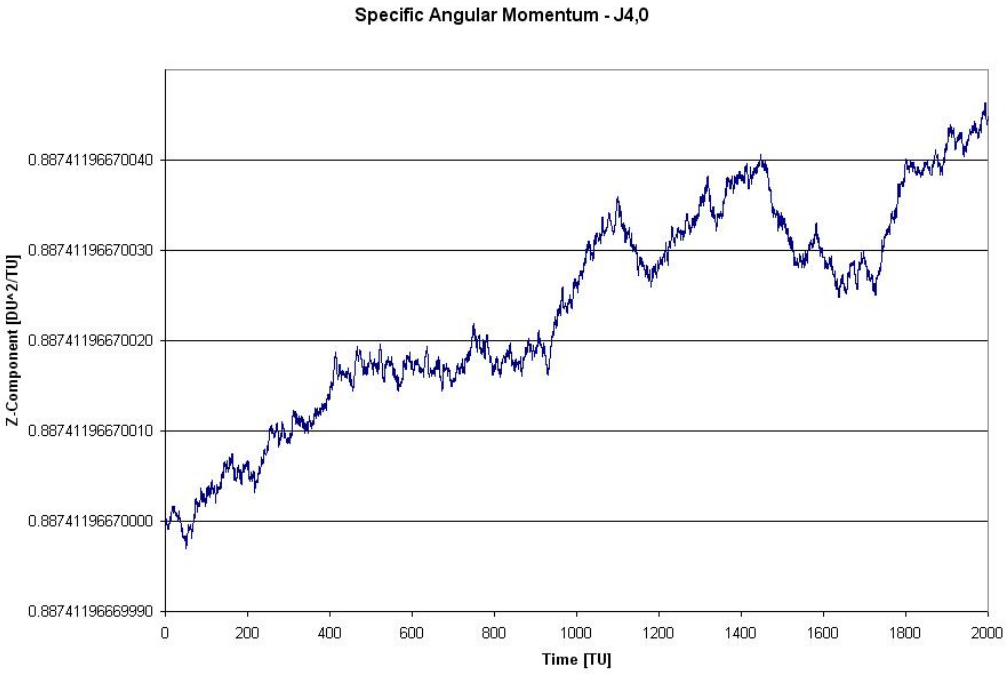

Figure A.7: Scenario 1, Case 4: H_k versus time

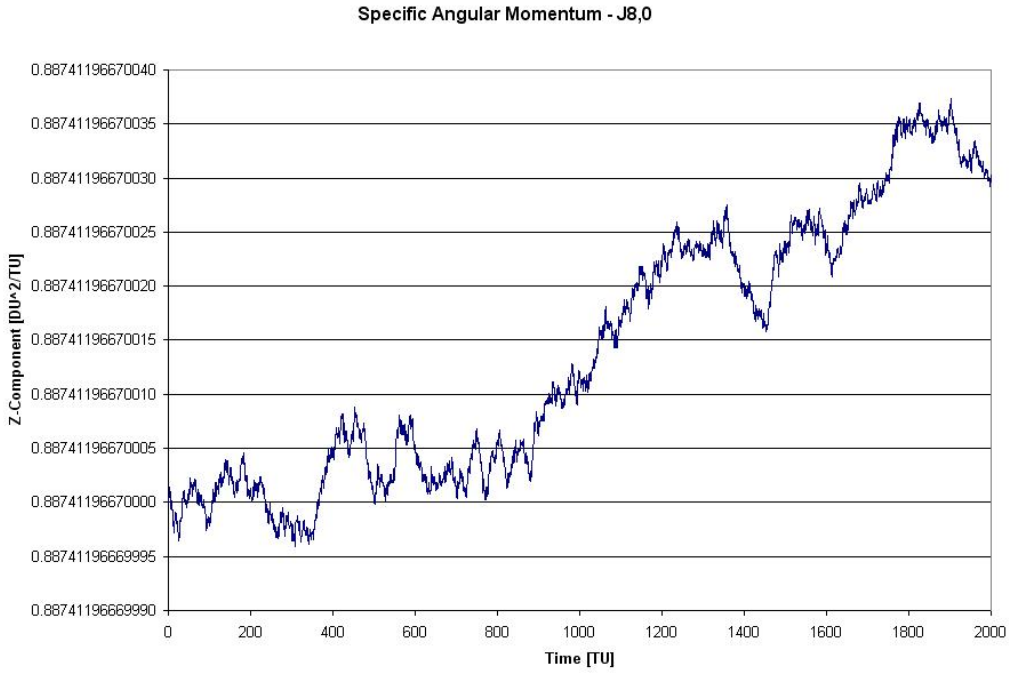

Figure A.8: Scenario 1, Case 6: H_k versus time

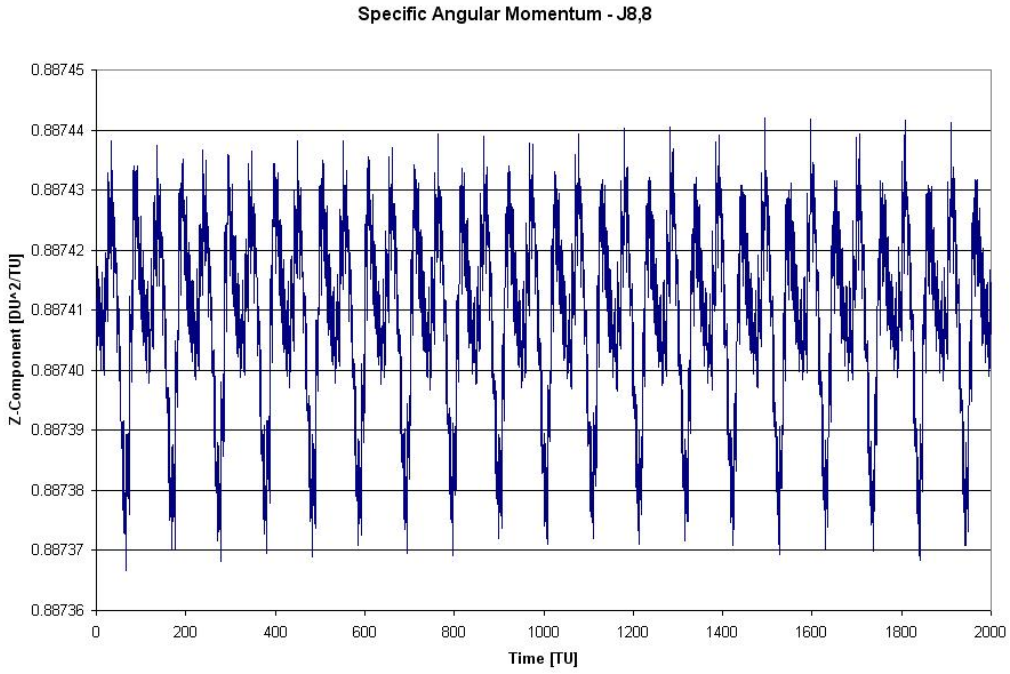

Figure A.9: Scenario 1, Case 7: H_k versus time

A.3 Scenario 1: Nodal Regression Graphs

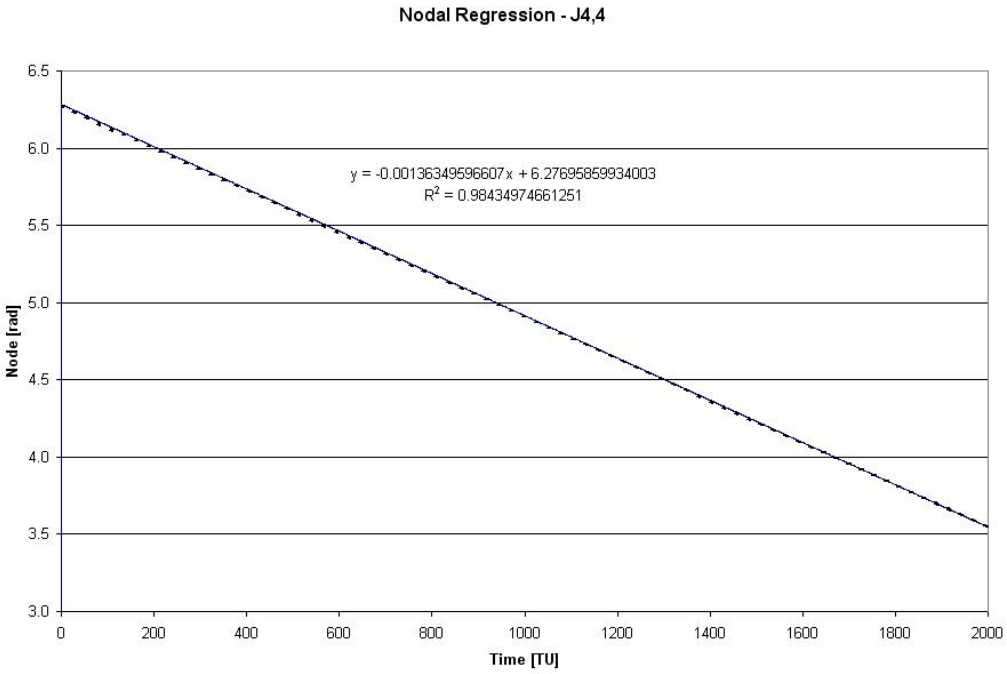

Figure A.10: Scenario 1, Case 5: $\dot{\Omega}$ versus time

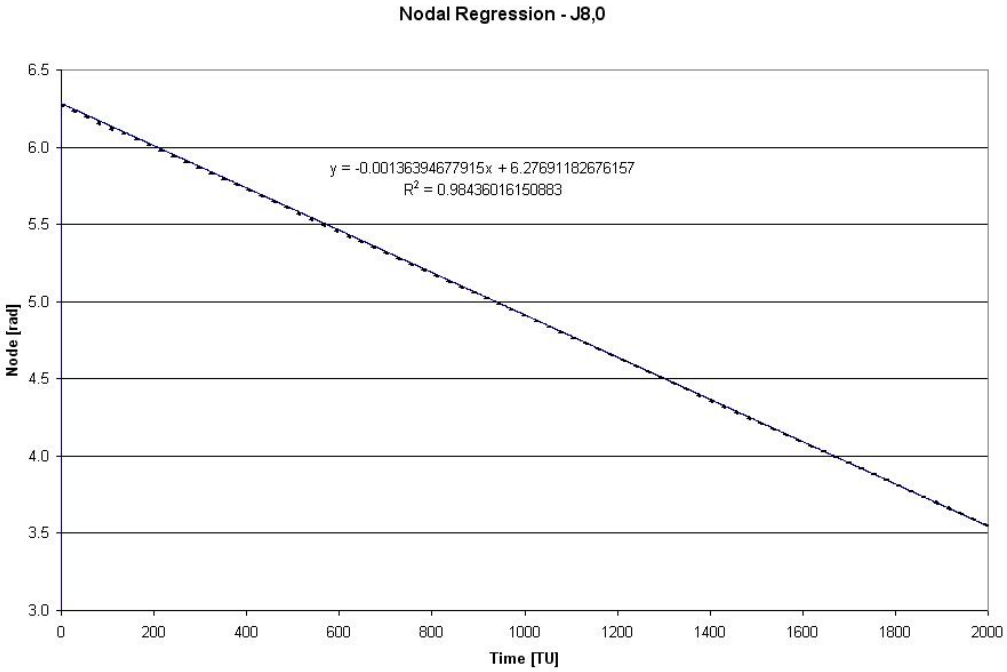

Figure A.11: Scenario 1, Case 6: $\dot{\Omega}$ versus time

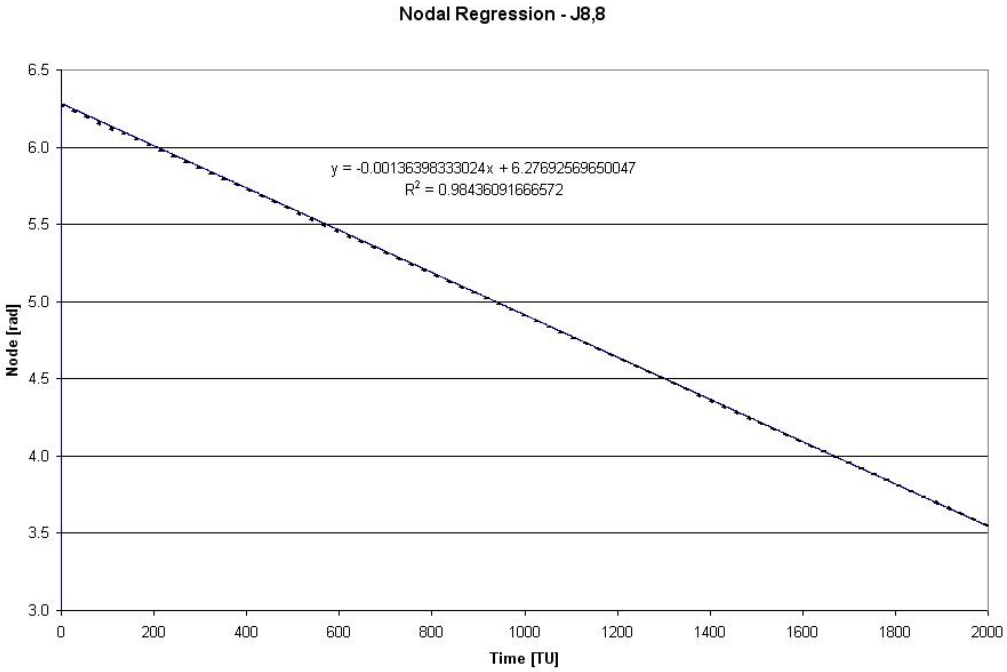

Figure A.12: Scenario 1, Case 7: $\dot{\Omega}$ versus time

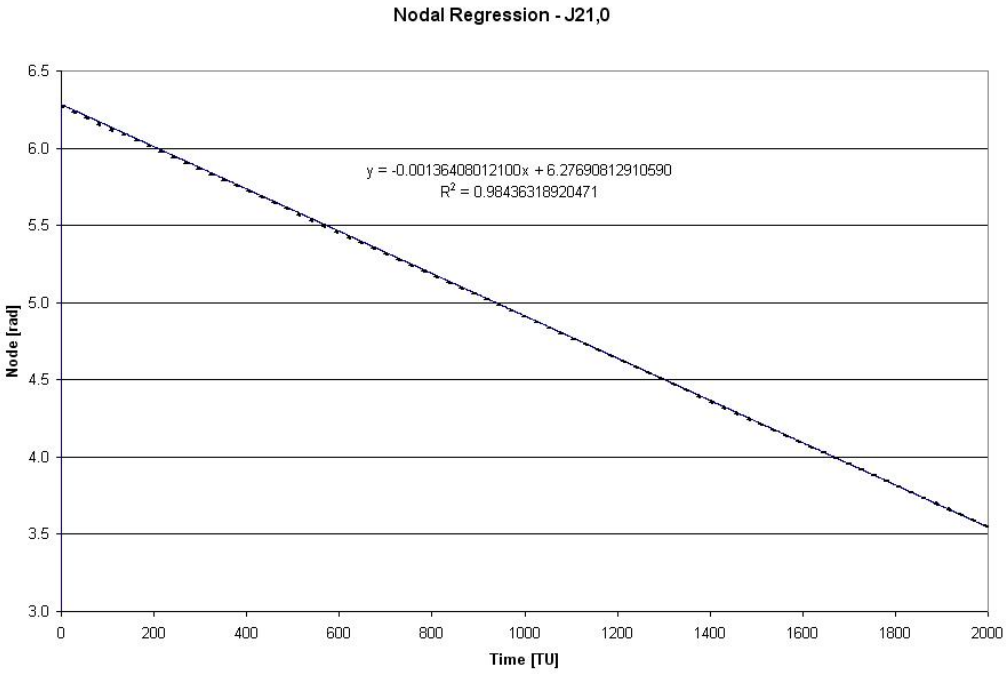

Figure A.13: Scenario 1, Case 8: $\dot{\Omega}$ versus time

A.4 Scenario 2: Hamiltonian Function Graphs

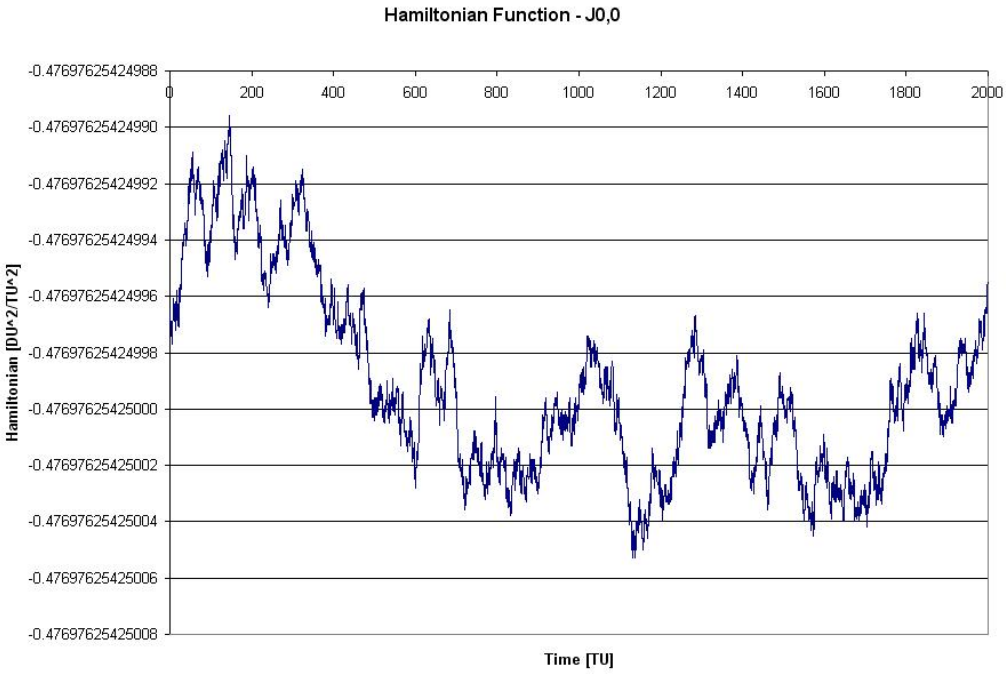

Figure A.14: Scenario 2, Case 1: $\mathcal{H}$ versus time

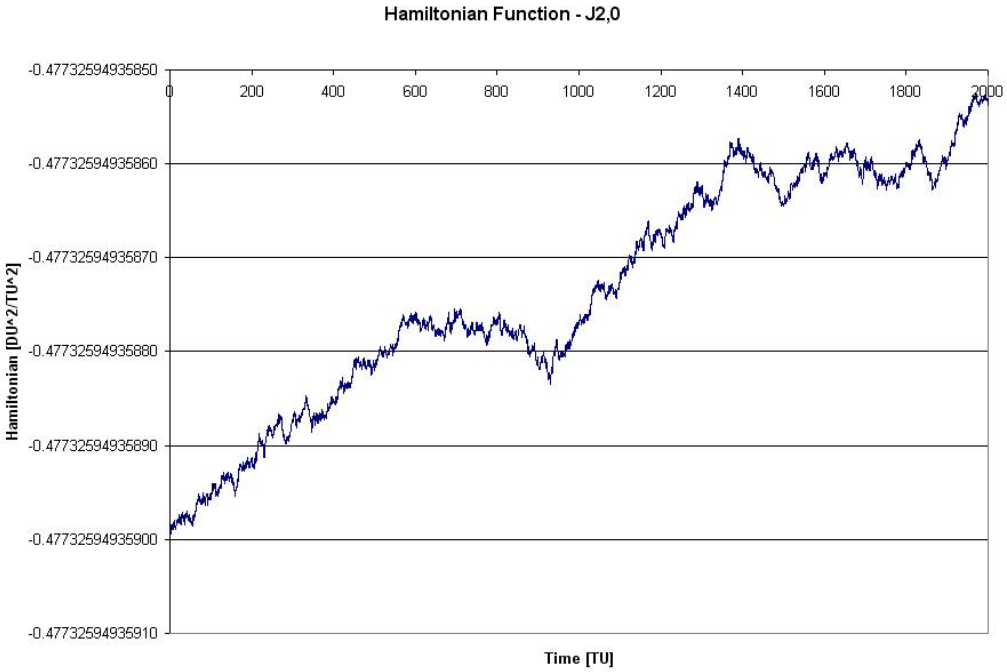

Figure A.15: Scenario 2, Case 2: $\mathcal{H}$ versus time

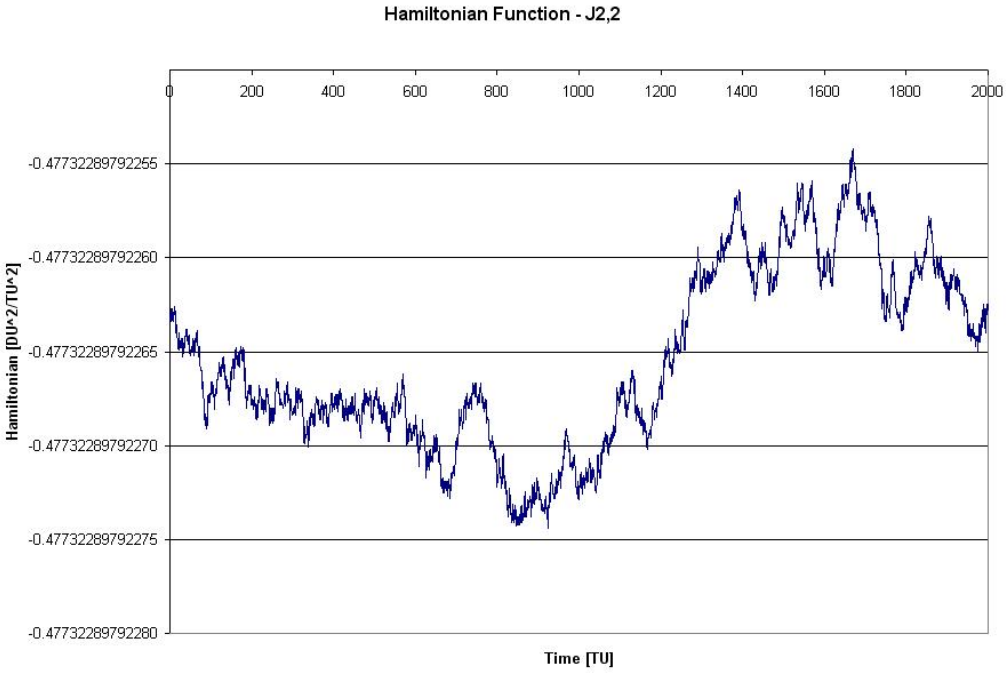

Figure A.16: Scenario 2, Case 3: $\mathcal{H}$ versus time

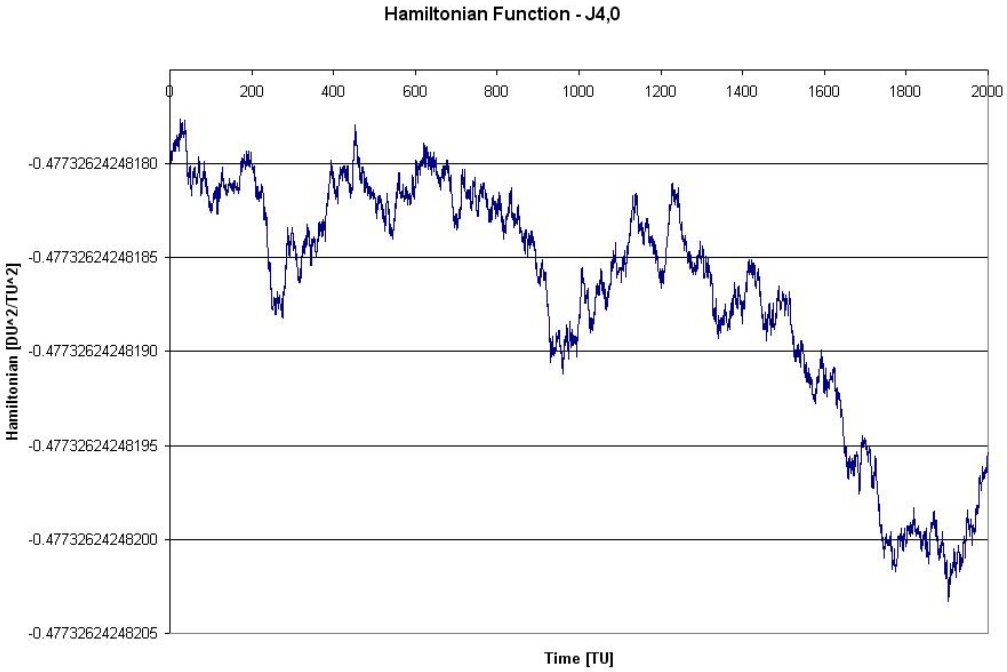

Figure A.17: Scenario 2, Case 4: $\mathcal{H}$ versus time

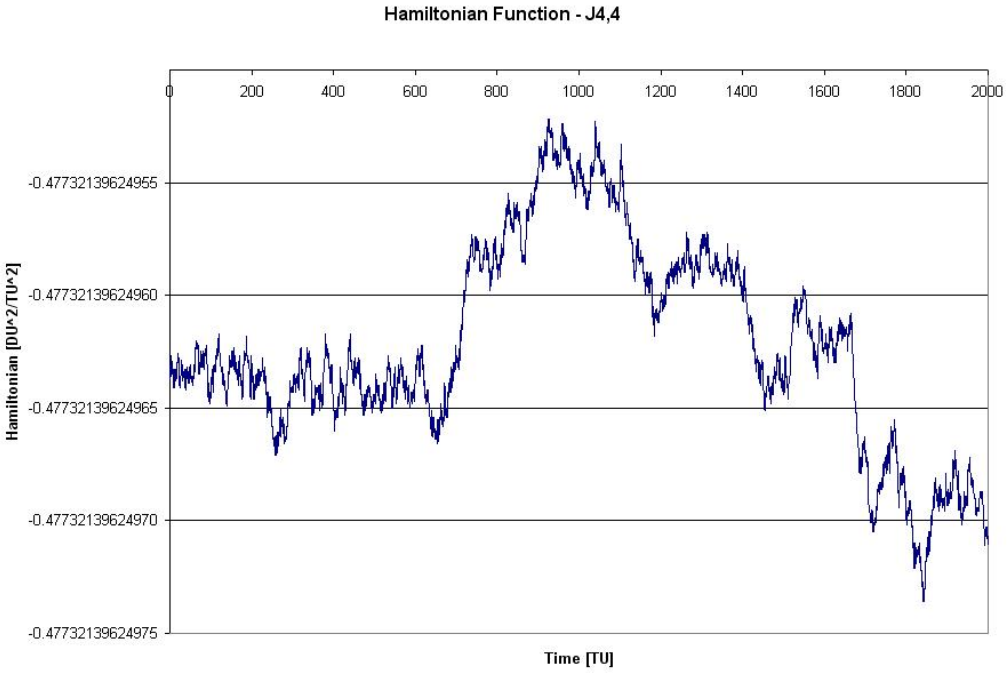

Figure A.18: Scenario 2, Case 5: $\mathcal{H}$ versus time

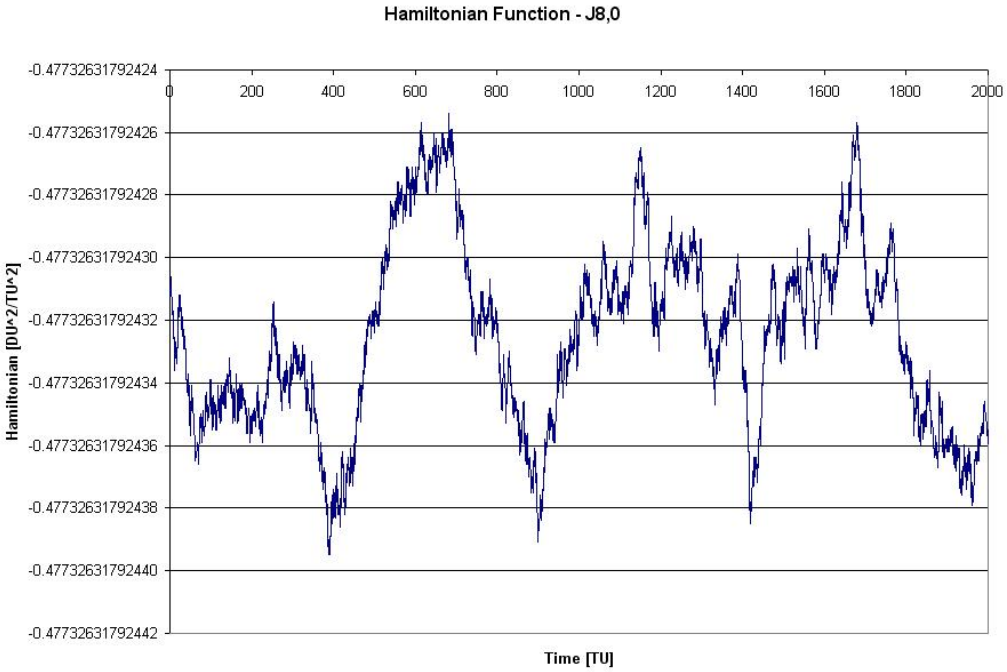

Figure A.19: Scenario 2, Case 6: $\mathcal{H}$ versus time

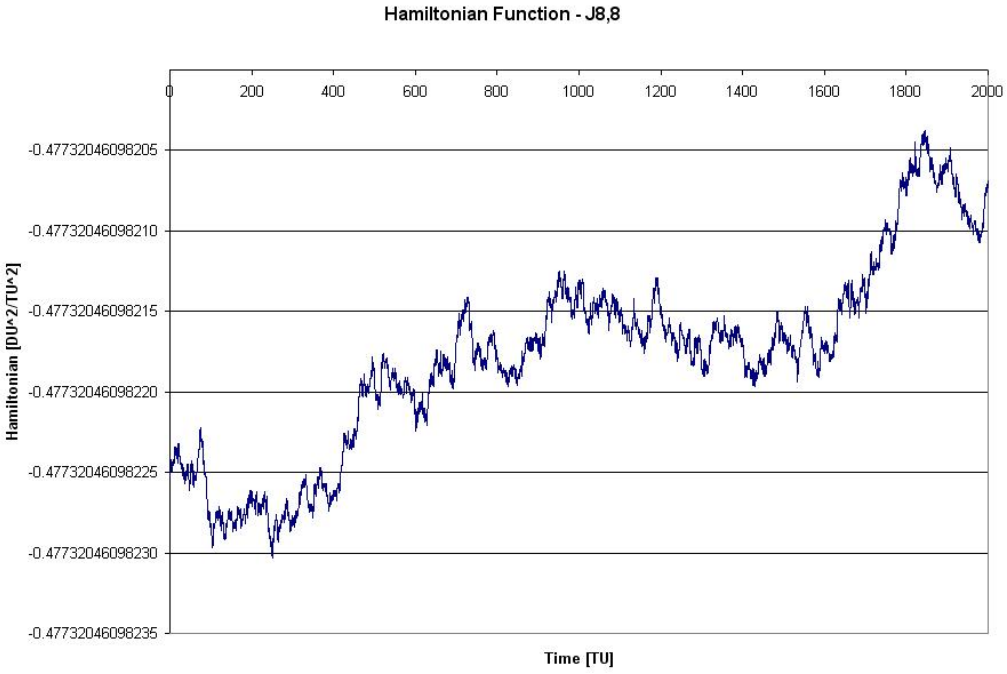

Figure A.20: Scenario 2, Case 7: $\mathcal{H}$ versus time

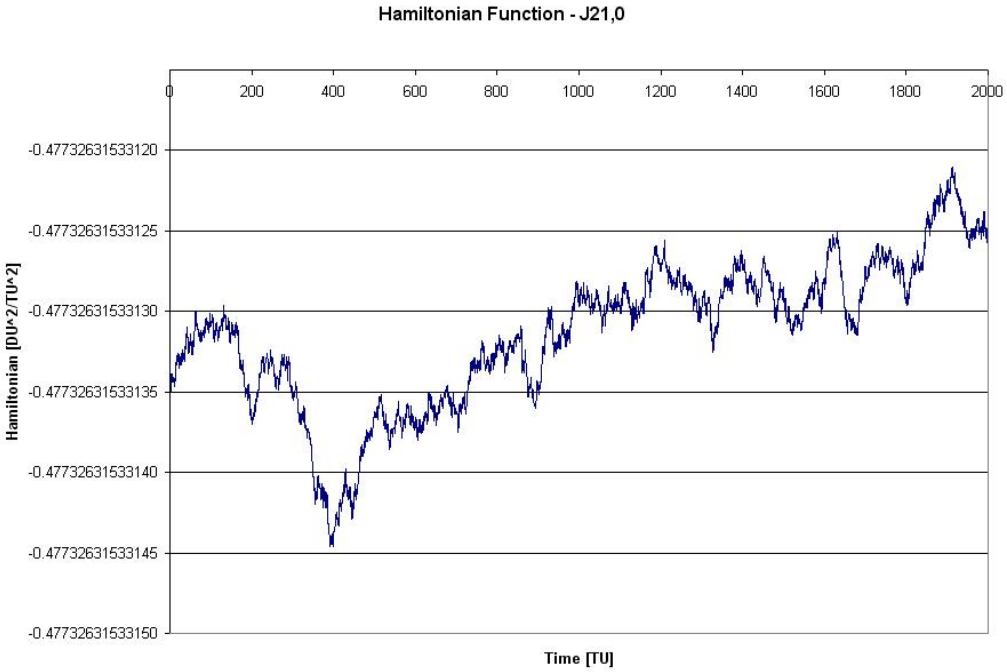

Figure A.21: Scenario 2, Case 8: $\mathcal{H}$ versus time

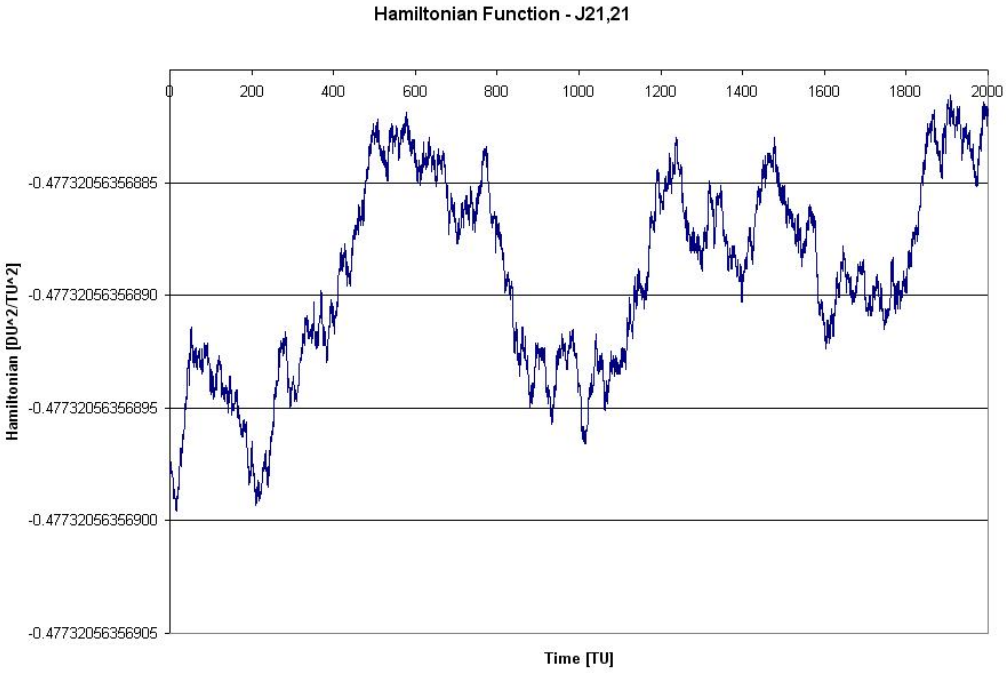

Figure A.22: Scenario 2, Case 9: $\mathcal{H}$ versus time

A.5 Scenario 2: Angular Momentum Graphs

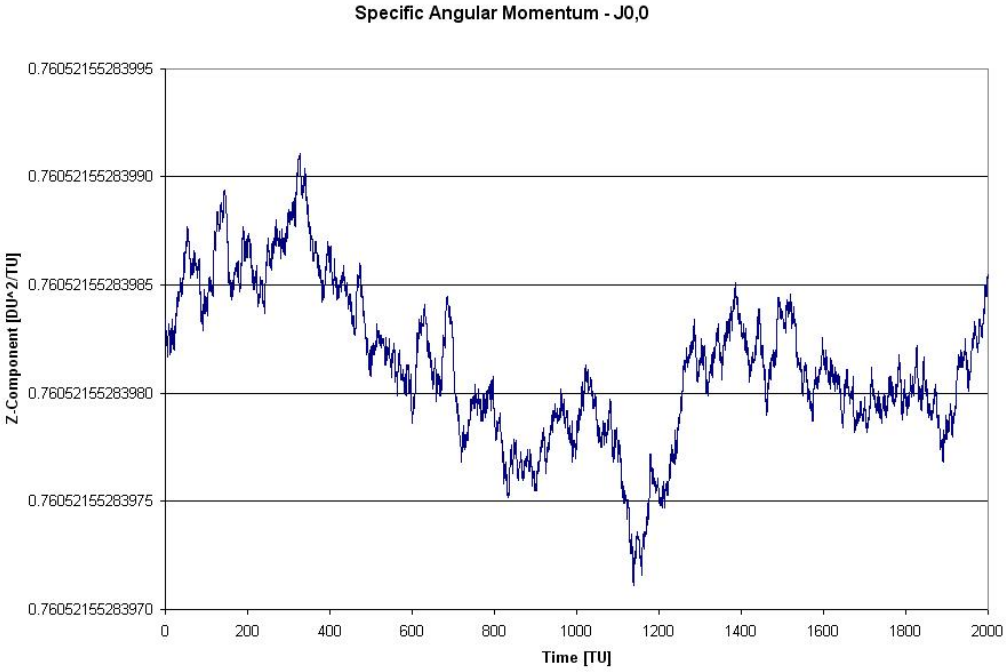

Figure A.23: Scenario 2, Case 1: H_k versus time

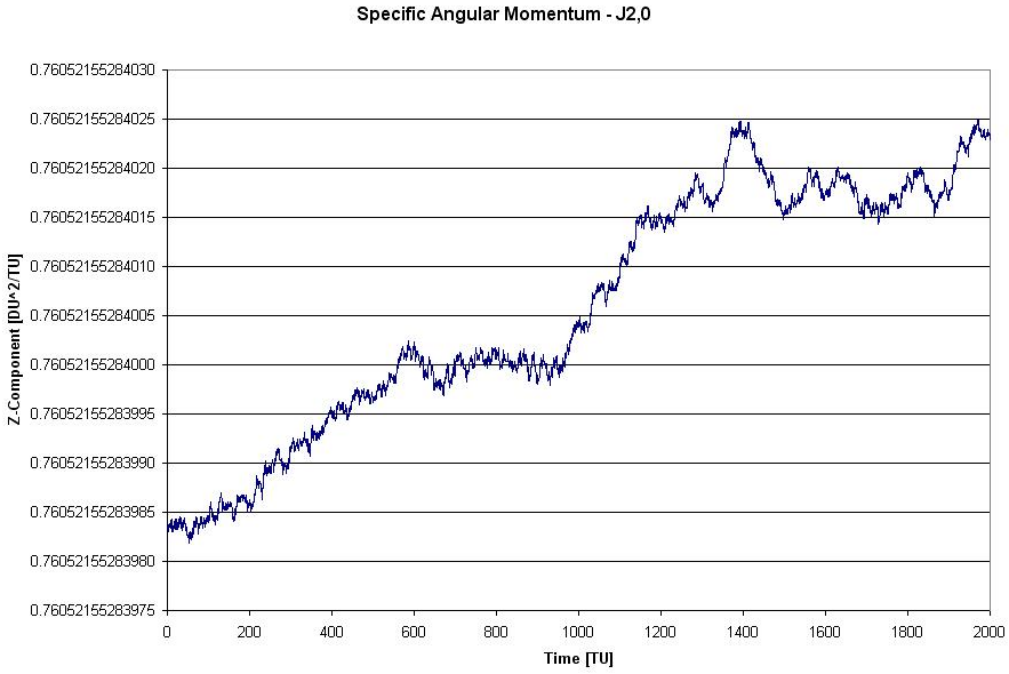

Figure A.24: Scenario 2, Case 2: H_k versus time

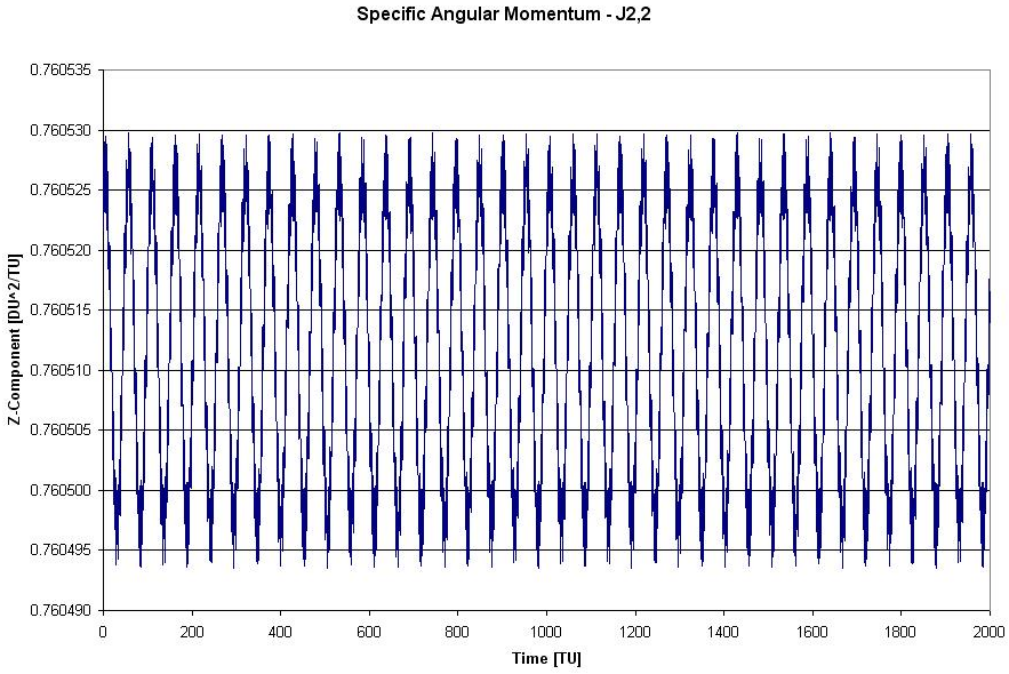

Figure A.25: Scenario 2, Case 3: H_k versus time

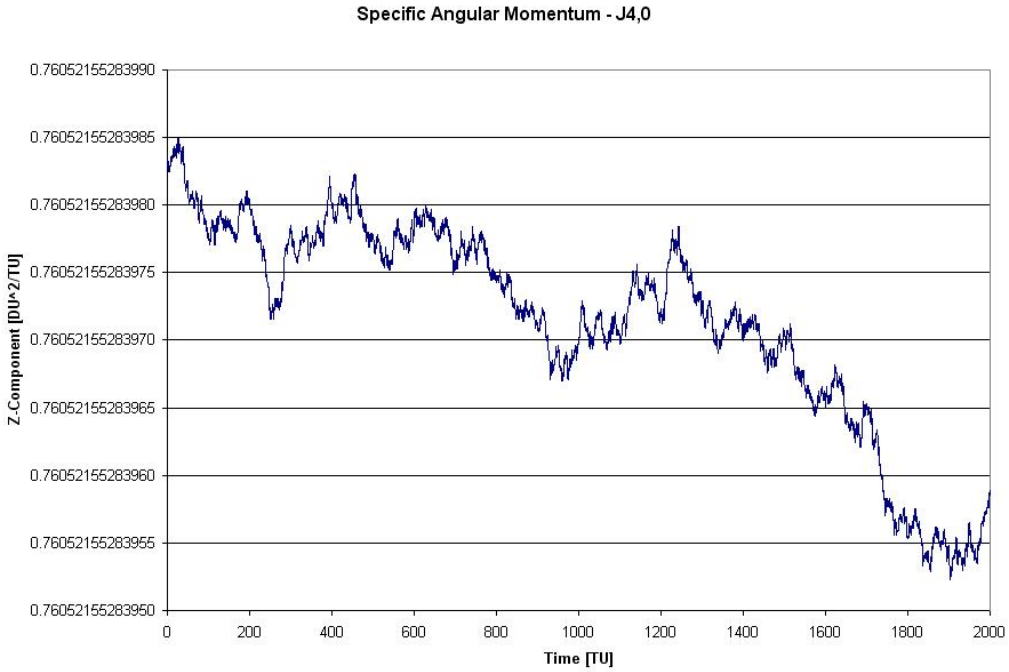

Figure A.26: Scenario 2, Case 4: H_k versus time

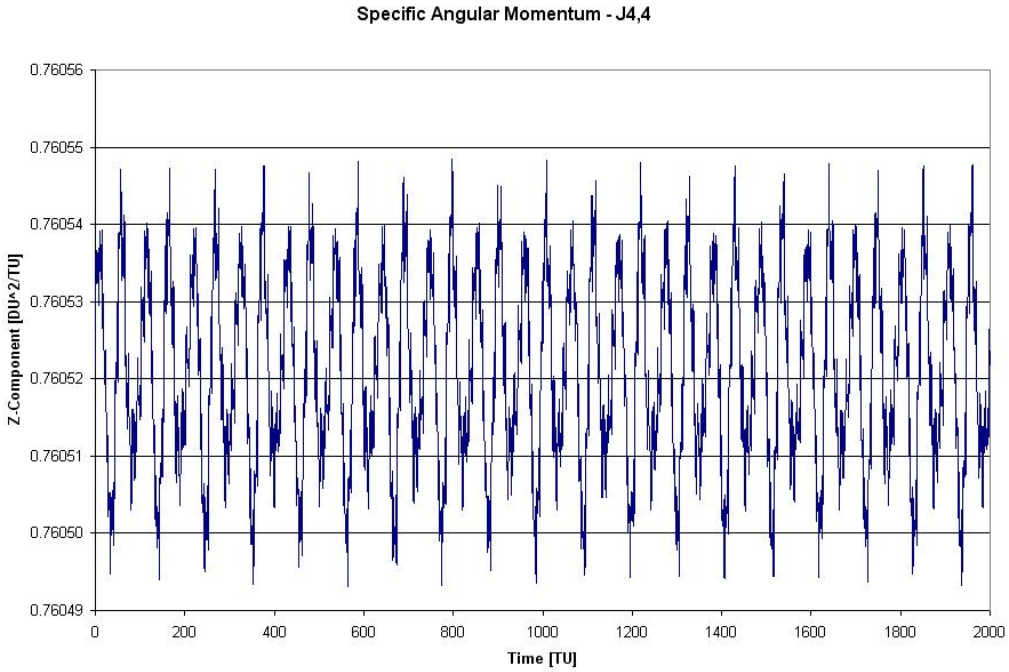

Figure A.27: Scenario 2, Case 5: H_k versus time

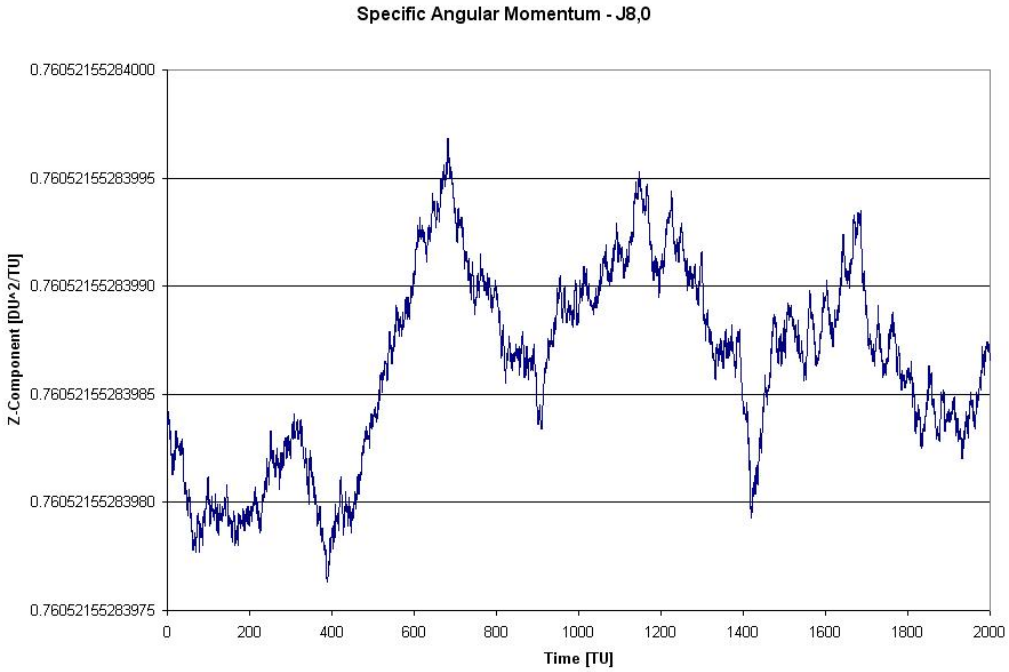

Figure A.28: Scenario 2, Case 6: H_k versus time

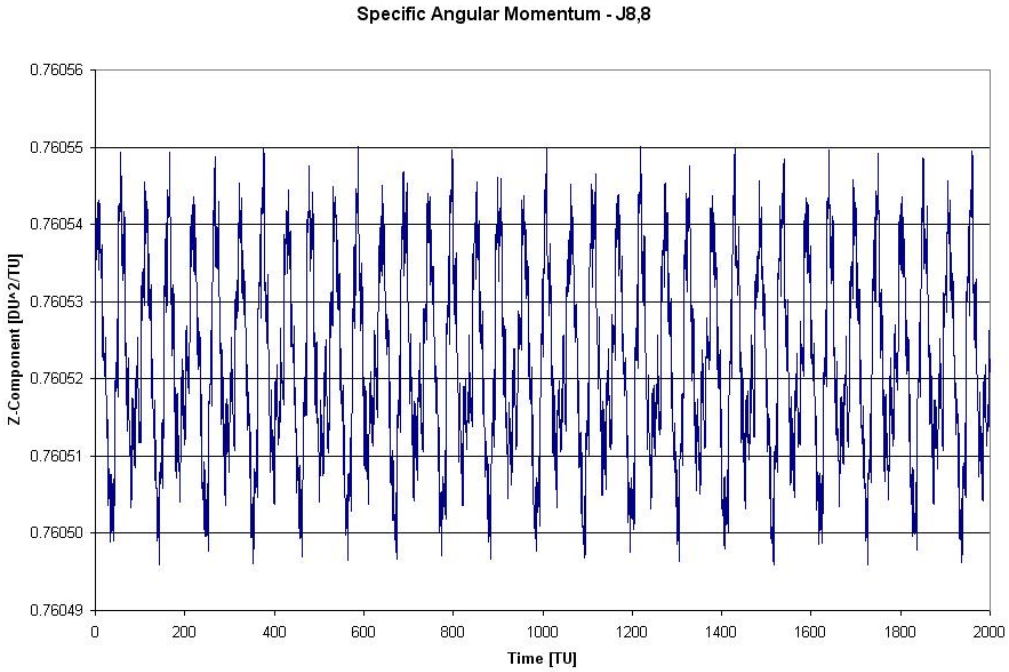

Figure A.29: Scenario 2, Case 7: H_k versus time

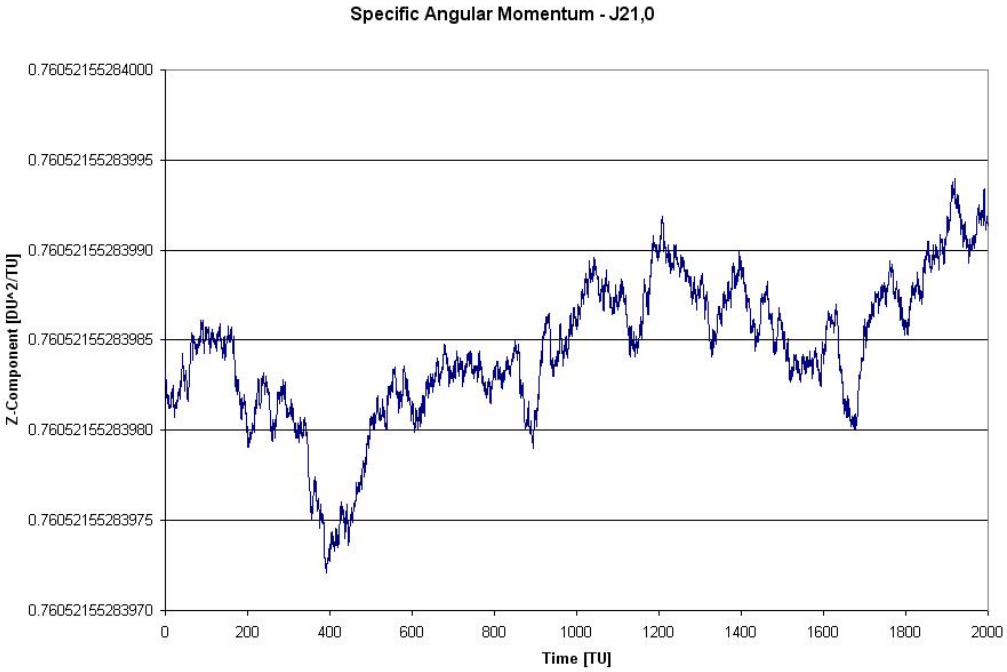

Figure A.30: Scenario 2, Case 8: H_k versus time

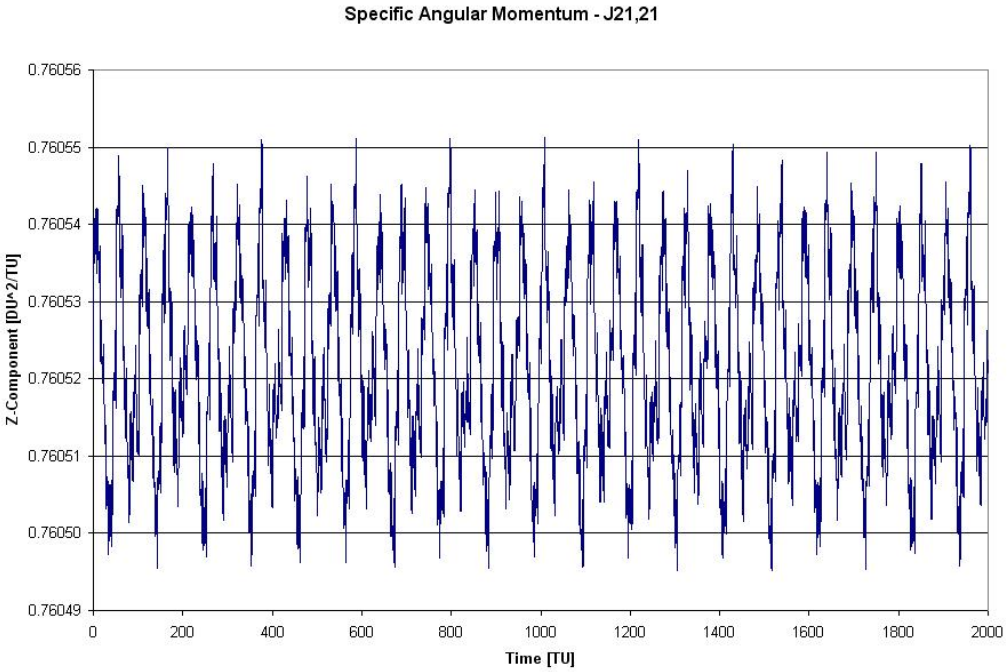

Figure A.31: Scenario 2, Case 9: H_k versus time

A.6 Scenario 2: Nodal Regression Graphs

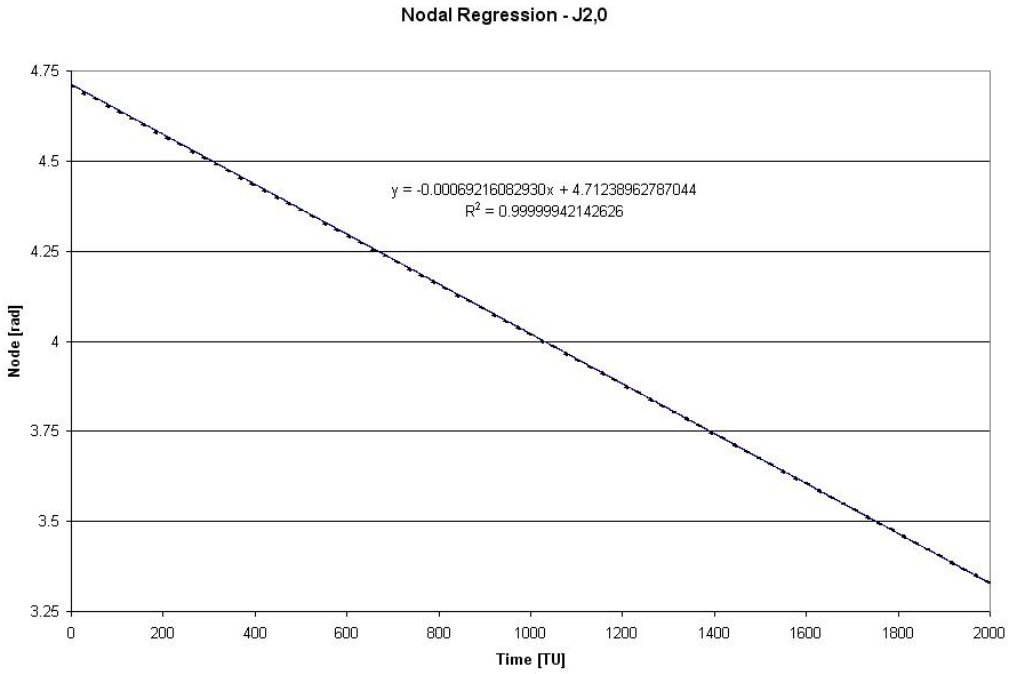

Figure A.32: Scenario 2, Case 2: $\dot{\Omega}$ versus time

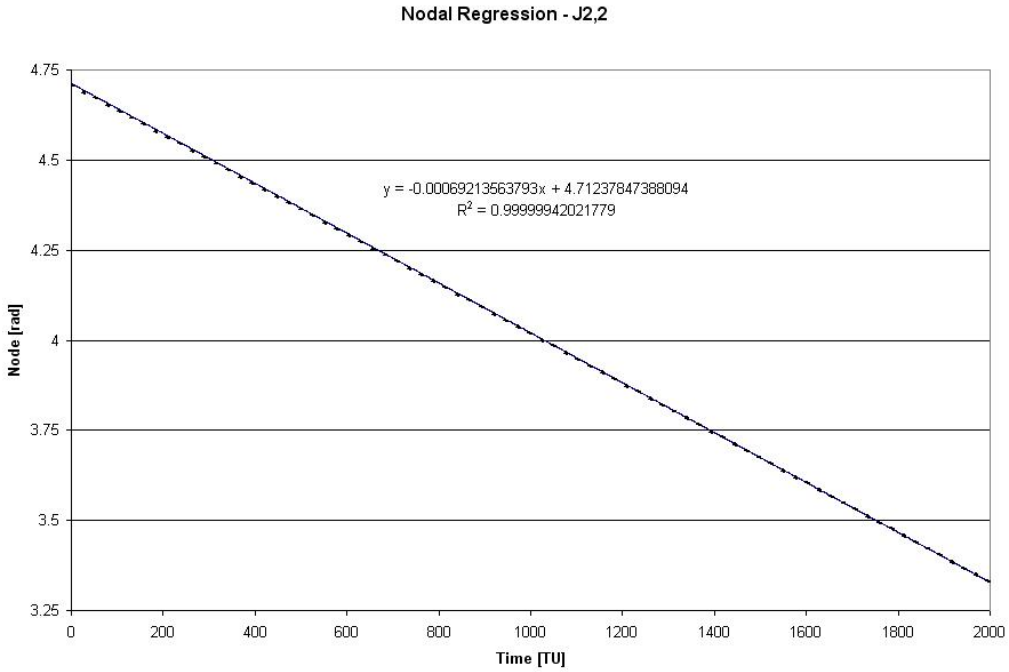

Figure A.33: Scenario 2, Case 3: $\dot{\Omega}$ versus time

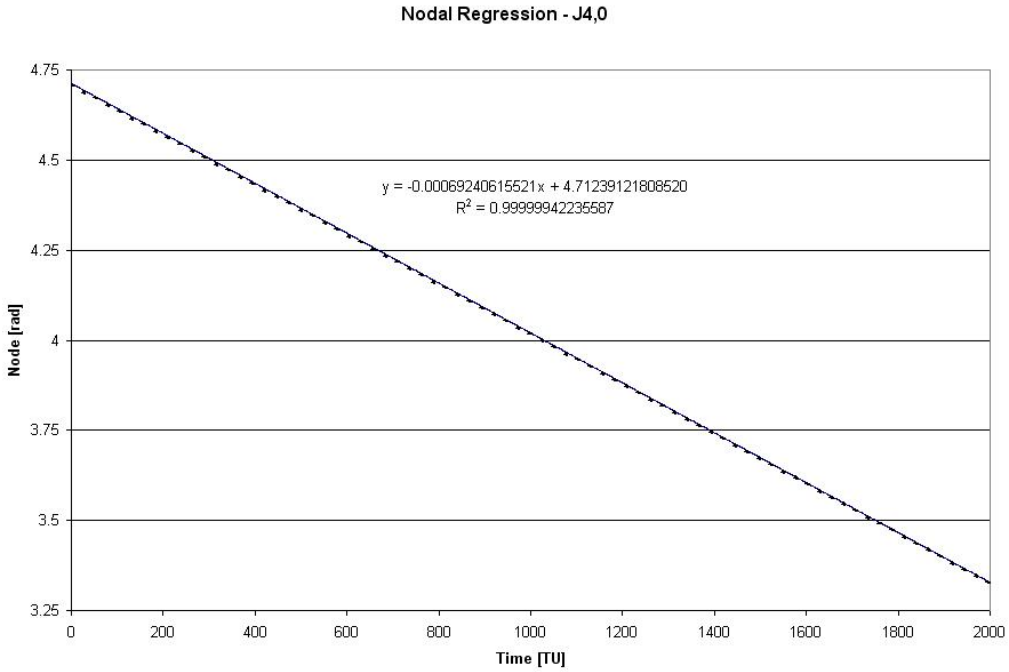

Figure A.34: Scenario 2, Case 4: $\dot{\Omega}$ versus time

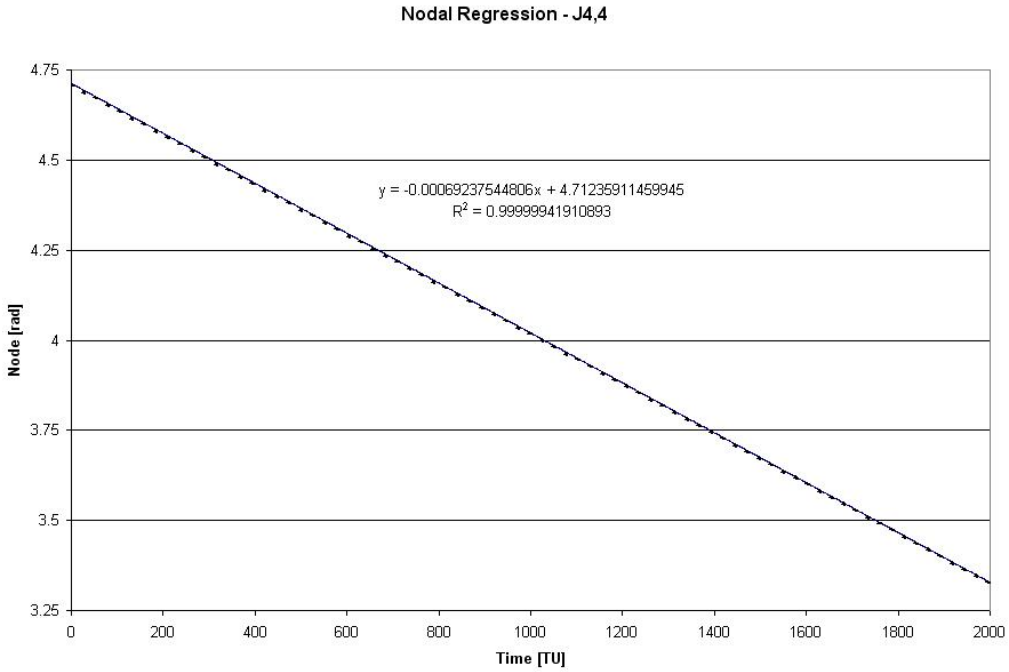

Figure A.35: Scenario 2, Case 5: $\dot{\Omega}$ versus time

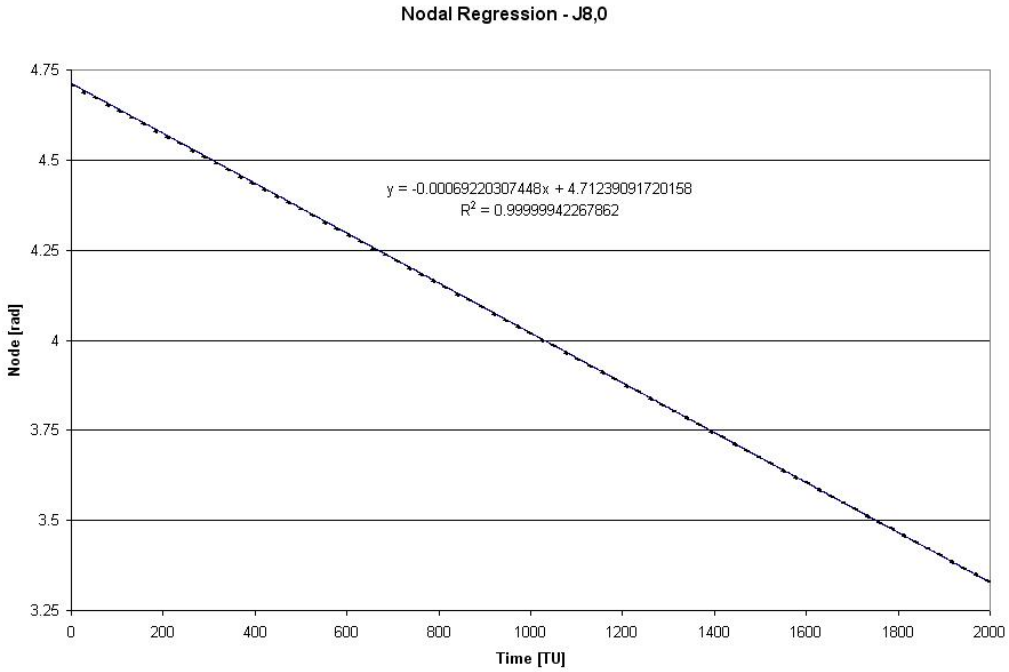

Figure A.36: Scenario 2, Case 6: $\dot{\Omega}$ versus time

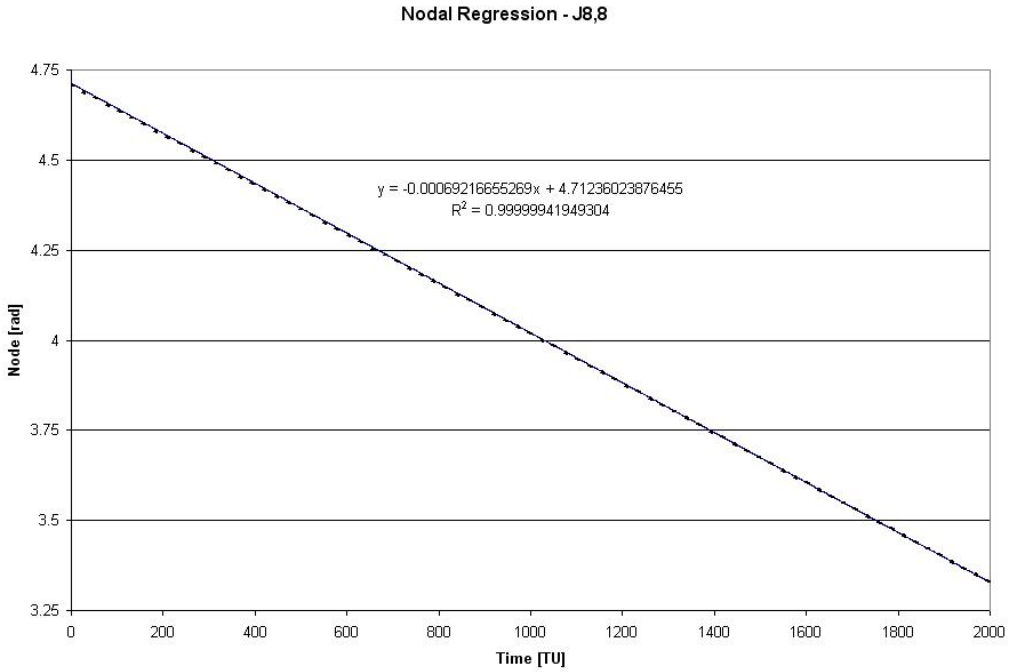

Figure A.37: Scenario 2, Case 7: $\dot{\Omega}$ versus time

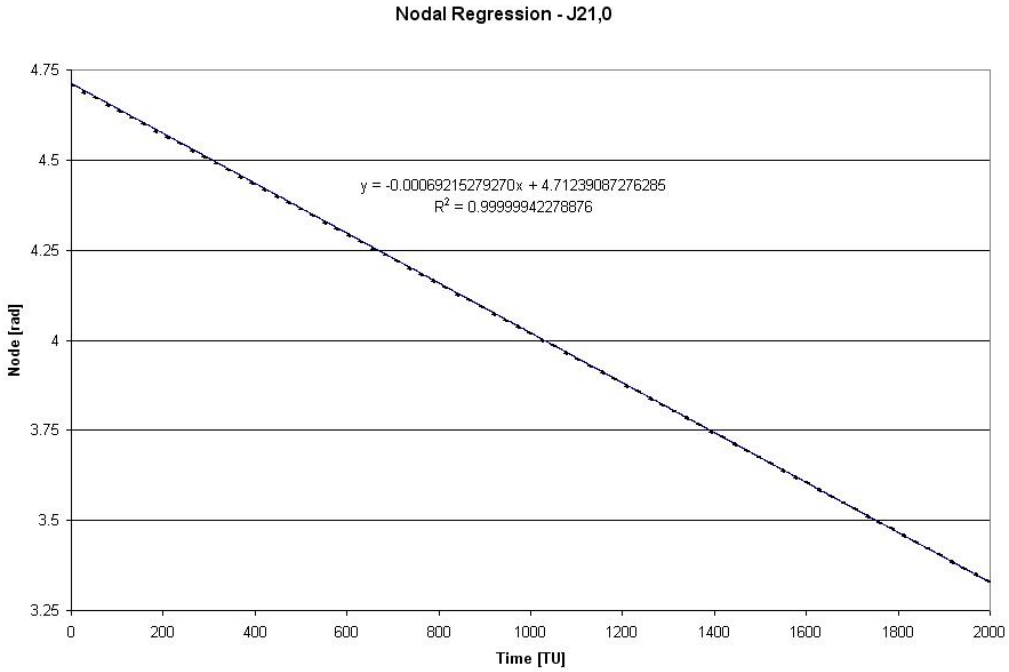

Figure A.38: Scenario 2, Case 8: $\dot{\Omega}$ versus time

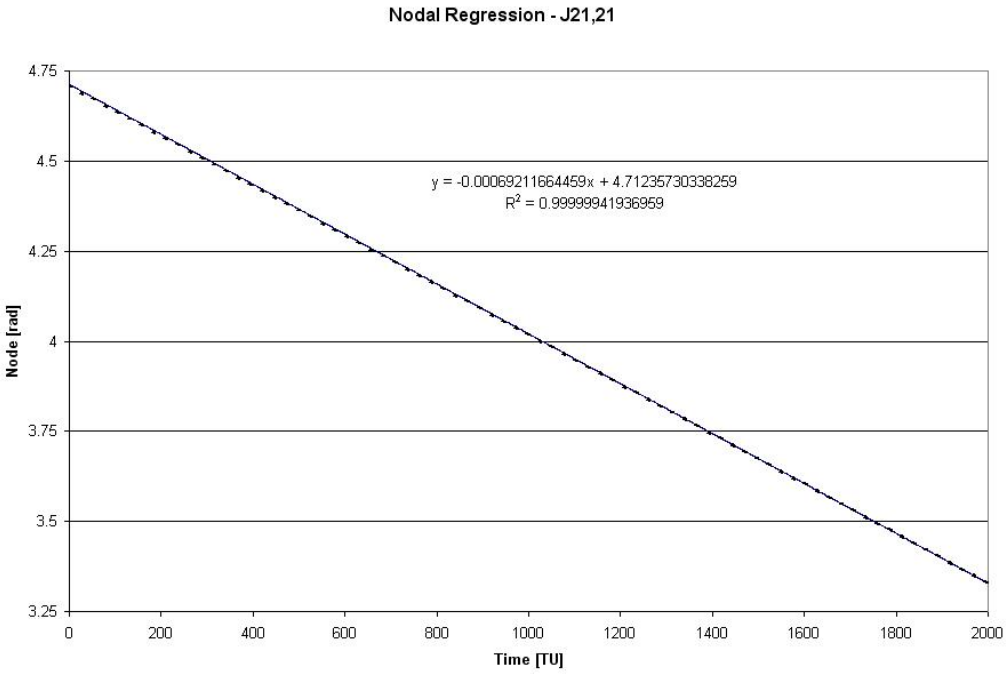

Figure A.39: Scenario 2, Case 9: $\dot{\Omega}$ versus time

A.7 Quantifying the Data: Initial Position and Velocity Error Graphs

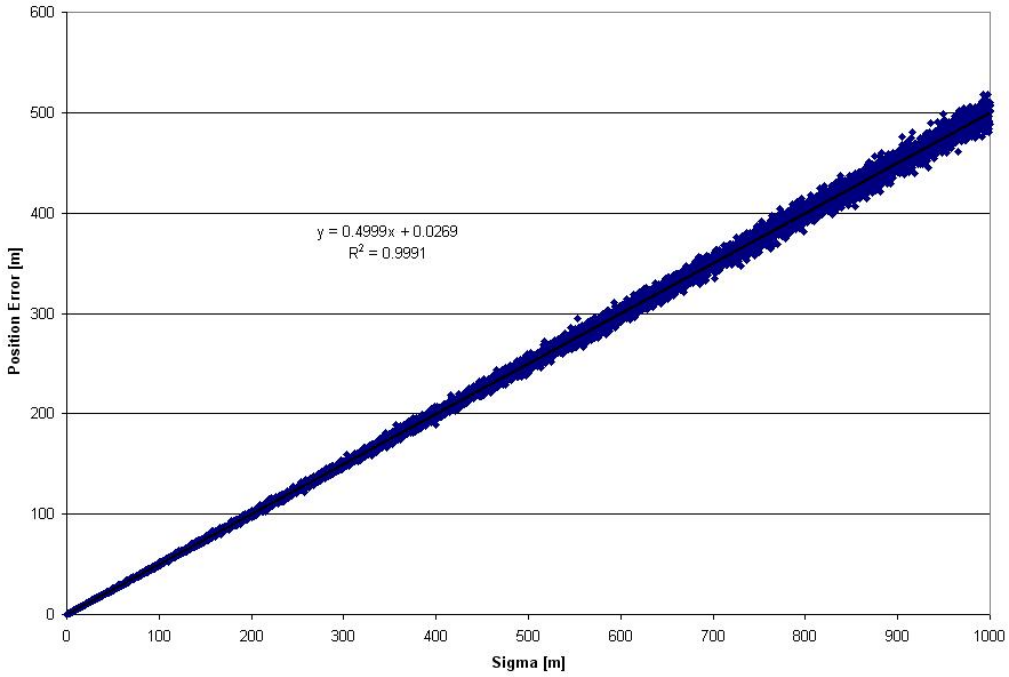

Figure A.40: Initial Position Error vs Sigma for $\Delta t = 0.1s$

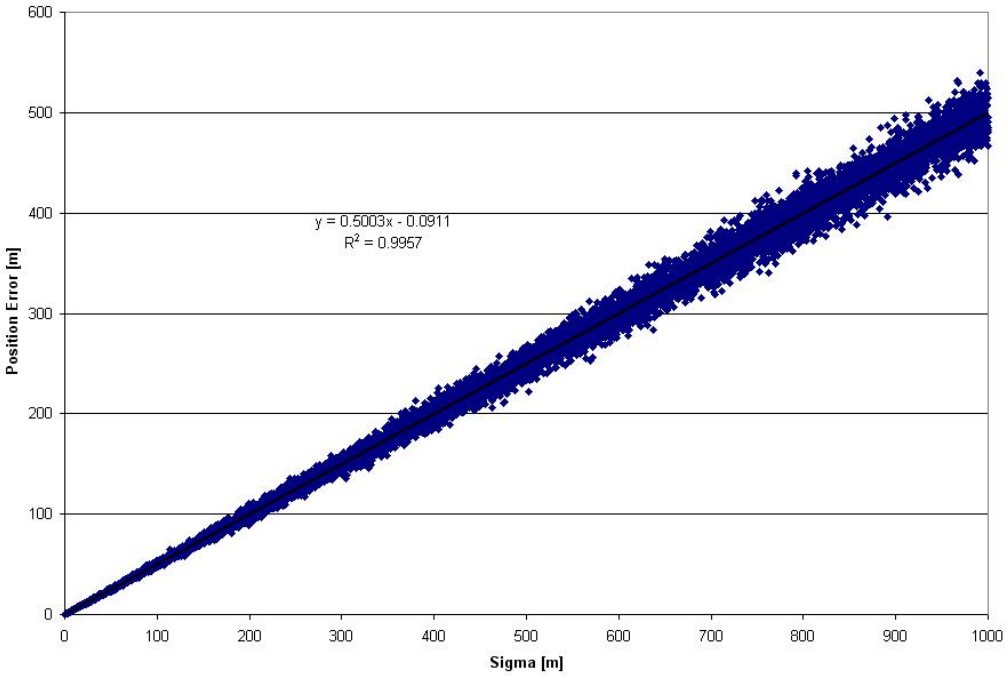

Figure A.41: Initial Position Error vs Sigma for $\Delta t = 0.5s$

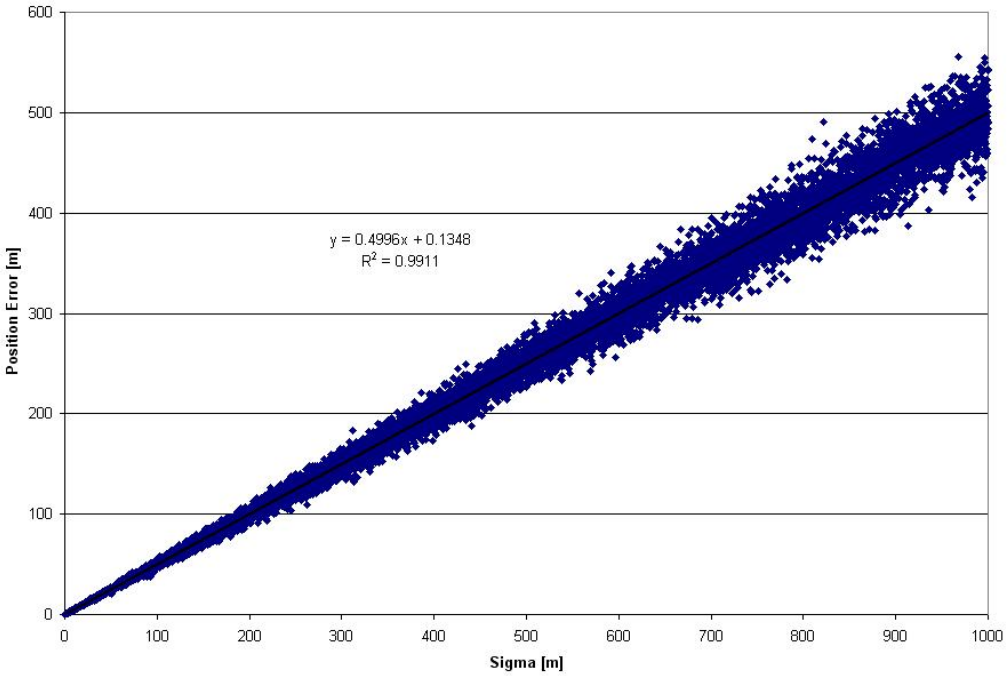

Figure A.42: Initial Position Error vs Sigma for $\Delta t = 1s$

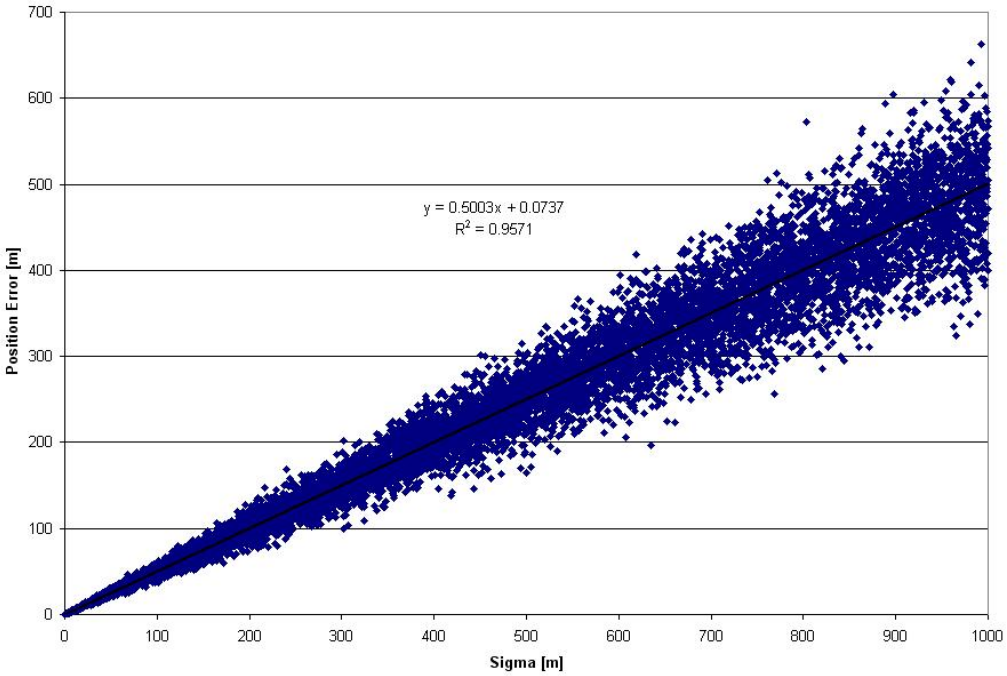

Figure A.43: Initial Position Error vs Sigma for $\Delta t = 5s$

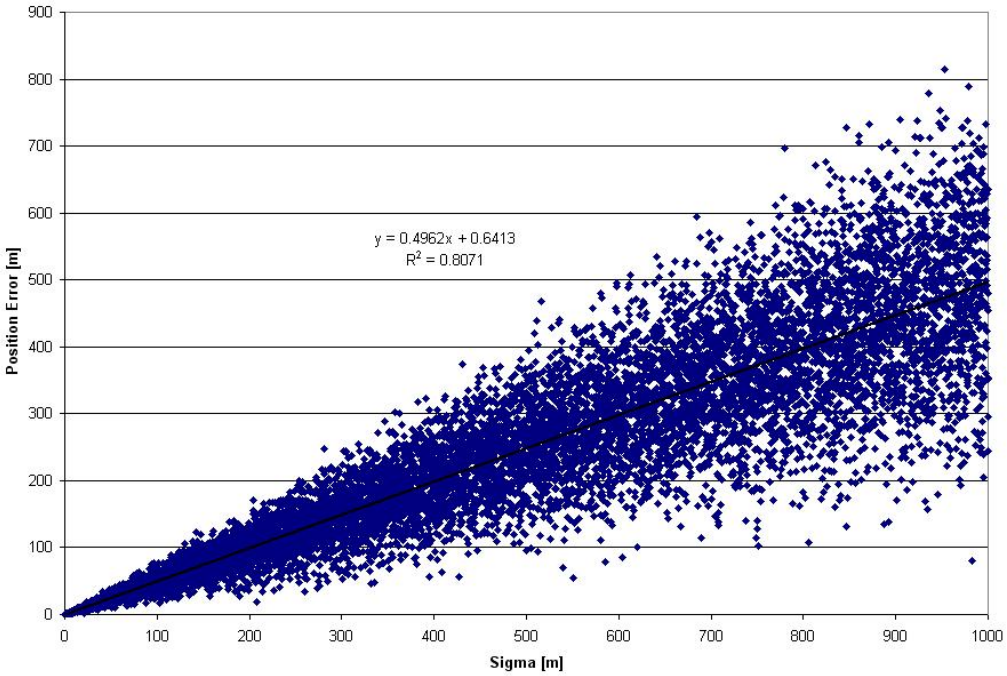

Figure A.44: Initial Position Error vs Sigma for $\Delta t = 30s$

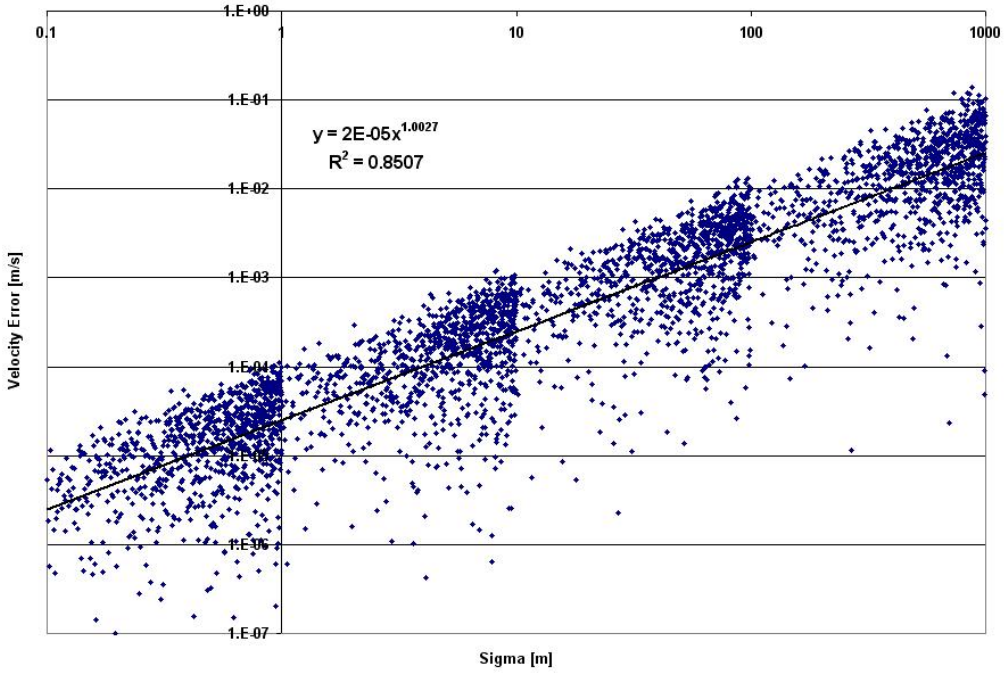

Figure A.45: Initial Velocity Error vs Sigma for $\Delta t = 0.5s$

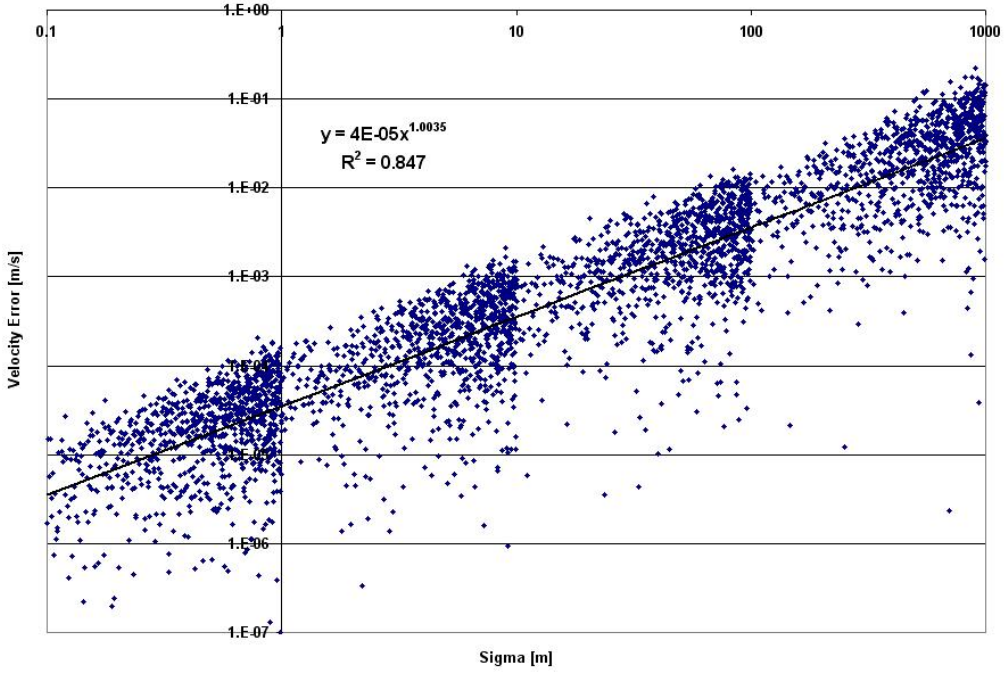

Figure A.46: Initial Velocity Error vs Sigma for $\Delta t = 1s$

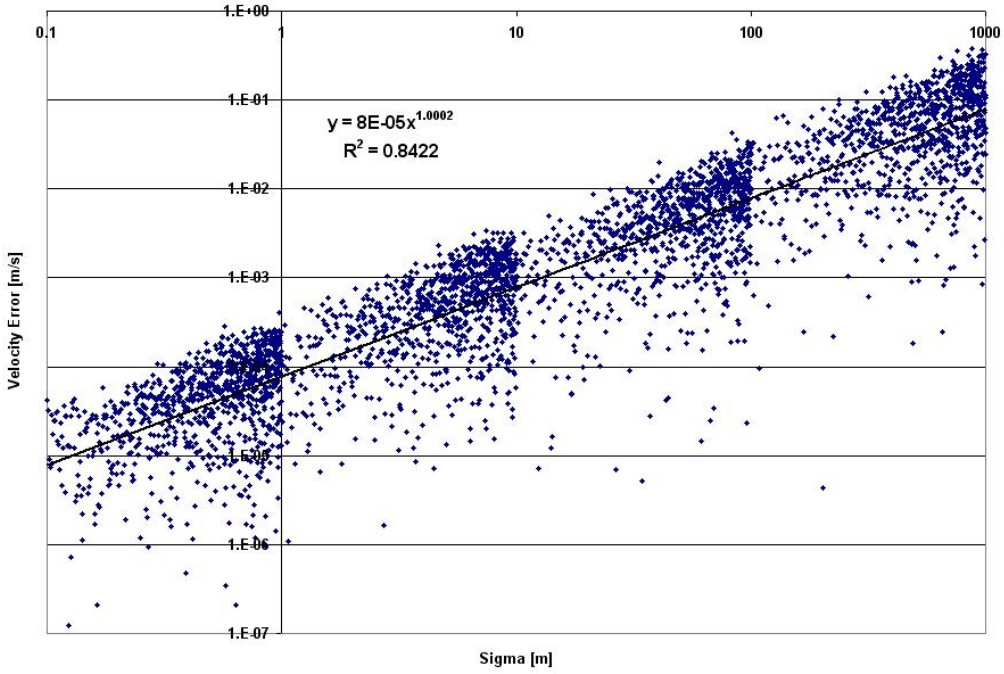

Figure A.47: Initial Velocity Error vs Sigma for $\Delta t = 5s$

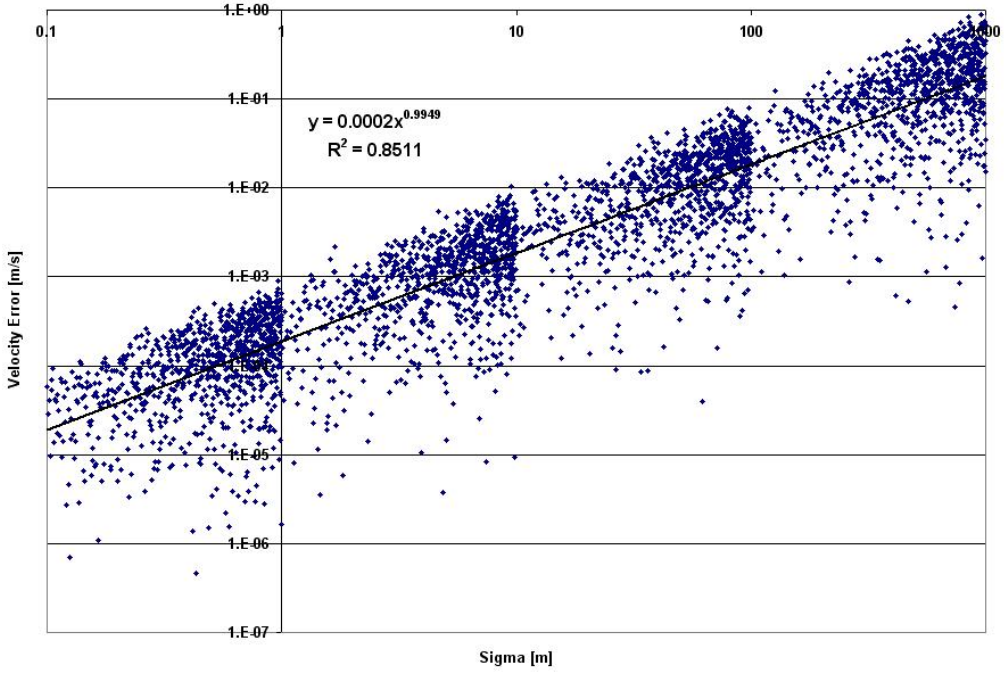

Figure A.48: Initial Velocity Error vs Sigma for $\Delta t = 30s$

Appendix B. Matlab Code

B.1 Hamiltonian Function Matlab Code

Listing B.1: Hamiltonian Function
(appendix2/TotalEnergyauto.m)

```
function [TE]=TotalEnergy_auto(C,S)
%%%%%%%%%%%%%%%%%%%%%%%%%%%%%%%%%%%%%%%%%%%%%%%%%%%%
% This function takes the coefficients C and S
% created from the EGM96 function and using the
% inertial position and velocity of a satellite
% computes the Hamiltonian of the system
%%%%%%%%%%%%%%%%%%%%%%%%%%%%%%%%%%%%%%%%%%%%%%%%%%%%

clc

% Define constants
%w_Earth = [0;0;0.0000729211585530d0];
% From Vallado's book

w_Earth = [0;0;0.058833592d0];
% Canonical Units From Wiesel

ord=1; %must be at least 1
       %order 1 gets me C00, S00 and P00
maxtess=0;

% Get the data from the file
In=dlmread('I:\My Documents\Thesis\EarthSat\Data\...
    Circular45ShortTBP\ecr.txt');
limit=length(In);
%limit=30;

% Put the data into new matrices time, x and xdot
a=1;
b=1;
while b < limit
        time(a)=In(b);
        a=a+1;
        b=b+3;
end

c=1;
d=2;
while d < limit
    x(c,1)=In(d,1);
    x(c,2)=In(d,2);
    x(c,3)=In(d,3);
    c=c+1;
    d=d+3;
end

e=1;
```

```
   f=3;
   while f < limit+1
       xdot(e,1)=In(f,1);
       xdot(e,2)=In(f,2);
51     xdot(e,3)=In(f,3);
       e=e+1;
       f=f+3;
   end

56 % Call the subroutine EGM96 to produce C and S
   [C,S,mu,R_Earth] = EGM96(ord);
   C=double(C);
   S=double(S);
   mu=double(1);
61 R_Earth=double(1);

   % Input the position and velocity vectors
   limit2=limit/3;

66 % Open the files for writing
   fid=fopen('I:\My Documents\Thesis\EarthSat\Data\Circular45ShortTBP...
      \TotalEnergy_grob.txt', 'wt');
   fid2=fopen('I:\My Documents\Thesis\EarthSat\Data\...
      Circular45ShortTBP\TotalEnergy_grob_graph.txt', 'wt');
   for y=1:limit2
       x1=[x(y,1) x(y,2) x(y,3)]';
71     xdot1=[xdot(y,1) xdot(y,2) xdot(y,3)]';
       % Calculate the inertial velocity
       crossterm=double(w_Earth*((x1(2,1)*xdot1(1,1))-(x1(1,1)*xdot1...
          (2,1))));
       crossterm=crossterm(3);
       KE1=0.5*dot(xdot1,xdot1)+crossterm; % (m/sec)^2
76
       % Calculate the potential energy
       r1=norm(x1); % m
       r1=double(r1);
       U_Coeff1=-mu/r1; % (m/sec)^2
81     U_Coeff1=double(U_Coeff1);

       % Calculate the summation for Geopotential
       U1(1)=1;
       U1=double(U1);
86
       % Create a matrix P for the Legendre Polynomials
       % where Pnm is actually P(m+1,n+1)
       P1(1,1)=1;

91     % For shorthand let cos(theta) = p
       % In ECI coordinate frame cos(theta) = z/r = p
       p1=(x1(3)/r1);
       p1=double(p1);
       %fprintf('p1 = %0.15f',p1);
```

```
96      P1(1,2)=(p1);
        P1(2,2)=-P1(1,1)/sqrt(1-p1^2);

        % for m = 0 see equation 4.44 page 113 in Modern Astrodynamics
        for n=2:ord
101         P1(1,n+1)=(((2*(n-1)+1)*p1*P1(1,n))-((n-1)*P1(1,n-1)))/(n)...
                ;
            for m=0:n-2
                P1(m+2,n)=(((n-1)-m)*p1*P1(m+1,n)-((n-1)+m)*P1(m+1,n...
                    -1))/sqrt(1-p1^2);
            end
        end
106
        UE1(1)=U_Coeff1*U1(1);
        TE1(1)=KE1+UE1(1);
        i=2;
        for n=1:ord-1
111         if maxtess < n
                mmax=maxtess;
            else
                mmax=n;
            end
116         for m=0:mmax
                ang=atan2(x1(2,1),x1(1,1));
                inter=C(n+1,m+1)*cos(m*ang)+S(n+1,m+1)*sin(m*ang);
                U1(i)=U1(i-1)+(P1(m+1,n+1)*inter*((r1/R_Earth)^(-n)));
                U1=double(U1);
121             UE1(i)=U_Coeff1*U1(i);
                UE1=double(UE1);
                TE1(i)=KE1+UE1(i);
                TE1=double(TE1);
                TEDIFF1(i)=TE1(i)-TE1(i-1);
126         i=i+1;
            end
        end

        fprintf(fid,'Time: %1.6f\n',time(y));
131     k=1;
        for n=0:ord-1
            if maxtess < n
                mmax=maxtess;
            else
136             mmax=n;
            end
            for m=0:mmax
               if n==ord-1
                if m==n
141            fprintf(fid,'Order J%1.0f,%1.0f:\n',n,m);
               fprintf(fid,'Total Energy is %0.15f\n',TE1(k));
                end
               end
                if n==ord-1
```

```
146             if m==mmax
                fprintf(fid2,'%4.14f            %0.15f\n',time(y),TE1(k...
                   ));
                end
                end
    %             if n==m
151 %                 if n==ord-1
    %                     fprintf(fid,'%1.14f            %0.15f\n',time...
       (y),TE1(k));
    %                 end
    %             end
                k=k+1;
156         end
        end
        fprintf(fid,'\n');

    end
161      fclose(fid);
         fclose(fid2);
    fprintf('DONE\n');
```

Listing B.2: EGM 96 Data
(appendix2/EGM96.m)

```
function [C,S,mu,R_Earth]=EGM96(ord)
%%%%%%%%%%%%%%%%%%%%%%%%%%%%%%%%%%%%%%%%%%%%%%%%%%%%%%%%%%%%%%%%
% This function takes data from the gravity model in
% egm96.dat and creates two orderXorder matrices C and S
% that coordinate with the normalized coefficients Cnm
% and Snm.  The matrix is tied to the coefficient in the
% following way: Cnm = C(n+1,m+1) and Snm=S(n+1,m+1)
%%%%%%%%%%%%%%%%%%%%%%%%%%%%%%%%%%%%%%%%%%%%%%%%%%%%%%%%%%%%%%%%

% Initialize the C and S matrices
C=zeros(ord,ord);
S=zeros(ord,ord);

% Read in the data from the file and store in a 1XN matrix
EGM96=double(dlmread('EGM96.dat'));

% Used for checking my values to the original
% fid=fopen('EGM96_grob.txt','wt');
%
% for m=1:500
%     for n=1:2
%         fprintf(fid,'%1.0f     ',EGM96(m,n));
%     end
%     for n=3:4
%         fprintf(fid,'%1.11e     ',EGM96(m,n));
%     end
%     fprintf(fid,'\n');
% end
%
% fclose(fid);

%Define mu and radius of the earth
mu=EGM96(1,1); % m^3/sec^2
R_Earth=EGM96(2,1); % m

% Do a for loop to populate the C and S matrices
% with the data from the file
n=3;
for i=1:ord
    for j=1:i
        C(i,j)=EGM96(n,3);
        S(i,j)=EGM96(n,4);
        n=n+1;
        j=j+1;
    end
    i=i+1;
end

% Unnormalize the C and S coefficients
for k=0:ord-1
```

```
51      for l=0:k
            if l==0
                eps=1;
            else
                eps=2;
56          end
            fact=(eps*(2*k+1)*factorial(k-l))/factorial(k+l);
            C(k+1,l+1)=double(sqrt(fact)*C(k+1,l+1));
            S(k+1,l+1)=double(sqrt(fact)*S(k+1,l+1));
        end
61  end

    % Used for checking my values to the original
    % fid=fopen('EGM96_grob.txt','wt');
    %
66  % for n=0:ord-1
    %     for m=0:n
    %         fprintf(fid,'%1.0f     ',n);
    %         fprintf(fid,'%1.0f     ',m);
    %         fprintf(fid,'%1.11e     ',C(n+1,m+1));
71  %         fprintf(fid,'%1.11e     \n',S(n+1,m+1));
    %     end
    % end
    % fclose(fid);

76  end
```

B.2 Inertial Angular Momentum Matlab Code

Listing B.3: Inertial Angular Momentum
(appendix2/angularmom.m)

```
function angularmom
% This function reads in time, position and velocity data
% from a text file, calculates the Inertial Angular Momentum
% and outputs the z-component to a text file.

% Put the data from eci.txt into new matrices time, x and xdot
clc
In=dlmread('I:\My Documents\Thesis\EarthSat\Data\Circular30LongTBP...
   \eci.txt');
limit=length(In);

a=1;
b=1;
while b < limit
        time(a)=In(b);
        time=double(time);
        a=a+1;
        b=b+3;
end

c=1;
d=2;
while d < limit
    x(c,1)=In(d,1);
    x(c,2)=In(d,2);
    x(c,3)=In(d,3);
    x=double(x);
    c=c+1;
    d=d+3;
end

e=1;
f=3;
while f < limit+1
    xdot(e,1)=In(f,1);
    xdot(e,2)=In(f,2);
    xdot(e,3)=In(f,3);
    xdot=double(xdot);
    e=e+1;
    f=f+3;
end

limit2=limit/3;
fid = fopen('I:\My Documents\Thesis\EarthSat\Data\...
   Circular30LongTBP\Lz_grob.txt', 'wt');
fprintf(fid,'Time (TU)      Z component of angular momentum\n');
fprintf(fid,'-----------------------------------------\n');
for j=1:limit2
```

```
        x1=[x(j,1) x(j,2) x(j,3)];
        xdot1=[xdot(j,1) xdot(j,2) xdot(j,3)];
49      H=cross(x1,xdot1);
        fprintf(fid,'%1.6f',time(j));
        fprintf(fid,'            %0.15f\n',H(3));
    end
    fclose(fid);
54  fprintf('DONE\n');
```

B.3 Change in Ascending Node Matlab Code

Listing B.4: Nodal Regression
(appendix2/nodalregress.m)

```
function nodalregress
% Put the data into new matrices time, x and xdot
clc
In=dlmread('I:\My Documents\Thesis\EarthSat\Data\Circular30LongTBP...
    \eci.txt');
limit=length(In);

a=1;
b=1;
while b < limit
        time(a)=In(b);
        time=double(time);
        a=a+1;
        b=b+3;
end

c=1;
d=2;
while d < limit
    x(c,1)=In(d,1);
    x(c,2)=In(d,2);
    x(c,3)=In(d,3);
    x=double(x);
    c=c+1;
    d=d+3;
end

e=1;
f=3;
while f < limit+1
    xdot(e,1)=In(f,1);
    xdot(e,2)=In(f,2);
    xdot(e,3)=In(f,3);
    xdot=double(xdot);
    e=e+1;
    f=f+3;
end

limit2=limit/3;
fid = fopen('I:\My Documents\Thesis\EarthSat\Data\...
   Circular30LongTBP\Nodal_Regress_grob.txt', 'wt');
for j=1:limit2
    x1=[x(j,1) x(j,2) x(j,3)];
    xdot1=[xdot(j,1) xdot(j,2) xdot(j,3)];
    H=cross(x1,xdot1);
    N=[-H(2) H(1) 0];
    if N(2) < 0
    omega=2*pi - acos(N(1)/norm(N));
```

```
        else
        omega=acos(N(1)/norm(N));
        end
        if omega < 0.0
51          omega = 2*pi - omega;
        end
        fprintf(fid,'%1.6f',time(j));
        fprintf(fid,'            %0.15f\n',omega);
    end
56  fclose(fid);
    fprintf('DONE\n');
```

B.4 Least Squares Matlab Code

Listing B.5: Least Squares
(appendix2/leastsquares.m)

```
function leastsquares
% This program estimates data using a simplified
% dynamics model, creates an initial estimate
% using linear least squares and then updates
% the estimate using non-linear least squares

clc

t=0:60:600;
% asssume accuracy to meters
sigma=.1; % Accuracy of the sensor and noise level

% Create the simulated data
   % Define the constants and ICs
   R0=[1.05*6378137;0;0];
   V0=[0;6538.656905;3600.9857675];
   g=-9.81;

   %Run a for loop to calculate position
   for i=1:length(t)
      R(:,i)=R0+V0*t(:,i)+[0;0;.5*g*t(:,i)^2];
   end

   % Add random noise to the data
   P=rand(3,length(t));
   z=R+P*sigma;

% Run linear least squares to find an initial estimate
% Define constants and initiate sums
Q=[sigma^2*eye(3,3)];
H=[eye(3,3),zeros(3,3)];
TQIT_sum=0;
TQIz_sum=0;
% Run a for loop to complete the two summations
for i=1:length(t)
   STM=[eye(3,3),t(:,i)*eye(3,3);zeros(3,3),eye(3,3)];
   T=H*STM;
   TQIT=T'*inv(Q)*T;
   TQIz=T'*inv(Q)*z(:,i);
   TQIT_sum=TQIT_sum+TQIT;
   TQIz_sum=TQIz_sum+TQIz;
end
% Calculate the covariance
P_x=inv(TQIT_sum);
% Calcalute the initial state
state_init=P_x*TQIz_sum;

% Run non-linear least squares to caculate the accuracy
```

```
   % Initiate the sums
   TQIT_sum2=0;
   TQIr_sum=0;
52 % Run a for loop to calculate the sums
   for j=1:length(t)
       STM=[eye(3,3),t(:,j)*eye(3,3);zeros(3,3),eye(3,3)];
       % Find the state and add a particular solution
       state=STM*state_init+[0;0;0.5*g*(t(:,j))^2;0;0;g*t(:,j)];
57     % Treat as a linear problem
       G=[eye(3,3),zeros(3,3)]*state;
       H2=[eye(3,3),zeros(3,3)];
       r=z(:,j)-G;
       T2=H2*STM;
62     TQIT=T2'*inv(Q)*T2;
       TQIr=T2'*inv(Q)*r;
       TQIT_sum2=TQIT_sum2+TQIT;
       TQIr_sum=TQIr_sum+TQIr;
   end
67 %C Calculate the covariance
   P_dx=inv(TQIT_sum2);
   % Calculate the initial state variance
   dstate_init=P_dx*TQIr_sum;
   % Calculate the updated initial state
72 state_init=state_init+dstate_init;
   % Calculate the initial state error
   R_diff=[abs(R0(1)-state_init(1));abs(R0(2)-state_init(2));abs(R0...
      (3)-state_init(3))];
   V_diff=[abs(V0(1)-state_init(4));abs(V0(2)-state_init(5));abs(V0...
      (3)-state_init(6))];
   % Output the data to the screen
77 fprintf('Position error is:\nx-direction %1.12e\ny-direction %1.12...
      e\nz-direction %1.12e\n',R_diff(1),R_diff(2),R_diff(3));
   fprintf('Velocity error is:\nx-direction %1.12e\ny-direction %1.12...
      e\nz-direction %1.12e\n',V_diff(1),V_diff(2),V_diff(3));
```

Bibliography

1. "Cheyenne Mountain - Joint Space Operations Center". Mission Statement. Available at https://www.cheyennemountain.af.mil/jspoc05.htm.
2. "EGM96: The NASA GSFC and NIMA Joint Geopotential Model". Results from a study, 1996. Available at http://cddisa.gsfc.nasa.gov/926/egm96/egm96.html.
3. "Mean Element Theory". An article in the AGI online knowledge base, March 2005. Available at http://www.agi.com/resources/help/stk613/helpSystem/stk/vehSat_meanElements.htm.
4. Annis, Charles. "R-Squared". An article in Statistical Engineering, January 2008. Available at http://www.statisticalengineering.com/r-squared.htm.
5. Escobal, Pedro Ramon. *Methods of Orbit Determination*. John Wiley & Sons, Inc., New York, NY, first edition, 1965.
6. Kelso, T.S. "Space Surveillance". An article in Satellite Times, September/October 1997. Available at http://celestrak.com/columns/v04n01/.
7. Meirovitch, Leonard. *Methods of Analytical Dynamics*. Dover Publications, Inc., Mineola, NY, first edition, 2003.
8. Vallado, David A. *Fundamentals of Astrodynamics and Applications*. Microcosm Press, El Segundo, CA, second edition, 2001.
9. Wiesel, William E. *Spaceflight Dynamics*. Irwin/McGraw Hill, Boston, MA, second edition, 1995.
10. Wiesel, William E. *Modern Astrodynamics*. Aphelion Press, Beavercreek, OH, first edition, 2003.
11. Wiesel, William E. *Modern Orbit Determination*. Aphelion Press, Beavercreek, OH, first edition, 2003.

REPORT DOCUMENTATION PAGE

Form Approved
OMB No. 074-0188

1. REPORT DATE *(DD-MM-YYYY)*	2. REPORT TYPE	3. DATES COVERED *(From – To)*
14-03-2008	**Master's Thesis**	September 2006-March 2008

4. TITLE AND SUBTITLE

UNCORRELATED TRACK AVOIDANCE

5a. CONTRACT NUMBER

5b. GRANT NUMBER

5c. PROGRAM ELEMENT NUMBER

6. AUTHOR(S)

Grob, Darrell L., Captain, USAF

5d. PROJECT NUMBER

5e. TASK NUMBER

5f. WORK UNIT NUMBER

7. PERFORMING ORGANIZATION NAMES(S) AND ADDRESS(S)

Air Force Institute of Technology
Graduate School of Engineering and Management (AFIT/EN)
2950 Hobson Way
WPAFB OH 45433-7765 DSN: 785-3636

8. PERFORMING ORGANIZATION REPORT NUMBER

AFIT/GA/ENY/08-M10

9. SPONSORING/MONITORING AGENCY NAME(S) AND ADDRESS(ES)

AFRL/RDSM
Dr. Chris Sabol
535 Lipoa Pkwy Ste 200
Kihei, HI 96753 (808) 874-1594

10. SPONSOR/MONITOR'S ACRONYM(S)

11. SPONSOR/MONITOR'S REPORT NUMBER(S)

12. DISTRIBUTION/AVAILABILITY STATEMENT

APPROVED FOR PUBLIC RELEASE; DISTRIBUTION UNLIMITED

13. SUPPLEMENTARY NOTES

14. ABSTRACT

The purpose of this thesis is to examine what data requirements are necessary to avoid continual series of uncorrelated tracks when gathering observations. The constants of the motion for simple two-body motion for a satellite orbiting the Earth, known as the classical orbital elements do not remain constant due to zonal and sectoral harmonic variations in the Earth's gravitational field. There are other elements of the motion that should be considered and this paper discusses the constancy of three elements: the Hamiltonian of the Earth-Centered Rotating System, Z-component of inertial angular momentum, and the time rate of change of the right ascension of the ascending.

With an understanding of the constancy of these elements, simulated data was used to determine the effects sensor performance and observation quantity have on the ability to effectively estimate these constants. This information was used to determine an appropriate level of fidelity for a model to be utilized as a supplement in fitting observation data with current data available in the Satellite Catalog.

15. SUBJECT TERMS

Uncorrelated Tracks, Hamiltonian Function, Angular Momentum, Right Ascension, Data Mining, Space Surveillance

16. SECURITY CLASSIFICATION OF:			17. LIMITATION OF ABSTRACT	18. NUMBER OF PAGES	19a. NAME OF RESPONSIBLE PERSON
REPORT	ABSTRACT	c. THIS PAGE			**William E. Wiesel, PhD (ENY)**
U	U	U	UU	112	**19b. TELEPHONE NUMBER** *(Include area code)* (937) 255-3636 x4312; email: william.wiesel@afit.edu

Standard Form 298 (Rev: 8-98)
Prescribed by ANSI Std. Z39-18